BNL-90873-2009-BC

Evaluated Nuclear Data

P. Oblozinsky, M. Herman and S.F. Mughabghab

To be published in "Handbook of Nuclear Engineering - Chapter3"

2010

Energy Sciences & Technology Department
National Nuclear Data Center
Brookhaven National Laboratory
P.O. Box 5000
Upton, NY 11973-5000
www.bnl.gov

DISCLAIMER

3 Evaluated Nuclear Data

P. Obložinský, M. Herman and S.F. Mughabghab

Abstract This chapter describes the current status of evaluated nuclear data for nuclear technology applications. We start with evaluation procedures for neutron-induced reactions focusing on incident energies from the thermal energy up to 20 MeV, though higher energies are also mentioned. This is followed by examining the status of evaluated neutron data for actinides that play dominant role in most of the applications, followed by coolants/moderators, structural materials and fission products. We then discuss neutron covariance data that characterize uncertainties and correlations. We explain how modern nuclear evaluated data libraries are validated against an extensive set of integral benchmark experiments. Afterwards, we briefly examine other data of importance for nuclear technology, including fission yields, thermal neutron scattering and decay data. A description of three major evaluated nuclear data libraries is provided, including the latest version of the US library ENDF/B-VII.0, European JEFF-3.1 and Japanese JENDL-3.3. A brief introduction is made to current web retrieval systems that allow easy access to a vast amount of up-to-date evaluated nuclear data for nuclear technology applications.

1 Evaluation Methodology for Neutron Data

The evaluated (recommended) neutron cross section data represent the backbone of data needed for nuclear technology applications. The incident energies of interest cover an extremely broad energy range of 13 orders of magnitude. Thus, for fission

P. Obložinský
National Nuclear Data Center, Brookhaven National Laboratory, Upton, NY 11973-5000, e-mail: oblozinsky@bnl.gov

M. Herman
as above, e-mail: mwherman@bnl.gov

S.F. Mughbaghab
as above, e-mail: mugabgab@bnl.gov

and fusion reactor systems one needs neutrons from 10^{-5}eV to $2 \times 10^{+7}$eV (20 MeV), to be extended up to about 200 MeV for accelerator driven systems. If higher incident energies are needed, one resorts to on-fly calculations (not covered here) rather than to evaluated nuclear data libraries.

Such a large range of incident neutron energies represents enormous challenge for developers of evaluated nuclear data libraries. This is coupled to another challenge that stems from the fact that nuclear technology applications need data for about 400 atomic nuclei, covering the atomic mass range of A = 1 - 250, from hydrogen to the actinides.

There is no simple way to describe physics of neutrons interacting with atomic nuclei throughout this vast range of energies and different types of nuclei. Rather, nuclear physics uses different approaches and many different models to describe underlying physics. The role of experimental data in the evaluation process is absolutely crucial, with the understanding that measured data must be combined with physics-based models to fill-in the gaps and to gain confidence in the judgment as to what is the best reflection of nature.

The goals for the evaluations are to comply as closely as possible with experimental microscopic (differential) data and at the same time to accurately match results from simple benchmark (integral) experiments. The evaluation is a complex process, requiring detailed knowledge of nuclear reaction physics, experimental databases, nuclear modeling, considerable experience and attention to details. Once the whole set of isotopes (materials) is evaluated and a library is assembled, validation of the entire library is performed against hundreds of benchmark experiments.

The description of evaluation methodology given below reflects the state-of-art methods used in the development of the latest US evaluated data library, ENDF/B-VII.0. This library, released in December 2006, is described in detail in the extensive paper by Chadwick *et al.* [1]. The evaluated data are stored in the internationally adopted ENDF-6 format [2].

1.1 Basic Ingredients

Basic ingredients of the evaluation process for neutron cross section data include the EXFOR database of microscopic experimental data, Atlas of Neutron Resonances and nuclear reaction model codes. Consequently, the evaluation methodology consists of three parts:

- Careful analysis of microscopic[1] experimental data.

[1] "Microscopic" is the term used by nuclear data physicists to describe properties of individual nuclei and their interactions, which should be distinguished from properties of large-scale ensambles

- The low energy region (thermal energy, resolved resonances and unresolved resonances) is treated by methods developed to analyze neutron resonances.
- The fast neutron region is evaluated using methods based on nuclear reaction model calculations and experimental data.

Nuclear theory and modeling has played a central role in developing complete cross section evaluations, by which we mean representations that cover all incident projectile energies, outgoing particle and photon energies as well as angular distributions. Nuclear reaction theory codes provide a powerful tool to interpolate and extrapolate from the measured data, and naturally incorporate constraints such as unitarity, and energy and momentum conservation. A number of reaction physics codes have been developed that support this work:

- Statistical, preequilibrium, direct and fission models, for use in modeling medium and heavy nucleus reactions, notably Los Alamos National Laboratory code GNASH [3, 4, 5] and code EMPIRE (Brookhaven National Laboratory, [6, 7]), often used in conjunction with coupled-channels optical model code ECIS (CEA Saclay, [8]),
- R-matrix codes for light nucleus reactions, and for lower incident energy reactions on heavier targets, notably the Los Alamos code EDA [9] and the Oak Ridge code SAMMY [10],
- Atlas code system [11] for analyzing neutron resonances in terms of multi-level Breit-Wigner formalism by Mughabghab at Brookhaven to produce comprehensive evaluation of resonance parameters, thermal cross sections, and average resonance parameters for the Atlas of Neutron Resonances [12].

Fig. 1 qualitatively summarizes nuclear reaction models and related codes as used in the ENDF/B-VII.0 evaluations for various combinations of mass number and incident energy. In light nuclei the excited states are generally sparse and well isolated. This feature necessitates use of special few-body techniques that are feasible due to a limited number of nucleons in the system. We have used the explicit R-matrix theory, implemented in the Los Alamos code EDA, for evaluations of nuclides up to the atomic mass A $\approx$ 10 (with a few exceptions). This approach, although formally strict, relies on experimental input. In Fig. 1 the few-body regime is depicted as a vertical rectangle at the left of the picture. Note, that in this case the same methodology is applied throughout the whole energy range.

Increasing the number of nucleons in the target makes usage of few-body models impractical. On the other hand, the large number of excited states facilitates approaches that, to a certain extent, are built upon statistical assumptions. This "statistical regime" appears in Fig. 1 to the right of A$\sim$10. We have to deal with three distinct energy regions for these nuclei:

- Resolved resonance region (including thermal neutrons),
- Unresolved resonance region, and

---

of nuclei. Thus, microscopic cross section is the interaction probability of one neutron incident on a single target nucleus.

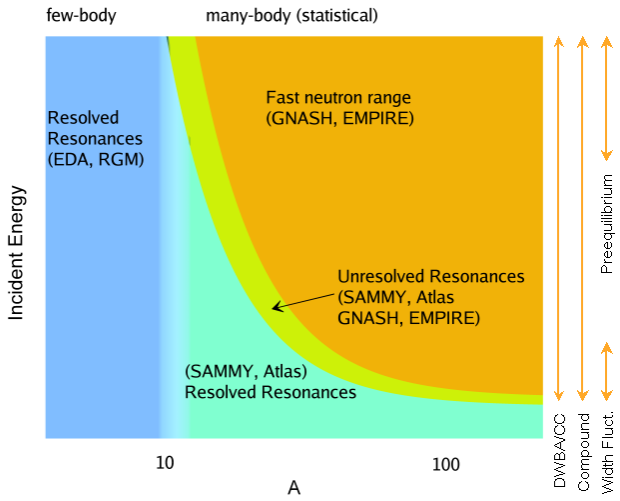

Fig. 1 Schematic representation depicting the use of various evaluation techniques and related codes (in brackets) depending on target mass and incident energy. Arrows to the right of the figure indicate major reaction mechanisms in the fast neutron region and their energy range of applicability.

- Fast neutron region.

Since the density of neutron resonances increases with A, the upper limit of the resolved resonance region decreases when moving to heavier nuclei. A neighboring region is known as the unresolved resonance region in which overlapping resonances usually produce quite smooth cross sections. Each of these three regions needs different techniques and different reaction modeling.

Except for very light nuclei, there is no theory capable of predicting individual resonances. Therefore, realistic evaluations require experimental data for neutron resonances. In ENDF/B-VII.0 the Reich-Moore approach derived from the R-matrix theory, as implemented in the Oak Ridge code SAMMY, was utilized for the important actinides. For about 150 fission product nuclei, the multi-level Breit-Wigner formalism, and statistical methods from the Atlas of Neutron Resonances [12] were used at BNL.

The unresolved resonance region is a transitional region that could be treated with the methods from the resolved region as well as in the terms of the models used in the fast neutron region.

The fast neutron region involves a whole suite of nuclear reaction models with a strong statistical component resulting from the averaging over many resonances. The Hauser-Feshbach formulation of the compound nucleus is a key model for any evaluation in the fast neutron region, although in the low energy range it must be corrected to account for the width fluctuation effects. At incident energies above some

10 MeV, preequilibrium emission has to be taken into account and one implements a variety of semi-classical and quantum-mechanical models.

While most of the nuclear reaction models used for the evaluations are predominantly phenomenological, their usage involves a huge number of input parameters. Developement of the ENDF/B-VII.0 library largely benefited from the Reference Input Parameter Library (RIPL) [13, 14, 15] , an international project coordinated by the International Atomic Energy Agency, Vienna.

1.2 Thermal and Resolved Resonance Region

Usually the first step in neutron resonance evaluation is inspection of the well-known compendium of data produced over years by S. Mughabghab, BNL, traditionally known as BNL-325. Its last 5^{th} edition has been published in 2006 as "Atlas of Neutron Resonances: Resonance Parameters and Thermal Cross Sections" [12], representing a considerable update to the 1981 [16] and 1984 editions [17]. Often, one is satisfied with these data and adopts them as they are. Indeed, these latest thermal values and resonance parameters provided a basis for more than 150 new evaluations included in ENDF/B-VII.0. In many other cases, however, one performs additional evaluation by applying sophisticated R-matrix analysis to most recent experiments using the Oak Ridge code SAMMY [10].

1.2.1 Thermal Energy Region

Accurate knowledge of the thermal neutron capture and fission cross sections are of paramount importance for many applications and considerable experimental as well as evaluation effort was expended in obtaining precise and consistent constants at a neutron energy of 0.0253 eV (velocity v_0 = 2200 m/s). The parameters under consideration are the absorption ($\sigma_{\rm abs}$), radiative capture (σ_γ) and fission (σ_f) cross sections, the neutron yield data ($\bar{\nu}, \eta$) as well as Westcott factors g_w. Some of these quantities are interrelated as

$$\eta = \bar{\nu}\frac{\sigma_f}{\sigma_{\rm abs}} = \frac{\bar{\nu}}{1+\alpha}, \tag{1}$$

where $\bar{\nu} = \bar{\nu}_p + \bar{\nu}_d$ is the average number of neutrons emitted per neutron induced fission obtained by the sum of prompt and delayed values,

$$\sigma_{\rm abs} = \sigma_\gamma + \sigma_f \quad \text{and} \quad \alpha = \frac{\sigma_\gamma}{\sigma_f}. \tag{2}$$

When the scattering cross section (σ_s) is known, the absorption cross section can be determined absolutely to a high degree of accuracy from a measurement of the total cross section as $\sigma_{\rm abs} = \sigma_{\rm tot} - \sigma_s$.

The capture[2] cross section for a single resonance is usually represented by the Breit-Wigner formalism. In the case of several s-wave resonances, the thermal capture cross section at $E = 0.0253$ eV is given by

$$\sigma_\gamma(E) = \frac{2.608 \times 10^6}{\sqrt{E}} \left(\frac{A+1}{A}\right)^2 \sum_j \frac{g_J \Gamma_{nj}^0 \Gamma_{\gamma j}}{\Gamma_j^2 + 4(E - E_{0j})^2}. \tag{3}$$

In this relation, Γ_{nj}, $\Gamma_{\gamma j}$ and Γ_j are the neutron scattering, radiative and total width of the resonance j, respectively; E_{0j} is the resonance energy, A is the atomic mass number of the target nucleus, and g_J is the statistical spin weight factor defined as

$$g_J = \frac{2J+1}{2(2I+1)}, \tag{4}$$

where J is the resonance spin and I is the target nucleus spin. As an example, Fig. 2 shows the evaluated capture cross sections for ^{133}Cs in the thermal along with the low energy resonance region compared with the available experimental data.

Similarly, the fission cross section can be described as a sum over positive and negative energy resonance contributions. In the framework of the Breit-Wigner formalism, the fission cross section can be obtained from

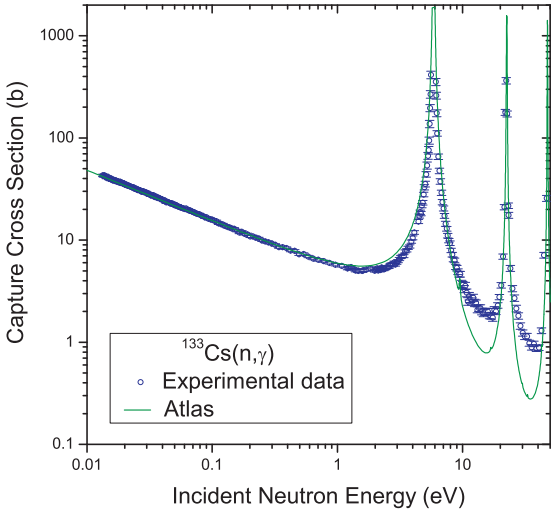

Fig. 2 Neutron capture cross section for ^{133}Cs in the thermal and resolved resonance energy region computed from Atlas are compared with experimental data. The calculated cross section is Doppler-broadened to 300^o K; the experimental resolution is not included. Two bound levels were invoked in order to fit the thermal constants.

[2] "Capture" is the short-hand term used by nuclear physicists to describe radiative capture, *i.e.*, (n,γ) cross sections. This differs from what nuclear engineers might consider "capture", which is given by the sum of neutron removal cross sections, *i.e.*, $(n,\gamma)+(n,p)+(n,\alpha)+\cdots$.

$$\sigma_f(E) = \frac{2.608 \times 10^6}{\sqrt{E}} \left(\frac{A+1}{A}\right)^2 \sum_j \frac{g_J \Gamma_{nj}^0 \Gamma_{fj}}{\Gamma_j^2 + 4(E-E_{0j})^2}, \tag{5}$$

where

$$\Gamma_j(E) = \Gamma_{nj}(E) + \Gamma_{\gamma j} + \Gamma_{fj}. \tag{6}$$

The formalism for neutron elastic scattering is more complicated. Thus, elastic cross section for a single resonance can be expressed by the sum of three terms

$$\sigma_n(E) = 4\pi \frac{2l+1}{k^2} \sin^2\phi_l + \pi \frac{g_J}{k^2} \frac{\Gamma_n \Gamma \cos(2\phi_l) + 2(E-E_0)\Gamma_n \sin(2\phi_l)}{(E-E_0)^2 + \frac{1}{4}\Gamma^2}, \tag{7}$$

where k is the neutron wave number, ϕ_l are the phase shifts determined by k and the potential scattering radius R'. The 1st term describes potential scattering, σ_{pot}, which is nearly constant as a function of energy. The second term stands for the symmetric resonance cross section. The 3rd term, containing $2(E-E_0)\Gamma_n \sin(2\phi_l)$ in the numerator describes interference between potential (hard-sphere) and resonance scattering which is negative at $E < E_0$ and positive at $E > E_0$.

In order to obtain the thermal scattering cross section one should resort to extended version of the above expression, such as provided by the multi-level Breit-Wigner formalism. We note that in the low-energy approximation simplified expressions can be obtained, including that for potential scattering

$$\sigma_{\text{pot}} \approx 4\pi R'^2. \tag{8}$$

The neutron scattering can be also expressed in terms of spin-dependent free nuclear scattering lengths, a_+ and a_-, associated with spin states $I+1/2$ and $I-1/2$, as

$$a_\pm = R' + \sum_j \frac{\lambda_j \Gamma_{nj}}{2(E-E_{0j}) - i\Gamma_j}, \tag{9}$$

where $\lambda_j = 1/k$ is de Broglie's wavelength divided by 2π. We note that $a_\pm$ contain imaginary components and the summation is carried out over all s-wave resonances with the same spin.

The total coherent scattering length for non-zero spin target nuclei, is then the sum of the spin-dependent coherent scattering widths, a_+ and a_-, weighted by the spin statistical factor, $g_+ = (I+1)/(2I+1)$ and $g_- = I/(2I+1)$,

$$a = g_+ a_+ + g_- a_- . \tag{10}$$

The total scattering cross section can then be expressed as

$$\sigma_s = 4\pi \left(g_+ a_+^2 + g_- a_-^2\right). \tag{11}$$

If the results of the calculated cross sections do not agree with measurements within the uncertainty limits, then one or two negative energy (bound) levels are invoked.

The potential scattering length or radius, R', is an important parameter which is required in the calculation of scattering and total cross sections. It can be expressed as

$$R' = R(1 - R^{\infty}), \tag{12}$$

where R is the channel or interaction radius, and R^{∞} is related to the distant s-wave resonance contribution. We note that R' can be determined to a high degree of accuracy from the measured coherent scattering amplitude by Eq. (9) when the resonance data are complete.

1.2.2 Westcott Factors and Resonance Integrals

In general, in the thermal energy region capture cross sections follow the 1/v law, where v is the neutron velocity. Deviations from this behavior are due to the proximity of the 1st resonance to the thermal energy of 0.0253 eV, notable examples being ^{113}Cd, ^{149}Sm and ^{155}Gd. Westcott factors, ideally equal to unity, can be used as a suitable measure of the validity of this law. They are defined as the ratio of the Maxwellian averaged cross section, σ, to the thermal cross section, σ_0

$$g_w = \frac{\sigma}{\sigma_0} = \frac{1}{\mathrm{v}_0\sigma_0} \int_0^{\infty} \frac{1}{\pi^{1/2}} \frac{\mathrm{v}^3}{\mathrm{v}_T^3} e^{-\mathrm{v}^2/\mathrm{v}_T^2} \sigma(\mathrm{v}) d\mathrm{v}, \tag{13}$$

where v_0 = 2200 m/s and v_T is the most probable velocity for Maxwellian spectrum at temperature T.

Resonance integrals represent useful quantities that characterize cross sections in the thermal and resonance region. For a particular reaction $\sigma_x(E)$, such as total, elastic scattering, capture and fission ($x = \mathrm{tot}, s, \gamma, f$), in a $1/E$ spectrum these are defined as

$$\mathrm{I}_x = \int_{0.5eV}^{\infty} \sigma_x(E) \frac{dE}{E}, \tag{14}$$

where the low energy is determined by the cadmium cutoff energy usually set to 0.5 eV, while the upper energy is sometimes set to 100 keV [18]. It is important to note that both the thermal energies and resonances contribute to the resonance integrals.

Often Westcott factors and resonance integrals are readily available in tabulated form, an example being JEFF-3.1 library [18]. They can also be conveniently obtained from web using retrieval systems such as Sigma [19] developed and maintained by the National Nuclear Data Center at Brookhaven.

1.2.3 Resolved Resonance Energy Region

Neutron time-of-flight techniques that employ accelerator facilities as neutron sources are used to perform high-resolution cross-section measurements in the resonance region. Then, the measured data are analyzed by a state-of-the-art tool such as SAMMY [10]. This code combines multichannel multilevel R-matrix formalism

with corrections for experimental conditions to fit experimental data using generalized least squares fitting procedures.

Resolved resonances are described by the R-matrix collision theory, which is exact, and the resulting formalism is fairly transparent, though the expressions look rather formidable. In practical applications several approximations are widely used. The most precise is Reich-Moore , followed by the multi-level Breit-Wigner (MLBW) and the least precise single-level Breit-Wigner (SLBW). In ENDF/B-VII.0 library Reich-Moore is mostly used for actinides, MLBW is adopted for majority of other materials, while SLBW was essentially abandoned and its use is restricted to the unresolved resonance region.

R-matrix channels are characterized by the two particles with spin i and I, the orbital angular momentum l, the channel spin s (where $s = i \pm I$), and the total spin J (where $\mathbf{J} = \mathbf{s} + \mathbf{l}$) and parity π. Those channels having the same J and π (the only two quantum numbers that are conserved) are collected in the same spin group. Resonances (which appear generally as peaks in the cross sections) are assigned to particular spin groups depending on their individual characteristics; initial assignments may be changed as knowledge is gained during the evaluation process. The goal of the evaluation is to determine those values for the resonance energy (peak position), channel widths and spin for each of the resonances that provide the best fit to the measured data.

In general, partial cross sections can be obtained from a collision matrix U_{ab}, which connects entrance channels a with exit channels b. The formalism, applied to neutron reactions, implies $a = n$ and

$$\sigma_{nb} = \frac{\pi}{k^2}\, g_J \left|\delta_{nb} - U_{nb}\right|^2 , \tag{15}$$

where k is the neutron wave number and δ_{nb} is the Kronecker delta symbol. These partial cross sections must be summed over the appropriate entrance and exit channels to yield observable cross sections. The statistical factor g_J is the probability of getting the correct angular momentum J from the spins of collision partners, and π/k^2 relates probability and cross section.

In the Reich-Moore formalism as implemented in ENDF-6 the only reactions requiring explicit channel definitions are total, elastic scattering and fission; capture is obtained by subtraction (although it is possible to obtain it directly from the collision matrix elements). Neutron channels are labeled by quantum numbers, l, s, and J.

The channel spin s is the vector sum of the target spin I and the neutron spin $i = 1/2$), and takes on the range of values $|I - 1/2|$ to $I + 1/2$. The total angular momentum J is the vector sum of l and s, and runs from $|l - s|$ to $l + s$. The fission channels f1 and f2 do not correspond to individual two-body fission product breakup, but to Bohr-channels in deformation space, which is why two are adequate for describing many neutron-induced fission cross sections.

If one sums over all incident channels n and exit channels b, and invokes unitarity, the resulting total cross section can be expressed in terms of the diagonal matrix elements as

$$\sigma_{\rm tot}(E) = \frac{2\pi}{k^2} \sum_{lsJ} \sum_{l's'J'} g_J {\rm Re}\left[1 - U_{lsJ,l's'J'}\right] . \tag{16}$$

The elastic cross section is obtained by summing the incident neutron channels over all possible lsJ values and the exit neutron channels over those quantities $l's'J'$ that have the same ranges as lsJ. Conservation of total angular momentum requires that $J' = J$; ususally additional, simplifying conservation rules are imposed, namely $l' = l$ and $s' = s$. The six-fold summation then reduces to the familiar form

$$\sigma_{nn}(E) = \frac{2\pi}{k^2} \sum_{lsJ} g_J \left|1 - U_{lsJ,lsJ}\right|^2 . \tag{17}$$

The absorption (non-elastic) cross section is obtained by subtraction

$$\sigma_{\rm abs}(E) = \sigma_{\rm tot}(E) - \sigma_{nn}(E). \tag{18}$$

Fission is obtained from the collision matrix by summing Eq. (15) over all incident lsJ values and over the two exit fission channels, $b = f1$ and $b = f2$,

$$\sigma_f(E) = \frac{2\pi}{k^2} \sum_{lsJ} g_J \left(\left|U^{lsJ}_{nf1}\right|^2 + \left|U^{lsJ}_{nf2}\right|^2 \right) . \tag{19}$$

The level-matrix form of the collision matrix is given as

$$U^J_{nb} = e^{-i(\phi_n + \phi_b)} \left\{ 2 \left[(1 - {\rm K})^{-1} \right]_{nb} - \delta_{nb} \right\} , \tag{20}$$

where

$$(1 - {\rm K})_{nb} = \delta_{nb} - \frac{i}{2} \sum_r \frac{\Gamma_{nr}^{1/2} \Gamma_{br}^{1/2}}{E_r - E - i\,\Gamma_{\gamma r}/2} . \tag{21}$$

Here, ϕ_b is zero for fission, $\phi_n = \phi_l$, and the summation is over those resonances r which have partial widths in both of the channels n and b; E_r is the resonance energy; $\Gamma_{\gamma r}$ is the "eliminated" radiation width; Γ_{nr} and Γ_{br} are the partial widths for the r^{th} resonance in channels n and b.

The shift factor has been set equal to zero in the above equations ($E'_r \rightarrow E_r$); hence they are strictly correct only for s-wave resonances. Originally, the ENDF Reich-Moore format was used for low-energy resonances in fissile materials, which are s-waves. However, it is believed that the "no-shift" formulae can be safely applied to higher l-values also, since the difference in shape between a shifted resonance and one that is not shifted at the same energy has no practical significance.

One of the tasks of the evaluator is to assign the orbital momentum, l, for resonances where this has not been done experimentally. In the Atlas of Neutron Resonances this was done by the Bayesian approach that assigns these values probabilistically. The first investigators to apply Bayes' conditional probability for the determination of parities of ^{238}U resonances were Bollinger and Thomas [20]. Subsequently, Perkins and Gyullassy [21] and Oh *et al.* [11] extensively applied this procedure in the evaluation of resonance parameters.

For a resonance with a neutron width weighted by the spin statistical factor, $g_J\Gamma_n$, the probability that this resonance is p-wave is given according to Bayes' theorem of conditional probability by

$$P(p|g_J\Gamma_n) = \left(1 + \frac{P(g_J\Gamma_n|s)\,\langle D_1\rangle}{P(g_J\Gamma_n|p)\,\langle D_0\rangle}\right)^{-1}, \tag{22}$$

where $\langle D_1\rangle / \langle D_0\rangle$ are the level-spacing ratio, and $P(g_J\Gamma_n|s)$ is the probability that the neutron width is $g_J\Gamma_n$ if the resonance is s-wave and similarly for p-waves. The Bayesian equation can be solved by taking into account the Porter and Thomas distribution [22] and taking into account (2J+1) degeneration of nuclear levels.

Fig. 3 and 4 illustrates the Porter-Thomas analysis as applied to the s- and p-wave resonances of ^{133}Cs. From this procedure also the average level spacings and strength functions for the s- and p- waves are determined, see Eqs. (26, 27).

1.3 Unresolved Resonance Region

In the unresolved resonance region (URR), the situation is different than in the resolved resonance energy region. The experimental resolution is larger than the width of the resonances and individual resonance parameters can no more be extracted from cross section fitting. The formalism used for cross section treatment in URR is therefore based on average values of physical quantities obtained in the resolved resonance range. The values for statistical quantities are determined from the resolved energy region and used as starting values for the unresolved evaluation.

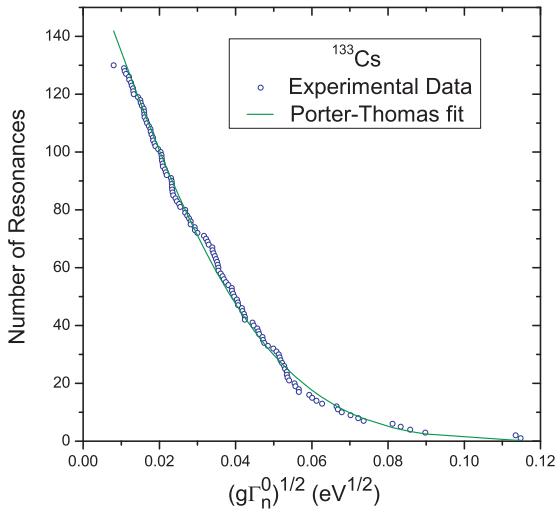

Fig. 3 Porter-Thomas distribution of reduced neutron widths, $g\Gamma_n^0$, for s-wave resonances of ^{133}Cs in the energy region below 3400 eV.

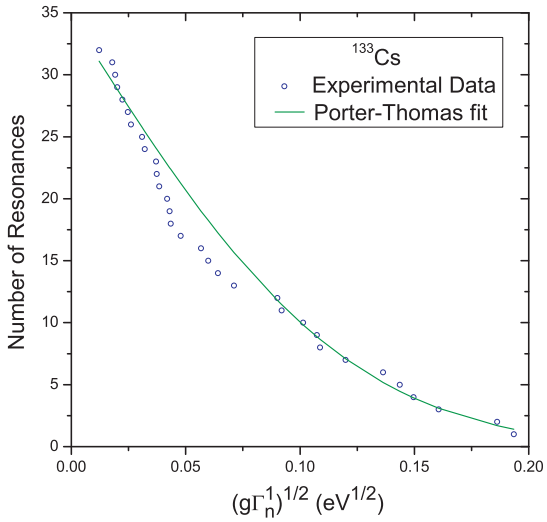

Fig. 4 Porter-Thomas distribution of reduced neutron widths, $g\Gamma_n^1$ for p-wave resonances of ^{133}Cs in the energy region below 387 eV where the p-wave resonances are detected.

The theoretical basis for URR description is the Lane-Lynn approach [23], which for capture gives

$$\langle \sigma_\gamma \rangle = \sum_{Jl} \langle \sigma_\gamma \rangle_{Jl} = \frac{2\pi^2}{k^2} \sum_{Jl} \langle \Gamma_\gamma \rangle_l S_l V_l E_n^{1/2} g_J \frac{F(\alpha_{Jl})}{\langle \Gamma_J \rangle}, \tag{23}$$

where the averaged quantities are given in brackets $\langle\ \rangle$, V_l is the penetrability factor divided by kR; $F(\alpha_{Jl})$ is the fluctuation factor, α_{Jl} being the ratio of mean radiative and neutron widths; summation is carried over partial waves l and spins J.

The unresolved resonance region is treated within the single-level Breit-Wigner formalism, which requires the following parameters: the average level spacing, D_l, the strength functions, S_l, the average radiative widths, $\Gamma_{\gamma l}$, and R'. After determination of l values for all resonances, the reduced neutron widths are analyzed in terms of Porter-Thomas distribution [22] if the number of measured resonances is large enough for a statistical sample.

Instead of working with the Porter-Thomas distribution, it is often much simpler to analyze the resonance parameter data with the cumulative Porter-Thomas distribution. Since resonances with small neutron widths are usually missed in measurements, it is necessary to exclude resonances whose reduced widths are smaller than a certain magnitude. By setting a cutoff value, *i.e.* a minimum magnitude of reduced neutron width, the effect of missed small resonances on the resulting average parameters is reduced significantly. The result is

$$N(y) = N_r(1 - \mathrm{erf}(y)), \tag{24}$$

where erf is the error function, N_r is the corrected total number of resonances, and $N(y)$ is the total number of resonances with reduced neutron width larger than a specified value y,

$$y = (\Gamma_n^l/2 < \Gamma_n^l >)^{1/2}, \tag{25}$$

where Γ_n^l is the reduced neutron width for orbital angular momentum l and $< \Gamma_n^l >$ is its average value. The two parameters N_r and $\langle g\Gamma_n^l \rangle$ are determined through the fitting procedure.

The resulting average level spacing D_l and neutron strength function S_l in a determined energy interval ΔE are then calculated by

$$D_l = \frac{\Delta E}{N_r - 1}, \tag{26}$$

$$S_l = \frac{\langle g\Gamma_n^l \rangle}{(2l+1)D_l}. \tag{27}$$

The average radiative widths of neutron resonances are determined from measurements in the resolved energy region by calculating the weighted as well as unweighted values. For nuclei with unmeasured radiative widths, the systematics of s-, p- and d-wave radiative widths as a function of atomic mass number are used [12].

Fig. 5 shows the evaluated capture cross sections in the unresolved energy resonance region, compared with the available experimental data for ^{133}Cs. The unresolved resonance region is extended up to the first excited level, which is 90 keV for ^{133}Cs. At higher energies (fast neutrons), the evaluations was done by the code EMPIRE. We note an excellent match of cross sections in the boundary of the two energy regions.

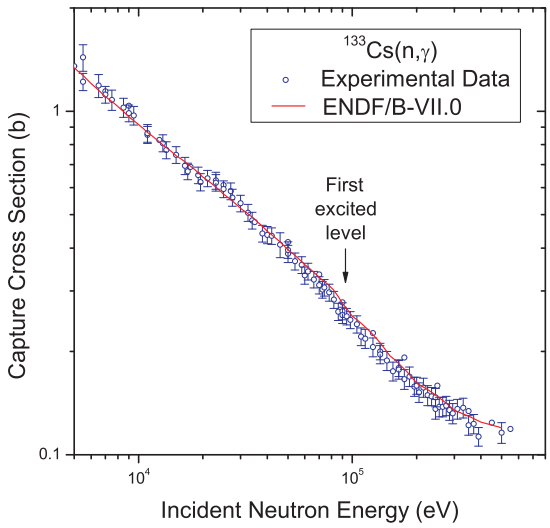

Fig. 5 Neutron capture cross section for ^{133}Cs in the unresolved resonance energy region extended up to the first excited level. The evaluation at higher energies was performed by EMPIRE. Evaluation adopted by ENDF/B-VII.0 is compared with experimental data.

We note that in the code SAMMY the unresolved resonance formalism is based on the methodology adopted by the statistical model code FITACS developed by F. Fröhner [24]. Values of the average parameters are found from fitting the calculated cross sections to experimental cross sections. The set of parameters that best reproduces the data cannot be reported directly to ENDF/B because the ENDF-6 format uses a less rigorous single-level Breit-Wigner representation. SAMMY/FITACS parameters must therefore be converted into average widths before insertion into ENDF/B library.

1.4 Fast Neutron Region

Fast neutron region is defined as incident energies above the unresolved resonance region (materials with $Z > 42$) or above resolved resonances that vary between hundreds keV - MeV for light nuclei and eV - keV for actinides. The upper end of the fast neutron region is in general 20 MeV, though in about 10% cases in ENDF/B-VII.0 this has been extended to 150-200 MeV. In this energy range several distinct nuclear reaction models are used to describe interaction of fast neutrons with atomic nuclei.

1.4.1 Optical Model and Direct Reactions

Spherical optical model is usually used to calculate transmission coefficients for all ejectiles involved in a reaction. In the case of spherical nuclei, the same calculations also determined reaction (absorption) cross sections. For deformed nuclei, the incident channel is treated in terms of coupled-channels rather than the spherical optical model. In the latter case, proper coupling also provided cross sections for inelastic scattering to collective levels and related angular distributions of scattered neutrons. In certain cases we also included direct scattering to the collective levels embedded in the continuum. Generally, we chose optical model potentials from a vast selection available in the RIPL library [15], but in the course of ENDF/B-VII.0 development the original RIPL potentials were often adjusted to improve agreement with recent experimental data or to match cross section obtained in the unresolved resonance evaluation, and in some cases totally new potentials were constructed.

1.4.2 Compound Nucleus Decay

The statistical model provides the basic underpinning for the whole evaluation procedure. The decay of the compound nucleus (CN) is modeled by the Hauser-Feshbach equations, using transmission coefficients and level densities to represent the relative probabilities of decay in the various open channels.

Schematically, the cross section for a reaction (a,b) that proceeds through the compound nucleus mechanism can be written as

$$\sigma_{a,b} = \sigma_a \frac{\Gamma_b}{\sum_c \Gamma_c}. \tag{28}$$

The summation over compound nucleus spin J and parity π, and integration over excitation energy E is implicit in Eq.(28). The decay width Γ_c is given by

$$\Gamma_c = \frac{1}{2\pi\rho_{CN}(E)} \sum_{c'} \int_0^{E-B_c} \rho_c(E') T_c(E - B_c - E') dE', \tag{29}$$

where B_c is the binding energy of particle c in the compound nucleus, ρ is the level density, and $T_c(\varepsilon)$ stands for the transmission coefficient for particle c having channel energy $\varepsilon = E - B_c - E'$. Again, for simplicity, we drop explicit reference to the spin and parity in Eq.(29) and the summation extends over all open channels c'. For low incident energies, Eq.(28) needs to be corrected for width fluctuation corrections. Since the evaluations extend at least up to 20 MeV, sequential multi-particle particle emission had to be included in the Hauser-Feshbach calculations, which in practice implies an energy convolution of multiple integrals of the type of Eq.(29).

In order to account for the competition between γ-emission and emission of particles along the deexcitation chain, our calculations always involve a full modeling of the γ-cascade that conserves angular momentum. The formalism for γ-rays transitions is based on the Giant Dipole Resonance (GDR) model known as the Brink-Axel hypothesis [25, 26]. GDR parameters are taken from the experimental compilation and/or systematics contained in the RIPL library. We note, that our calculations account for GDR splitting due to nuclear deformation. In GNASH, the γ-ray transmission coefficients are obtained from the γ-ray strength function formalism of Kopecky and Uhl [27]. EMPIRE allows for a suite of γ-ray strength functions. Typically, we used Mughabghab and Dunford's prescription known as GFL [28] or Plujko's modified Lorentzian referred as MLO1 [29]. In both codes the γ-ray strength functions can be, and often are, normalized to experimental information on $2\pi\Gamma_\gamma/D_0$ or adjusted to reproduce capture cross sections.

Nuclear level densities along with optical model transmission coefficients are the two most important ingredients of the statistical model. In GNASH , the description of the level densities in the continuum follows the Ignatyuk form of the Gilbert-Cameron formalism, including a washing-out of shell effects with increasing excitation energy. Most of the evaluations performed with EMPIRE employed level densities that are specific to the EMPIRE code. The formalism uses the super-fluid model below a critical excitation energy and the Fermi gas model at energies above it. Collective enhancements due to nuclear vibration and rotation are taken into account in the nonadiabatic approximation, *i.e.*, they are washed out when excitation energy increases. Differently from other formulations, EMPIRE-specific level densities explicitly account for the rotation-induced deformation of the nucleus and de-

termine spin distributions by subtracting rotational energy from the energy available for intrinsic excitations.

1.4.3 Width Fluctuation Correction

At low incident energies, the statistical approximation that entrance and exit channels are independent (Bohr independence hypothesis) is not valid anymore due to correlations between entrance and exit channels. The Hauser-Feshbach equations have to be modified in order to include the so-called width fluctuation correction factors accounting for the coupling between the incident and outgoing waves in the elastic channel.

The GNASH code does not calculate these correction factors but rather imports them as the result from an auxiliary code (usually COMNUC [30], which uses the Moldauer model). EMPIRE, by default, uses internal implementation of the HRTW approach [31] that can be summarized with the following equation

$$\sigma_{ab}^{HRTW} = V_a V_b \left(\sum_c V_c \right)^{-1} \left[1 + \delta_{ab} \left(W_a - 1 \right) \right]. \tag{30}$$

This formula is, essentially, equivalent to the Hauser-Feshbach expression (28) but the elastic channel is enhanced by the factor W_a. In Eq. (30) the quantities V_c replace optical model transmission coefficients that appear in the original Hauser-Feshbach formula.

1.4.4 Preequilibrium Models

The probability that a system composed of an incident neutron and a target nucleus decays before thermal equilibrium is attained becomes significant at incident energies above 10 MeV. In any preequilibrium model, the excited nuclear system (composite nucleus) follows a series of ever more complicated configurations, where more and more particle-hole (p-h) states are excited. In each stage, a possible emission of a particle competes with the creation of an intrinsic particle-hole pair that brings the system towards the equilibrium stage. Particle emission from the early stages is characterized by a harder spectrum and forward peaked angular distributions.

The exciton model is a semi-classical formulation of the preequilibrium emission that is used in GNASH and EMPIRE. The core of the model is the so called master-equation that governs time dependence of occupation probabilities, P_n, for various p-h stages

$$\hbar \frac{dP_n}{dt} = \sum_m \Lambda_{n,m} P_m - \Gamma_n P_n, \tag{31}$$

where the total decay width of the stage n is given in terms of the partial transition widths $\Lambda_{l,n}$ and partial width $\Gamma_{e,n}$ for the emission of particle e by

$$\Gamma_n = \sum_l \Lambda_{l,n} + \sum_e \Gamma_{e,n}. \tag{32}$$

Due to the two-body nature of the nuclear force, intrinsic transitions occur only between neighboring stages, and the transition matrix Λ is tri-diagonal; the off-diagonal terms accounting for backward and forward transitions.

In GNASH, the preequilibrium phase is addressed through the semiclassical exciton model in combination with the Kalbach angular-distribution systematics [32]. These systematics provide a reasonably reliable representation of the experimental database.

EMPIRE implements a suite of preequilibrium codes including two versions of the exciton model (PCROSS and DEGAS [33]), and the Monte-Carlo approach DDHMS [34, 35, 36] in addition to the quantum-mechanical Multistep Direct and Multistep Compound models.

A new Monte Carlo preequilibrium model allows unlimited emission of preequilibrium neutrons and protons, and is therefore well suited for the study of high-energy reactions up to a few hundreds of MeV. The model of choice in EMPIRE is the statistical Multi-step Direct (MSD) theory of preequilibrium scattering to the continuum originally proposed by Tamura, Udagawa and Lenske (TUL) [37]. The evolution of the projectile-target system from small to large energy losses in the open channel space is described in the MSD theory with a combination of direct reaction (DR), microscopic nuclear structure and statistical methods.

The modeling of Multi-step Compound (MSC) processes in EMPIRE follows the approach of Nishioka *et al.* (NVWY) [38]. The formal structure of the NVWY formula resembles the matrix representation of the master-equation typical for classical preequilibrium models. However, the NVWY formalism is strictly derived from basic principles. Microscopic quantities that constitute ingredients of the NVWY formula were linked to the macroscopic, experimentally known, quantities in Ref. [39] which was an essential step allowing for practical application of the theory.

1.4.5 Light Nuclei

In the case of light nuclei (from hydrogen to oxygen, A = 1 - 18, which mostly serve as coolants and moderators), the statistical approach cannot be applied and the above methodology should be replaced by the R-matrix approach. In the United States this approach is pursued by Los Alamos and virtually all light nuclei evaluations in ENDF/B-VII.0 were performed by the Energy Dependent Analysis (EDA) code developed over years by G. Hale [9, 40], which is based on R-matrix formalism in its most general form.

R-matrix theory is a general framework for describing nuclear reactions that is particularly well-suited for including resonances. It is mathematically rigorous phenomenological description of what is actually seen in an experiment. This is not a

model of neutron-nucleus interaction, rather it parametrizes measurements in terms of observable quantities. This theory properly describes multichannel nuclear reactions and builds in all the fundamental conservation laws, symmetries and analytic properties of nuclear interactions. The experimental cross section data from all relevant reactions, including neutron and charged particles, are taken into account and fitted simultaneously. This allows obtaining a single set of multichannel, multilevel R-matrix parameters that describe all the desired neutron-induced cross sections for light nucleus under consideration.

1.5 Fission

Nuclear fission remains the most complex topic in applied nuclear physics. Since its discovery, it has remained an active field of research, and from the evaluation point of view it poses one of the most difficult problems.

1.5.1 Fission Modeling

The status of fission modeling and related parametrization relevant to evaluation is summarized in the extensive paper dedicated to the Reference Input Parameter Library by Capote *et al.* [15]. The main concepts of nuclear fission theory are based essentially on the liquid-drop model [41, 42]. According to this model, when a nucleus is being deformed, the competition between the surface tension of a nuclear liquid drop and the Coulomb repulsion related to the nuclear charge leads to the formation of an energy barrier which prevents spontaneous decay of the nucleus by fission. The penetrability of this barrier depends on its hight and width and is a dominant factor in determining fission cross section. Decrease in height and/or width results in an exponential increase in barrier penetrability, which leads to the increased fission.

For most of the practical calculations one-dimensional fission barrier is considered. The present knowledge indicates that the pre-actinides have single-hump barriers, while the actinides have double- or triple-humped barriers. Usually, the barriers are parametrized as function of the deformation (β) by inverted parabolas,

$$B_i(\beta) = B_{fi} - \frac{1}{2}\mu\hbar^2\omega_i^2(\beta - \beta_i)^2, \quad i = 1, N \tag{33}$$

where N is the number of humps, the energies B_{fi} represent maxima of the deformation potential, β_i are the deformations corresponding to these maxima (saddle points), the harmonic oscillator frequencies ω_i define the curvature of the parabolas and μ is the inertial mass parameter approximated usually by a semi-empirical expression. Fig. 6 illustrates the relationship among the above mentioned quantities in a typical case of a double-humped fission barrier (N=2). The quasi-stationary states in the second well (the class II states) are also depicted in the plot.

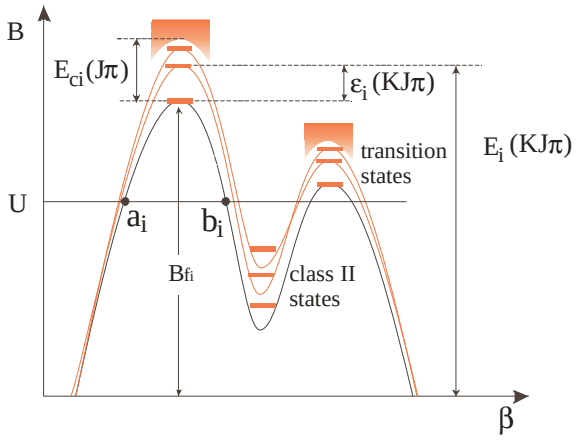

Fig. 6 Energy of a double-humped fission barrier in function of the deformation β along with associated barrier parameters: B_{fi} is the height of the fundamental fission barrier i; $\varepsilon_i(KJ\pi)$ is the energy of the transition state i; $E_{ci}(J\pi)$ is the cutoff energy, above which the continuum starts for a barrier i. Fission barriers associated with each discrete transition state are shown.

Above each barrier hump there is a spectrum of excited levels commonly referred to as transition states. Close to the top of the hump these levels are well separated and can be treated individually while at higher excitation energies (above E_{ci}) the concept of level densities must be invoked, as indicated in Fig. 6 with the shaded regions. The discrete transition states for all barriers i ($i = 1,2$ for a double-hump barrier) are obtained by building rotational levels on top of vibrational or non-collective levels that serve as a base (bandheads). They are characterized by a set of quantum numbers (angular momentum J, parity π and angular momentum projection on the nuclear symmetry axis K) with the excitation energies

$$E_i(KJ\pi) = B_{fi} + \varepsilon_i(KJ\pi) = B_{fi} + \varepsilon_i(K\pi) + \frac{\hbar^2}{2\Im_i}[J(J+1) - K(K+1)], \qquad (34)$$

where $\varepsilon_i(K\pi)$ are the bandhead energies and $\hbar^2/2\Im_i$ are the inertial parameters. A parabolic barrier with height $E_i(KJ\pi)$ and curvature $\hbar\omega_i$ is associated with each transition state.

The transmission coefficients through each hump are expressed in first-order approximation in terms of the momentum integrals for the humps

$$K_i(U) = \pm \left| \int_{a_i}^{b_i} \sqrt{2\mu[U - B_{fi}(\beta)]/\hbar^2}\, d\beta \right|, \quad i = 1,2, \qquad (35)$$

where a_i and b_i are the points indicated in Fig. 6 and U is the excitation energy in the fissioning nucleus. The $+$ sign is taken when the excitation energy U is lower than the hump under consideration and the $-$ sign when it is higher. In the case of a single parabolic barrier, Eq. (35) yields the well-known Hill-Wheeler transmission coefficient [43]

$$T_i^{HW}(U) = \frac{1}{1 + \exp\left[-(2\pi/\hbar\omega_i)(U - B_{fi})\right]}. \qquad (36)$$

The total fission transmission coefficient for a given excitation energy U, spin J and parity π is determined by summing the penetrabilities through barriers associated with all allowed transition levels, *i.e.*,

$$T_i(UJ\pi) = \sum_{K\leq J} T_i(UK\pi) + \int_{E_{ci}}^{\infty} \frac{\rho_i(\varepsilon J\pi)d\varepsilon}{1+\exp\left[-\frac{2\pi}{\hbar}\omega_i(U-B_{fi}-\varepsilon)\right]}. \quad (37)$$

The sum runs over all the discrete transition levels having the same spin J and parity π as those of the decaying compound nucleus, and the integration runs over the continuum of the transition levels described by the level densities $\rho_i(\varepsilon J\pi)$. Usually the wells are considered deep enough so that the transmission coefficient can be averaged over the intermediate structures. For a double-humped barrier the fission coefficient becomes

$$T_f(UJ\pi) = \frac{T_1(UJ\pi)T_2(UJ\pi)}{T_1(UJ\pi)+T_2(UJ\pi)+T_{\gamma_{II}}(UJ\pi)}, \quad (38)$$

where T_1 and T_2 are the penetrabilities of the inner and the outer humps, respectively, calculated according to Eq. (37), and $T_{\gamma_{II}}$ is the probability for gamma decay in the second well.

Finally, the relation used in the statistical model for the fission cross section is

$$\sigma_{a,f}(E) = \sum_{J\pi} \sigma_a(EJ\pi)P_f(EJ\pi), \quad (39)$$

where $\sigma_a(EJ\pi)$ is the population of the fissioning nucleus in the state $EJ\pi$ and $P_f(EJ\pi)$ represents the fission probability computed for a specific representation of fission barrier. The fission probability is usually defined as the ratio of the fission coefficient T_f to the sum of all the transmission coefficients including the competing channels $\sum_d T_d$,

$$P_f(EJ\pi) = \frac{T_f(EJ\pi)}{T_f(EJ\pi)+\sum_d T_d(EJ\pi)}. \quad (40)$$

Similar definitions apply for other decay probabilities.

In GNASH fission probabilities are calculated from the quantum-mechanical transmission coefficient through a simple double-humped fission barrier, using uncoupled oscillators for the representation of the barriers. The barrier penetrabilities are computed using the Hill-Wheeler formula for inverted parabolas. An additional parameter is used to account for level density enhancement due to asymmetry at saddle points [5].

Version 2.19 (Lodi) of the EMPIRE code introduced an advanced fission formalism that is applicable to multi-chance fission induced by light particles and photons. It uses an optical model for fission, *i.e.*, allows for an absorption through the imaginary potential in the second well, to calculate transmission through coupled single-, double- and triple-humped fission barriers. Such calculations can start from subbarrier excitation energies. In the case of a double-humped barrier, the expression is generalized to account for multi-modal fission. For light actinides, a triple-humped

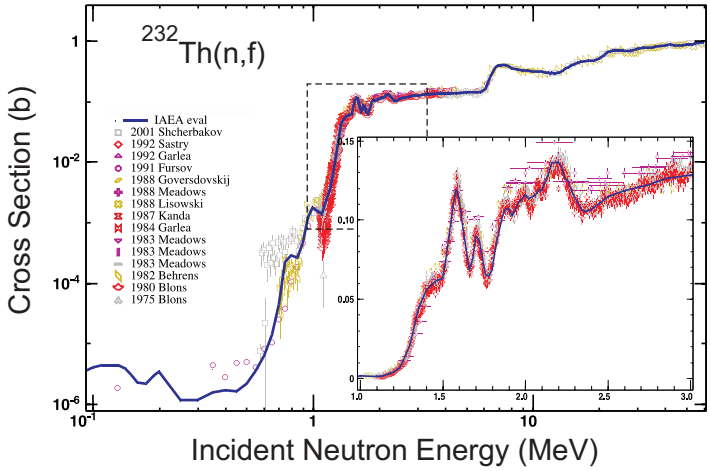

Fig. 7 Neutron-induced fission cross section on ^{232}Th compared with experimental data from EXFOR. Insert shows fine details of the resonance-like structure of these fission cross sections.

fission barrier with a shallow tertiary well, which accommodates undamped vibrational states, is employed. This fission model can provide good description of experimental data, including gross vibrational resonant structure at sub-barrier energies.

As an example of the complexity of the fission channel modeling in EMPIRE we show ^{232}Th fission cross sections in Fig. 7. Fine details can be seen in the insert, revealing complex resonance-like structure of fission in the threshold energy region. These fine details are fully described by the model, with the caviat that the fission model parametrization was obtained from careful fits to data.

1.5.2 Prompt Fission Neutron Spectra

One of the most intriguing aspects of evaluation of actinides are prompt neutron fission spectra. The Los Alamos (Madland-Nix) model of the prompt fission neutron spectrum and average prompt neutron multiplicity is based upon classical nuclear evaporation theory and utilizes an isospin-dependent optical potential for the inverse process of compound nucleus formation in neutron-rich fission fragments [44]. This model, in its exact energy-dependent formulation, has been used to calculate the prompt fission neutron spectrum matrix for the n + ^{235}U, n + ^{238}U, and n + ^{239}Pu systems, and these appear in ENDF/B-VII.0 with the tabulated distribution (LF=1) law.

Fig. 8 shows the average prompt fission neutron emission energy as a function of incident energy for ^{235,238}U and ^{239}Pu, for both the new ENDF/B-VII.0 evaluations and the old ENDF/B-VI evaluations.

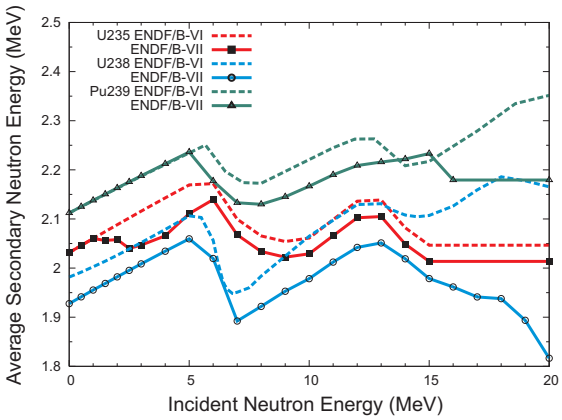

Fig. 8 First moments (average energies) of ^{235,238}U and ^{239}Pu prompt fission neutron spectra from ENDF/B-VII.0 calculated with the Los Alamos model [44] in comparison with those of ENDF/B-VI.

1.5.3 Pecularities of Fission Cross Section Evaluation

It is notoriously difficult to describe and parametrize the fission process. In particular, fission is extremely sensitive to fission barriers that are very difficult to predict and their actual values depend on other parameters such as nuclear level densities.

In view of this, in most cases fission cross sections are directly adopted from experiments. Then, the modeling is performed and used to evaluate all other reaction channels. This is the approach applied for years by Los Alamos, using the code GNASH. Most recently it has been used in the unprecedented evaluation of a complete set of ten uranium isotopes $^{232-241}$U as well as ^{239}Pu by Phil Young *et al.* [45], from keV energies to 30 MeV. These evaluations can be seen as the core of the ENDF/B-VII.0 library, with more details provided in the subsequent part of the present Chapter.

Recent advances in fission modeling, gradually implemented into the codes such as EMPIRE, allow cautious bypassing traditional mantra of using purely experimental data for fission cross section evaluations. An example would be ^{232}Th evaluation adopted by ENDF/B-VII.0. In that evaluation the fission channel was based on modeling with parametrization derived from fits to data, see Fig. 7.

2 Neutron Data for Actinides

In general, actinides are the most important materials (isotopes) in most of the nuclear technology applications. The 'big three' actinides, ^{235}U, ^{238}U and ^{239}Pu, usually play the dominant role. These three plus ^{232}Th constitute major actinides, the remaining about 15 actinides including other isotopes of U and Pu as well as Np, Am and Cm fall into the category of minor actinides.

It should be emphasized that major actinides are evaluated extremely carefully and attention paid to details is exceptionally high. The nuclear data community spent

considerable amount of time on these evaluations [45]. What is shown below is a glimpse on progress made between 2001 release of the US library ENDF/B-VII.8 and 2006 release of the ENDF/B-VII.0 library [1].

2.1 ^{235}U Evaluation

The ENDF/B-VII.0 evaluation in the unresolved resonance region was performed by ORNL. This was complemented with the evaluation in the fast neutron region performed by LANL. The remaining data were taken over from ENDF/B-VI.8.

^{235}U, Unresolved Resonance Region:

The SAMMY code has been used to perform the unresolved resonance evaluation of the ^{235}U cross sections from 2.25 keV up to 25 keV [46]. SAMMY generates average resonance parameters based on a statistical model analysis of the experimental average cross sections. The primary use of the average resonance parameters is to reproduce the fluctuations in the cross sections for the purposes of energy self-shielding calculations.

A good representation of the average cross section was achieved with the new evaluation as shown for the ^{235}U radiative capture in Fig. 9.

The thermal $\bar{\nu}$ value for ^{235}U , which was taken over from ENDF/B-VI.8, is $\bar{\nu}$ = 2.4367. This value is slightly higher than that from the neutron standards, 2.4355, but within experimental uncertainties in order to optimize agreement with the critical assembly benchmarks.

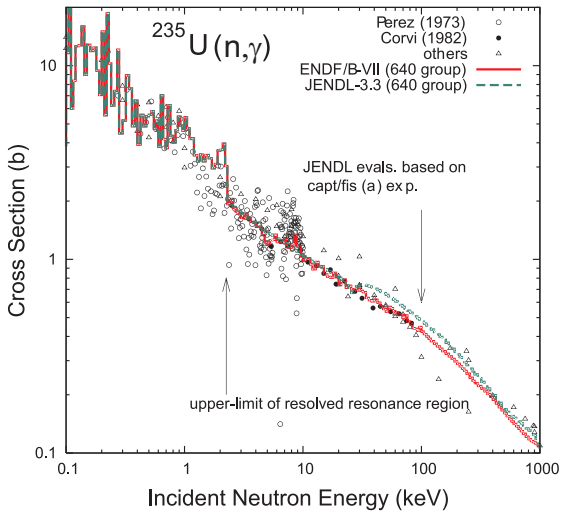

Fig. 9 Evaluated ^{235}U(n,γ) capture cross section compared with data and with the JENDL-3.3 evaluation.

^{235}U, Fast Neutron Region :

The new ^{235}U evaluation builds upon the previous ENDF/B-VI.8 file, with a number of improvements from Los Alamos. They include improved fission cross sections from the new standards, prompt $\bar{\nu}$ based on a covariance analysis of experimental data, (n,2n), (n,3n) cross sections based on new data, new prompt fission spectra taken from Madland, new delayed neutron time-dependent data, and improved inelastic scattering at 14 MeV and below.

The previous ^{235}U ENDF/B-VI.8 evaluation has performed reasonably well in integral validation tests based on simulations of critical assemblies. The principle deficiency the ENDF/B-VII.0 developers wanted to remove was an underprediction of reactivity. For instance, the calculated $k_{\rm eff}$ for Godiva, a fast critical assembly based upon highly enriched uranium (HEU) in a spherical configuration, was 0.9966, compared to experiment of 1.0000.

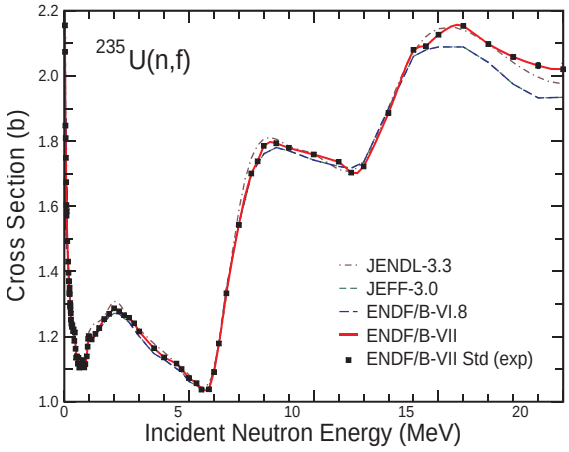

Fig. 10 Evaluated fission cross section compared with measured data, as represented by a covariance analysis of experimental data (referred to as ENDF/B-VII.0 Standard). Our new evaluation follows the Standard evaluation of the experimental data. Other evaluations from JEFF and JENDL are also shown.

The ^{235}U fission cross section is shown in Fig. 10, with comparison to the previous ENDF/B-VI.8 evaluation, and to the latest JEFF and JENDL evaluations. This new result comes from the recent international standards project, and the evaluation follows the statistical analysis of the measured data. This evaluation is 0.5-1.5% higher than the previous ENDF/B-VI Standard in the 1-5 MeV region, and significantly higher above 15 MeV. The impact of the higher fission cross section in the fast region (few MeV) is particularly important, having the effect of increasing the criticality of fast systems.

The Nuclear Energy Agency (NEA Paris) project studied the fission prompt neutron spectrum for ^{235}U. The final report [47] noted that significant uncertainties still exist in the prompt spectrum at thermal energies. Because of this uncertainty, adopted were Madland's new data for all energies except thermal, where the previous ENDF/B-VI evaluation was preserved.

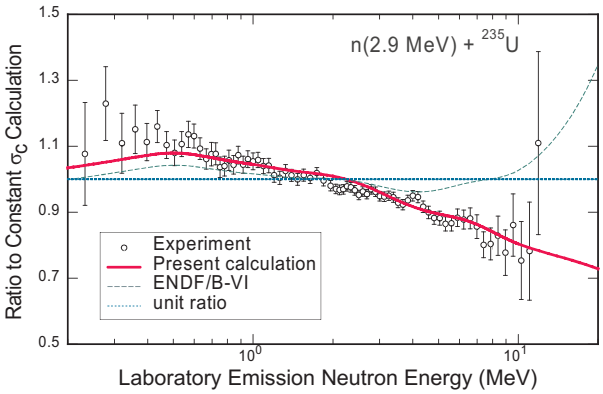

Fig. 11 Prompt fission spectrum for 2.9 MeV neutrons incident on ^{235}U shown as a ratio to the σ_c = constant approximation to the Los Alamos model. The data are from Boykov *et al.* [48].

In Fig. 11 we show the prompt fission neutron emission spectrum, compared with measurements by Boykov *et al.* [48] for 2.9 MeV neutrons on ^{235}U and plotted as a ratio to the σ_c = constant approximation to the Los Alamos model [44]. It is evident that the present ENDF/B-VII.0 agrees better with the Boykov *et al.* data.

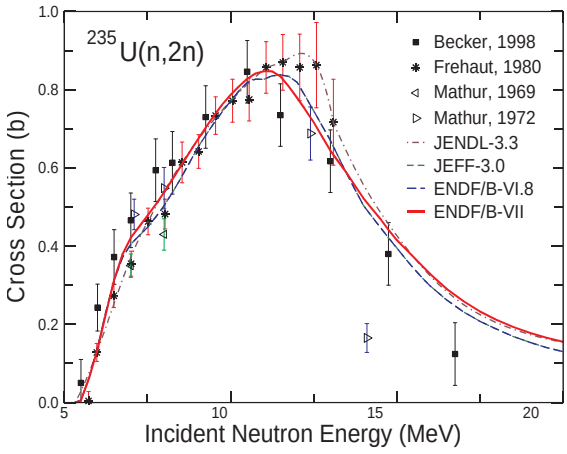

Fig. 12 Evaluated $^{235}\mathrm{U}(n,2n)$ cross section compared with data and with previous evaluations.

The new $^{235}\mathrm{U}(n,2n)$ cross section comes from a GNASH code theory prediction, baselined against the measured data. A comparison with experimental data, and with ENDF/B-VI.8, JEFF-3.0 and JENDL-3.3 is given in Fig. 12.

The previous ^{235}U evaluation was known to poorly model Livermore pulsed sphere data that measure the downscattering of 14 MeV neutrons, in the region cor-

responding to inelastic scattering (the 2-4 MeV excitation energy region in ^{235}U). The angle-integrated spectrum for 14 MeV is shown in Fig. 13, and the oscillatory structure between 9 and 13 MeV emission energy is due to the new inelastic scattering to collective states. This is the first time that preequilibrium and DWBA mechanisms for inelastic scattering have been included high into the continuum for evaluated actinide databases. In ENDF/B-VII.0 this approach was followed for ^{233,235,236,238}U, ^{239}Pu, ^{232}Th, and ^{231,233}Pa.

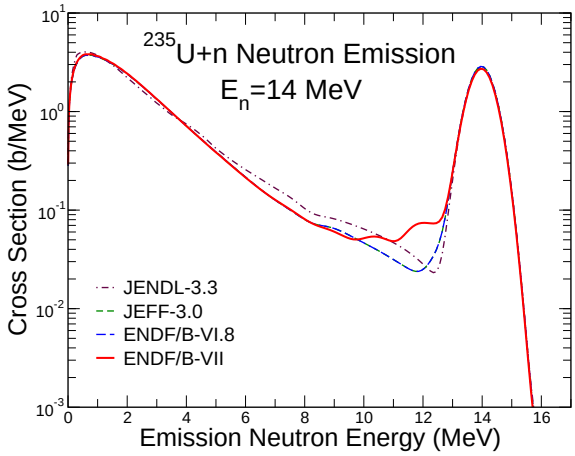

Fig. 13 Evaluated ^{235}U(n,xn) neutron production energy-spectrum compared with previous evaluations. No measured data exist, though our calculations were guided by measured data for ^{238}U.

2.2 ^{238}U Evaluation

In natural uranium ^{238}U is the dominant isotope, with 99.27% abundance and half-live of 4.468x10^{7} years. Although it is fast fissioner, not suitable for thermal systems, its high abundance stipulates that it must be evaluated very carefully.

^{238}U, Resolved and Unresolved Resonance Region:

Numerous criticality studies, involving low-enriched thermal benchmarks demonstrated a systematic $k_{\rm eff}$ under-prediction of about -0.5% (-500 pcm) or more with ENDF/B-VI.8. International activity was formed to solve this problem. First, the ^{238}U capture cross sections were investigated using specific integral experiments sensitive to the capture resonance integrals:

- Correlation between $k_{\rm eff}$ and ^{238}U capture fraction,
- Measurements of ^{238}U spectral indices and effective capture resonance integral,

- Post-irradiation experiments which measure the ^{239}Pu isotopic ratio as a function of burn-up.

These tests [49] supported a slight reduction of the effective resonance integral between 0.5% and 1%. A new analysis of the ^{238}U cross section in the resolved-resonance range was performed at ORNL in collaboration with the CEA [50]. The SAMMY [10] analysis of the lowest s-wave resonances below 102 eV led to resonance parameters slightly different from those of ENDF/B-VI.8 as shown in Table 1.

The ^{238}U(n,γ) thermal cross section, recently recommended by A. Trkov *et al.* [51], $\sigma_0 = 2.683 \pm 0.012$ *b*, was adopted. The scattering cross-section at thermal energy was also revisited and the effective scattering radius R_{eff} as well as the parameters of the external levels have been carefully assessed.

Table 1 Resonance parameters of the ^{238}U s-wave resonances in ENDF/B-VII.0 and ENDF/B-VI.8. Although the differences look small, they have positive impact on performance.

	ENDF/B-VII.0 R' = 9.48 fm		ENDF/B-VI.8 R' = 9.42 fm	
Energy eV	Γ_γ meV	Γ_n meV	Γ_γ meV	Γ_n meV
6.673	23.00	1.476	23.00	1.493
20.87	22.86	10.09	22.91	10.26
36.68	23.00	33.55	22.89	34.13
66.03	23.31	24.18	23.36	24.60
80.75	23.39	1.874	23.00	1.865
102.56	24.08	70.77	23.40	71.70

Fig. 14 shows an example of the SAMMY fit of capture measurements in the keV energy range. As suggested by integral experiments, this new evaluation proposes a slight decrease of the effective capture resonance integral by about 0.6%, compared to ENDF/B-VI.8. One expected consequence of this new evaluation is an increase of the calculated multiplication factor for low-enriched lattices from about 0.1 to 0.15% (100 to 150 pcm), depending on the moderation ratio. The combination of the new LANL ^{238}U inelastic data in the fast neutron region with the ORNL resonance parameter set gave a satisfactory correction of the reactivity under-prediction.

^{238}U, Fast Neutron Region :

The new ENDF/B-VII.0 evaluation is based upon evaluations of experimental data and use of GNASH and ECIS nuclear model calculations to predict cross sections and spectra. Prior to the present work, there were some longstanding deficiencies, as evident in critical assembly integral data testing. First, there was the reflector bias - the phenomenon whereby fast critical assemblies showed a reactivity swing in the calculated k_{eff} in going from a bare critical assembly (*e.g.*, Godiva (HEU) or

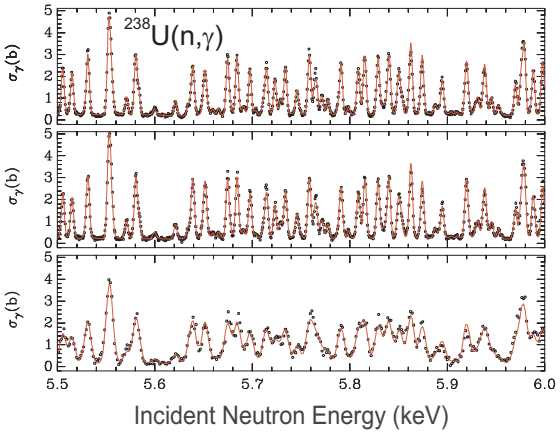

Fig. 14 Experimental capture data on ^{238}U (one sample measured by De Saussure and two samples by Macklin) compared to the results of the SAMMY fit in the range 5.5 - 6.0 keV.

Jezebel (^{239}Pu)) to ^{238}U-reflected critical assembly (*e.g.*, Flattop-25, or Flattop-Pu), whereas measurements showed $k_{\text{eff}} = 1$ for both assemblies.

Secondly, thermal critical assemblies involving ^{238}U have showed a calculated underreactivity for ENDF/B-VI.8. Thirdly, some intermediate energy critical assemblies involving large quantities of ^{238}U, such as Big-10, were modeled very poorly using ENDF/B-VI.8 data. The nuclear data improvements made for ENDF/B-VII.0 largely removed these deficiencies. Similar methods in the fast neutron region applied at the CEA/Bruyères-le-Châtel lead to similar improvements in the JEFF-3.1 library [52].

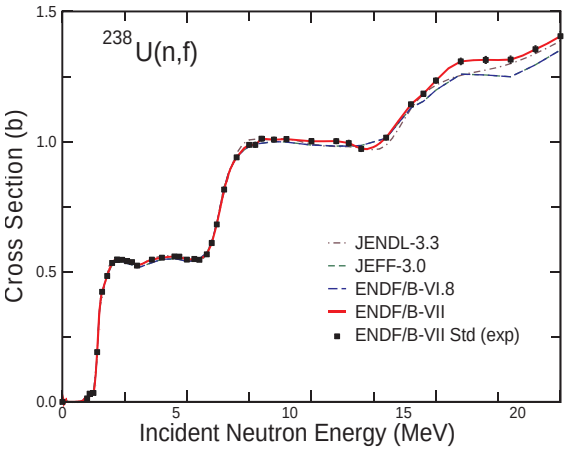

Fig. 15 Evaluated ^{238}U fission cross section, based on a covariance analysis of the experimental data from the Standards project (labeled Std).

The fission cross section was taken from the new recommendations of the IAEA Standards group, based on a Bayesian analysis of measured data. As can be seen in Fig. 15 the fission cross section differs from the previous ENDF/B-VI.8 cross

section in some important ways, being ≈1.5% larger in the 2-4 MeV region, and 1-5% larger in the 14-20 MeV region. Above 14 MeV the principle reason for the change is newer and more precise measurements from various laboratories, which were not available for ENDF/B-VI.

The prompt fission spectrum in ENDF/B-VII.0 for ^{238}U came from a new analysis by Madland using the Los Alamos model. The average energies are compared with Los Alamos model predictions in Fig. 16, and the agreement with experimental data is seen to be good.

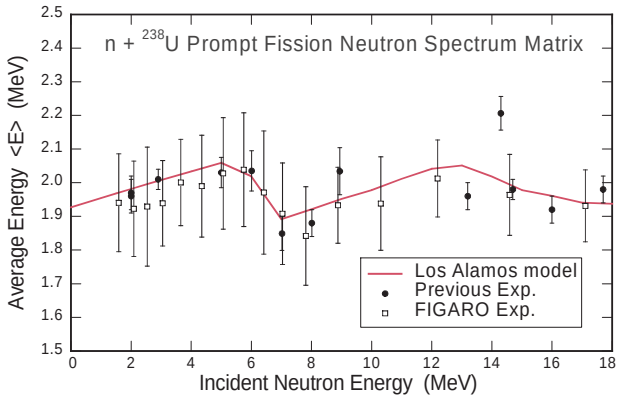

Fig. 16 First moment (average energies) of the n+^{238}U prompt fission neutron spectrum matrix calculated with the Los Alamos model shown together with those extracted from earlier experiments and the more recent CEA/Los Alamos FIGARO measurements [53].

Nuclear reaction modeling with the GNASH and ECIS codes played an important role for improving the treatment of inelastic scattering to discrete levels and to the continuum. This work impacts both the scattering in the fast region, as well as at 14 MeV and below. In the former case - inelastic scattering in the fast (few MeV) region - our improved data for inelastic scattering result in significant improvements in the critical assembly validation tests, not just for fast critical assemblies, but also for more moderated and thermal assemblies (the LEU-COMP-THERM series).

An example of the secondary neutron emission spectrum at 6.1 MeV incident energy on ^{238}U is shown in Fig. 17, for an emission angle of 45 degrees. It is evident that the new ENDF/B-VII.0 evaluation provides a much more accurate representation of the secondary spectrum, and its angular distribution, than the earlier ENDF/B-VI.8 evaluation.

Our evaluated neutron capture cross section is shown in Fig. 18, and is compared with the result from the Standards project (which represents a Bayesian analysis of a large amount of experimental data). It should be noted that in the 10's–100's keV region, the evaluated cross section lies below the bulk of the measurements that one might find in the CSISRS (EXFOR) experimental database. This is intentional, and

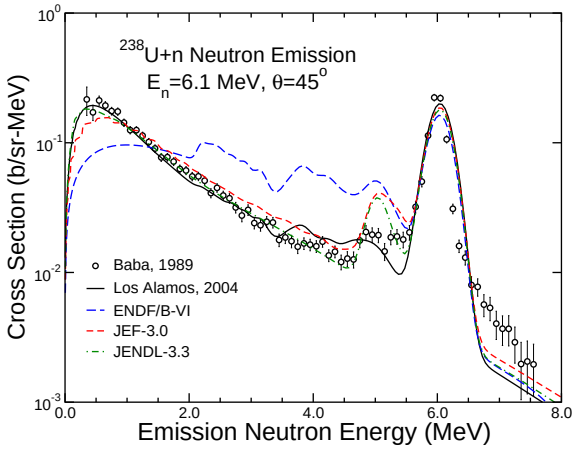

Fig. 17 Evaluated $^{238}\mathrm{U}(n,xn)$ neutron production energy-spectrum, compared with data, and with different evaluations.

represents the conclusions of evaluators who have studied the various measurements and concluded that the lower measurements are most accurate. See for instance, the NEA WPEC Subgroup-4 report [54].

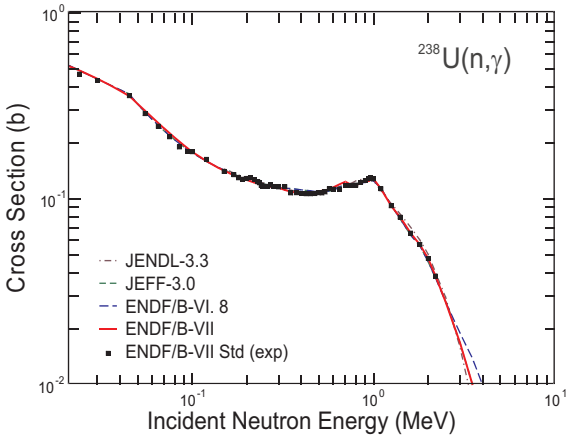

Fig. 18 Evaluated $^{238}\mathrm{U}(n,\gamma)$ neutron capture cross section, compared with data (labeled Std), and with previous evaluations. The standards evaluation resulted in uncertainties less than 3% over the E_n = 10^{-4} - 2.2 MeV region.

The neutron capture cross section of ^{238}U can be tested in an integral way, by comparing production of ^{239}U in a critical assembly for various neutron spectra in different critical assemblies, ranging from soft spectra to hard spectra. The results show that the evaluation reproduces integral capture rates reasonably well.

Like radiative capture, cross sections such as $(n,2n)$ and $(n,3n)$ are also important for production-depletion studies of uranium isotope inventories and transmutation. Our new evaluation of the $(n,2n)$ cross section is shown in Fig. 19 and is compared with ENDF/B-VI.8 and with measured data.

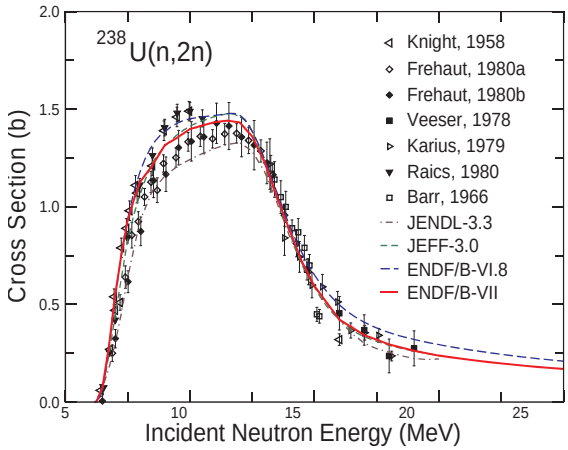

Fig. 19 Evaluated $^{238}\mathrm{U}(n,2n)$ cross section, compared with data and with previous evaluations.

2.3 ^{239}Pu Evaluation

^{239}Pu, Resonance Region:

The evaluation by Derrien and Nakagawa of the resonance region was taken over from the ENDF/B-VI.8 library without any change.

^{239}Pu, Fast Neutron Region :

The upgrades made to the ^{239}Pu evaluation included improved description of ^{239}Pu (n,2n), adoption of fission cross section from Standards, new analysis of the prompt fission spectrum, new delayed neutron time-dependent data, $\bar{\nu}$ modifications, and improved inelastic scattering at 14 MeV and below.

The earlier ^{239}Pu ENDF/B-VI.8 evaluation exhibited an under-reactivity, with the simulated Jezebel k_{eff} being ≈ 0.997. The new evaluation is more reactive, mainly because of the higher fission cross section in the fast region, with $k_{\mathrm{eff}} \approx 1.000$.

The new fission cross section is shown in Fig. 20 and is compared with the older ENDF/B-VI.8 evaluation. Because the earlier ^{235}U ENDF/B-VI.8 standard fission cross section was too low in the fast neutron energy region, and has now been increased in ENDF/B-VII.0, this leads to an increased ^{239}Pu fission cross section in this energy region too, since the plutonium fission cross section is strongly dependent on ^{239}Pu/^{235}U fission ratio measurements.

The prompt fission neutron spectrum, as a function of incident neutron energy, was reevaluated using the Madland-Nix approach. An example of the prompt fission spectrum is shown in Fig. 21, for 1.5 MeV neutrons incident on ^{239}Pu, compared with the Staples *et al.* data [55].

The new $(n,2n)$ cross section was based upon a Livermore – Los Alamos collaboration, involving GEANIE gamma-ray measurements of the prompt gamma-rays

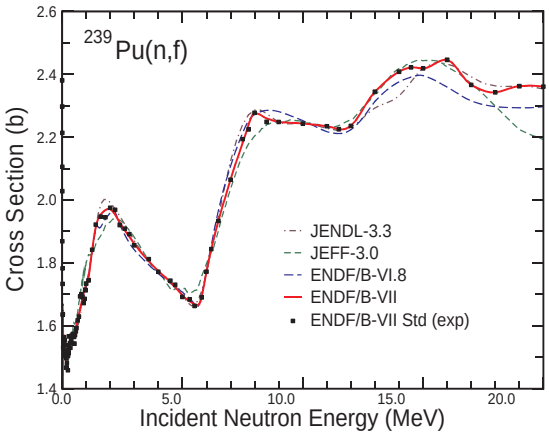

Fig. 20 Evaluated ^{239}Pu fission cross section compared with measured data, as represented by a covariance analysis of experimental data (referred to as ENDF/B-VII.0 Standard). The new evaluation follows the Standard evaluation of the experimental data. Other evaluations from JEFF and JENDL are also shown.

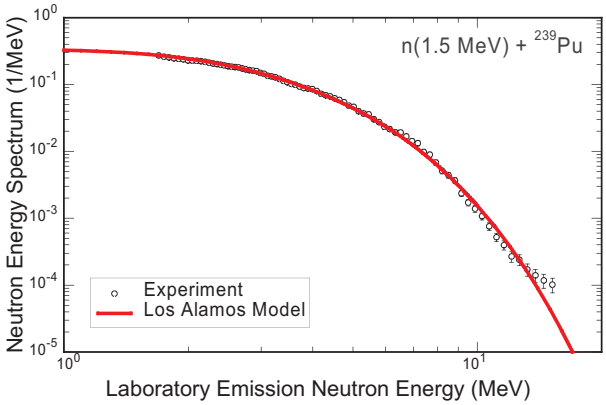

Fig. 21 Prompt fission neutron spectrum for 1.5 MeV neutrons incident on ^{239}Pu. The data of Staples *et al.* [55] are shown together with the least-squares adjustment to the Los Alamos model.

in ^{238}Pu, together with GNASH code theory predictions of unmeasured contributions to the cross section. Prior to this work, precision activation measurements had been made near 14 MeV by Lougheed *et al.* [56]. Other measurements based on measuring the two secondary neutrons were thought to be problematic and were therefore discounted in the evaluation.

As was the case for ^{235}U, the previous ^{239}Pu evaluation did not include enough inelastic scattering into the continuum for 14 MeV neutron energy and below, leading to poor performance in simulations of Livermore pulsed spheres in the 2-4 MeV excitation energy region. We inferred collective excitation strength from direct reaction analyses of ^{238}U data by Baba *et al.*, and assumed similar strengths for ^{239}Pu. Fig. 23 shows the new angle-integrated neutron spectrum data compared to the

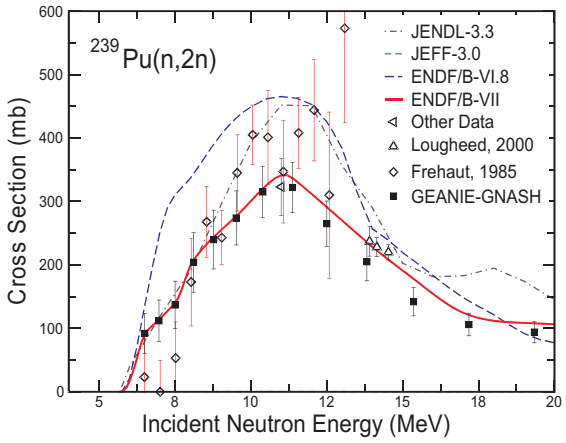

Fig. 22 Evaluated $^{239}\mathrm{Pu}(n,2n)$ cross section compared with data, and with previous evaluations.The evaluation was based upon the GEANIE-GNASH data and the Lougheed *et al.* 14 MeV data [56]. The ENDF/B-VII.0 evaluation (red line) is also referred to as the "GEANIE-project" evaluation.

ENDF/B-VI.8 evaluation (no measurements exist). This procedure led to a much improved MCNP modeling of the pulsed-sphere data.

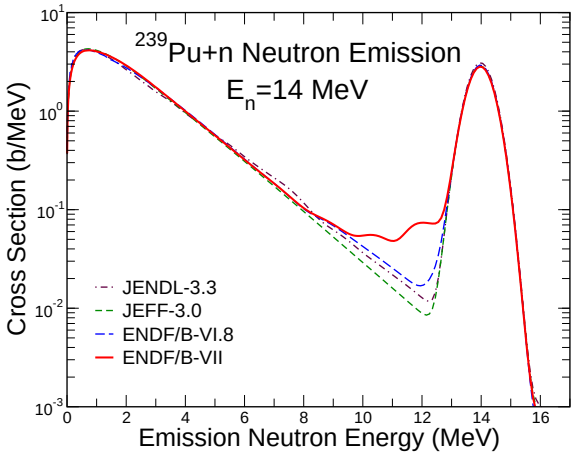

Fig. 23 Evaluated $^{239}\mathrm{Pu}(n,xn)$ neutron production energy-spectrum, compared with previous evaluations. No fundamental experimental data exist for this reaction, although Livermore pulsed data for transmission do exist.

2.4 ^{232}Th Evaluation

Recent developments in innovative fuel cycle concepts and accelerator-driven systems for the transmutation of nuclear waste have created a new interest in nuclear data for light actinides, with fission being crucially important for the design of new reactor systems. Additionally, there is strong scientific interest in the "thorium

anomaly" [57], which implies that in the thorium region the second-order shell effects split the outer fission barrier giving the so-called triple-humped structure.

The evaluation of ^{232}Th was completed in 2006 [58, 59]. The resonance parameters were obtained by Leal and Derrien [60] from a sequential Bayes analysis with the SAMMY code of the experimental database including Olsen neutron transmission at ORELA [61], not yet published capture data by Schillebeeckx (GELINA), and Gunsing (n-TOF) in the energy range 1 eV to 4 keV. Unresolved resonance parameters (4-100 keV) were derived by Sirakov *et al.* [62].

Evaluation in the fast energy region [63] was fully based on nuclear model calculations using the EMPIRE-2.19 code [7, 64, 65]. A crucial point was the selection of the proper coupled-channel optical model potential. The direct interaction cross sections and transmission coefficients for the incident channel on ^{232}Th were obtained from the dispersive coupled-channel potential of Soukhovitskii *et al.* (RIPL 608) [66]. Hauser-Feshbach [67] and HRTW [31] versions of the statistical model were used for the compound nucleus cross section calculations. Both approaches include fission decay probabilities deduced in the optical model for fission [68] and account for the multiple-particle emission and the full γ-ray cascade.

A new model to describe fission on light actinides, which takes into account transmission through a triple humped fission barrier with absorption, was developed [68] and applied for the first time to fission cross section evaluations. This formalism is capable of interpreting complex structure in the light actinide fission cross section in a wide energy range. The agreement with experimental fission cross sections is impressive as can be seen in Fig. 7 discussed earlier. The complex resonance structure in the first-chance neutron induced fission cross section of ^{232}Th has been very well reproduced. Prompt fission neutron spectra and $\bar{\nu}$ values were calculated using a new PFNS module of the EMPIRE code. The calculated $\bar{\nu}$ values were normalized to BROND-3 values [69], which are based on an extensive experimental database and contain covariance information.

The EMPIRE calculations were merged with the resonance data, including resonance covariance file and the delayed neutron data from the BROND-3 file [69]. Since the evaluation extends up to 60 MeV exclusive spectra are only given for the first 3 emissions, such as (n,3n) and (n,2np), while all the remaining channels are lumped into MT=5. Validation of the thorium file was carried out by Trkov and Capote [70], showing improvement over previous evaluations.

2.5 Minor Actinides

Minor actinides are defined broadly as fissionable nuclei beyond the four major actinides. They include minor isotopes of U and Pu as well as isotopes of Np, Am and Cm and ultimately also all heavier actinides. For example, advanced reactor systems are interested in 15 minor actinides, ^{233,234,236}U, ^{238,240,241,242}Pu, ^{237}Np, ^{241,242m,243}Am and ^{242,243,244,245}Cm.

2.5.1 ^{233}U Evaluation

The latest evaluation for ^{233}U [45] was specifically performed for ENDF/B-VII.0 library. The fission cross section is taken from a covariance statistical analysis of all experimental data, including ^{233}U/^{235}U fission ratio measurements converted using the ENDF/B-VII.0 standard ^{235}U cross section, as shown in Fig. 24. The somewhat higher ^{233}U fission cross section in the fission spectrum region produces better agreement with fast critical benchmark experiments.

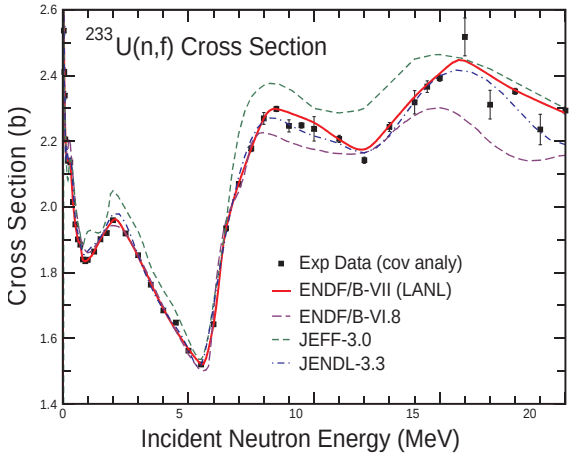

Fig. 24 Evaluated fission cross section that follows the measured data (shown as a covariance analysis of the experimental data). Other evaluations from JEFF and JENDL are also included.

2.5.2 ^{232,234,236,237,239,240,241}U Evaluations

These evaluations were done by the well established Los Lamos group lead by Phil Young [45]. Depending upon the isotope, varying amounts of measured data are available. In some cases, the experimental database is extremely sparse. For example, for ^{237}U, there are no direct measurements of the fission cross section at monoenergetic incident neutron energies, and there are no capture measurements. However, for ^{237}U and ^{239}U, indirect information does exist on the fission cross section in the few-MeV region, using surrogate (t,p) direct reaction experiments from Los Alamos, which have recently been re-analyzed by Younes and Britt at Livermore [71] and from a more recent LLNL experiment by Bernstein *et al.* [72]. These data allow an assessment of the equivalent neutron-induced fission cross section, and Younes and Britt have shown that such surrogate approaches can be accurate to better than 15 %.

In the case of ^{237}U, a measurement has been made of the fission cross section in a fast fission spectrum within a Flattop (fast) critical assembly, at two locations - the centre region and the tamper region (where the spectrum is softer). This kind of measurement also provides indirect information on the fission cross section.

2.6 Thermal Constants

It is useful to summarize the thermal constants in the ENDF/B-VII.0 neutron sublibrary for important materials and compare them with the values given in the neutron cross section standards sublibrary. This is done in Table 2. One can see that there are differences between the two sublibraries, though these are generally very small and within ≈ 0.5 standard deviation. The only item shown in this table that is considered a standard is the thermal ^{235}U(n,f) cross section.

Table 2 Thermal (0.0253 eV) constants obtained from the standards evaluation, $g_w^{\rm f}$ and $g_w^{\rm abs}$ are the Westcott factors . The neutron sublibrary values are given in brackets. The nubar obtained from the standards evaluation process for ^{252}Cf is $\bar{\nu}_{\rm tot}$ = 3.7692 $\pm$ 0.125%, comprised of $\bar{\nu}_p$=3.7606 and $\bar{\nu}_d$=0.0086. In ENDF/B-VI.8, $\bar{\nu}_{\rm tot}$ was 3.7676, comprised of $\bar{\nu}_p$=3.759 and $\bar{\nu}_d$=0.0086.

Quantity	^{233}U	^{235}U	^{239}Pu	^{241}Pu
σ_{nf}(b)	531.22± 0.25% (531.22)	584.33± 0.17% (585.09)	750.00± 0.24% (747.40)	1013.96± 0.65% (1011.85)
$\sigma_{n\gamma}$(b)	45.56± 1.50% (45.24)	99.40± 0.72% (98.69)	271.50± 0.79% (270.33)	361.79± 1.37% (363.05)
σ_{nn}(b)	12.11± 5.48% (12.15)	14.087± 1.56% (15.08)	7.800±12.30% (7.975)	12.13± 21.50% (11.24)
$g_w^{\rm f}$	0.9956±0.14% (0.9966)	0.9773± 0.08% (0.9764)	1.0554±0.20% (1.0542)	1.0454± 0.53% (1.046)
$g_w^{\rm abs}$	0.9996±0.11% (0.9994)	0.9788± 0.08% (0.9785)	1.0780±0.22% (1.0782)	1.0440± 0.19% (1.042)
$\bar{\nu}_{\rm tot}$	2.497 ±0.14% (2.497)	2.4355± 0.09% (2.4367)	2.8836±0.16% (2.8789)	2.9479± 0.18% (2.9453)

2.7 Nubars

The average number of neutrons per fission, also known as fission neutron multiplicity, represent quantities of exceptional importance. These quantities are evaluated with utmost care and high precision of data has been achieved. The total nubar (denoted as $\bar{\nu}$ or $\bar{\nu}_{\rm tot}$) is obtained as a sum of prompt and delayed nubars,

$$\bar{\nu}_{tot} = \bar{\nu}_p + \bar{\nu}_d \,. \tag{41}$$

For ^{235}U the energy dependence of the prompt $\bar{\nu}_p$ is shown in Fig. 25. This new ENDF/B-VII.0 evaluation follows covariance analysis of the experimental data, generally within uncertainties, and includes renormalization of the measured values to the latest standard value for ^{252}Cf.

For the ^{238}U the energy dependence of prompt fission neutron multiplicity, the ENDF/B-VII.0 data are identical to ENDF/B-VI, except the energy range was ex-

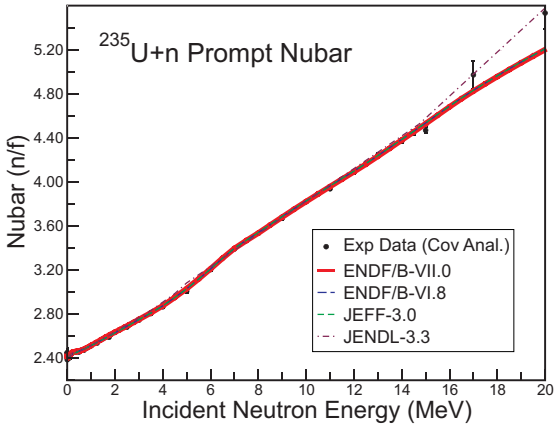

Fig. 25 Evaluated ^{235}U prompt fission neutron multiplicity, $\bar{\nu}_p$, compared with measured data, as represented by a covariance analysis of experimental data. Other evaluations from JEFF (Europe) and JENDL (Japan) are also shown.

tended from 20 to 30 MeV. The ENDF/B-VI data are based on an evaluation by Frehaut [73]. For the results and comparison see Fig. 26.

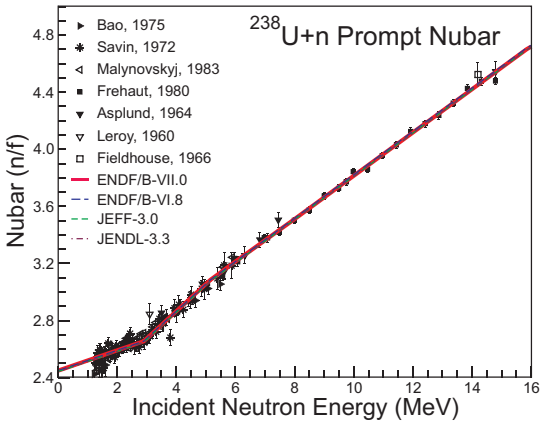

Fig. 26 Evaluated ^{238}U prompt fission neutron multiplicity, based on a covariance analysis of the experimental data.

The ^{239}Pu evaluated prompt fission nubar is shown in Fig. 27, compared with statistical covariance analysis of all measured data (again re-normalized to the latest californium standard). In the fast region, our evaluation follows the upper uncertainty bars of the statistical analysis of the experimental data, allowing us to optimize the integral performance in criticality benchmarks for the fast Jezebel ^{239}Pu spherical assembly.

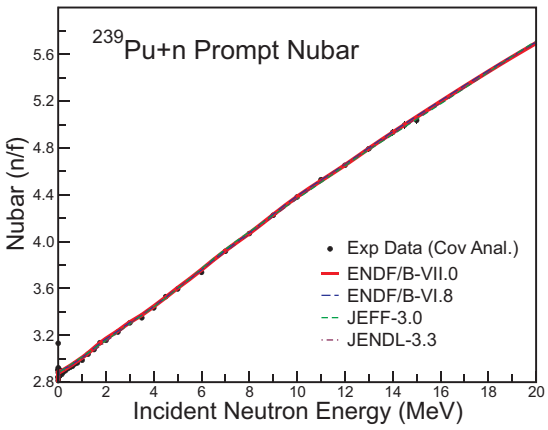

Fig. 27 Evaluated ^{239}Pu prompt fission neutron multiplicity, $\bar{\nu}_p$ compared with measured data, as represented by a covariance analysis of experimental data. Other evaluations from JEFF and JENDL are also shown.

2.8 Delayed Neutrons

Delayed neutrons originate from the radioactive decay of nuclei produced in fission and hence they are different for each fissioning system.

2.8.1 Fission-Product Delayed Neutrons

Delayed neutrons, also referred to as temporal fission-product delayed neutrons, are stored in ENDF-6 formatted files as MF=1, MT=455. Related experiments typically report data as a series of exponential terms. An experiment includes measurements characteristically made for a set of irradiation, cooling, and counting periods. Integrally detected delayed neutrons, adjusted for efficiencies and assigned uncertainties, are fit for maximum likelihood with an exponential series.

The most common function used has been a series of six exponential terms emulating the sum of contributions of six uncoupled delayed-neutron precursors or precursor groups of differing time constants – hence the use of "six-group fits" in common parlance. This series is generally given in terms of $\bar{\nu}_d$ – the total number of delayed neutrons per fission – times the normalized sum of six exponential terms giving the temporal production at time t following a fission event.

The delayed neutron yields in ENDF/B-VII.0 were carried over from ENDF/B-VI.8, with the exception of the modifications to ^{235}U thermal $\bar{\nu}_d$ as described in the next subsection. Therefore, these yields are based on experimental data. The 6-group parameters describing the time dependence of the delayed neutrons are discussed in more detailed below. But we note that an explicit incident energy dependence is not given in the ENDF file as was also the case in the previous ENDF/B-VI.8 evaluation. The 6-group values in the ENDF file correspond to fast neutron incident energies.

CINDER'90 calculations of a single fission pulse were replaced with a series of calculations for a variety of irradiation periods followed by decay times to 800 s,

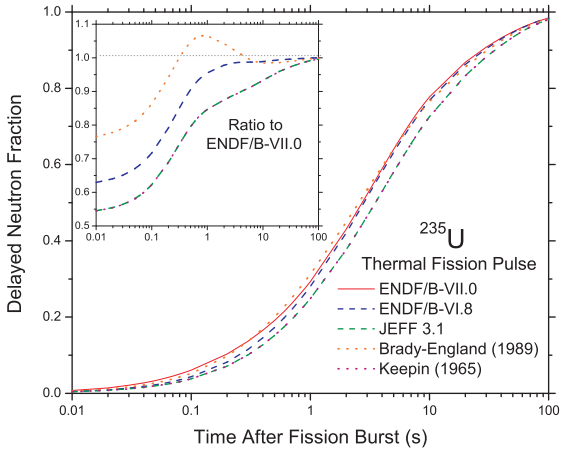

Fig. 28 Delayed neutron fraction as function of time following a ^{235}U thermal fission pulse for ENDF/B-VII.0, ENDF/B-VI.8, JEFF 3.1, Brady-England [74] and Keepin [75]. The inset shows the ratio of the delayed neutron fractions for the other evaluations to the ENDF/B-VII.0.

defining delayed neutron production in terms of irradiation and cooling times improving fits at very short and very long cooling times [76]. Subsequent improvements in P_n and half-life data were obtained using evaluated measured data of Pfeiffer [77] and NUBASE2003 [78]. Use of the earlier systematics of Kratz and Herrmann was then replaced by results obtained with our own model.

A new CINDER'90 data library, including all delayed neutron data developed, now includes 534 delayed neutron precursors, with 477 precursors in the fission-product range $65 < A < 173$. Use of the FPY data [79] results in the production of 281 to 440 of these precursors yielded in the 60 fission systems. These data have been used to produce new temporal delayed neutron fits for all 60 fission systems. Fits for some systems are included in this release of ENDF/B-VII.0; spectra, where present, are taken from the ENDF/B-VI.8 files using the new group abundances.

For illustration, in Fig. 28 we show delayed neutron fraction emitted as function of the time following a ^{235}U thermal fission pulse. As shown in the inset, differences between ENDF/B-VII.0 and the other evaluations are smaller than 20% for times larger than 1 second.

2.8.2 ^{235}U Thermal $\bar{\nu}_d$

When G. R. Keepin [75] measured delayed nubar ($\bar{\nu}_d$) for ^{235}U, he found a difference between thermal and fast values: 0.0158 ± 0.0005 and 0.0165 ± 0.0005, respectively. Since second-chance fission was above the energy of his measurements, he assumed it was an experimental error, and recommended the cleaner fast data for kinetics applications, including thermal. This posed a problem for thermal reactor designers: use the more accurate fast value, or the more relevant thermal data. Mostly, they opted for the latter.

Experiments continued to send mixed signals. References [80] and [81] supported a difference between fast and thermal values, and thermal reactor kinetics

calculations failed to show a problem with the lower value. Fast measurements, and summation calculations tended to raise the 0.0167 value even higher.

Two recent developments provided a plausible resolution of this problem:

1. Fission theory allowed an energy-variation of delayed nubar in the resonance region [82, 83]. The change in ^{235}U delayed nubar is a series of small dips, one at each resonance, but for engineering purposes, only the average value over the thermal region is important. As the energy increases, the fluctuations decrease and the value approaches the higher fast value.
2. Analysis of beta-effective measurements supported the view that thermal delayed nubar is about 5% lower than the fast value [84, 85, 86].

The ENDF/B-VII.0 ^{235}U delayed nubar file is not a re-evaluation of the data, but a minimum adjustment to ENDF/B-VI which reflects current usage and recognizes the thermal-fast difference. An appropriate time to re-visit this issue will be when the ANS-19.9 Standard is finalized. The delayed value at thermal energy ($\bar{\nu}_d$ = 0.01585) was taken from JENDL-3.3. It then ramps linearly to 0.0167 at 50 keV. JENDL ramps to 0.0162, but 0.0167 minimizes the change to ENDF/B-VI. Above 50 keV, the ENDF/B-VI data are unchanged. To avoid disturbing thermal criticality benchmark results, which depend on total nubar, the thermal prompt value was changed to keep total nubar the same, $\bar{\nu}_{\rm tot}$ = 2.42000 to 2.42085.

2.9 Fission Energy Release

The ENDF/B-VII.0 library includes new information for the energy released in fission for the major actinides, ^{235,238}U and ^{239}Pu. A recent study by Madland [87] found a new representation for the prompt fission product energy $E_{FR}(e_{\rm inc})$, prompt neutron energy $E_{NP}(e_{\rm inc})$, and prompt photon energy $E_{GP}(e_{\rm inc})$ functions. Their sum, the average total prompt fission energy deposition, is given by

$$< E_d(e_{\rm inc}) >= E_{FR}(e_{\rm inc}) + E_{NP}(e_{\rm inc}) + E_{GP}(e_{\rm inc}). \tag{42}$$

This expression is based upon published experimental measurements and application of the Los Alamos model [44] and it shows that, to first order, these quantities can be represented by linear or quadratic polynomials in the incident neutron energy $e_{\rm inc}$,

$$E_i(e_{\rm inc}) = c_0 + c_1 e_{\rm inc} + c_2 e_{\rm inc}^2, \tag{43}$$

where E_i is one of E_{FR}, E_{NP} or E_{GP}.

The recommended coefficients for ^{235,238}U and ^{239}Pu are provided in Table 3. The average total prompt energy deposition $< E_d >$, obtained using these coefficients in Eqs. (42, 43) is shown in Fig. 29. Madland's recommended c_0 values for E_{FR} have been adopted in the new ENDF/B-VII.0 files for ^{235,238}U and ^{239}Pu.

Table 3 Madland's recommended energy release polynomial coefficients, in MeV. See Eq. (43 for explanation.

Nuclide	Parameter	c_0	c_1	c_2
^{235}U	E_{FR}	169.13	-0.2660	0.0
	E_{NP}	4.838	+0.3004	0.0
	E_{GP}	6.600	+0.0777	0.0
^{238}U	E_{FR}	169.8	-0.3230	0.004206
	E_{NP}	4.558	+0.3070	0.0
	E_{GP}	6.6800	+0.1239	0.0
^{239}Pu	E_{FR}	175.55	-0.4566	0.0
	E_{NP}	6.128	0.3428	0.0
	E_{GP}	6.741	+0.1165	-0.0017

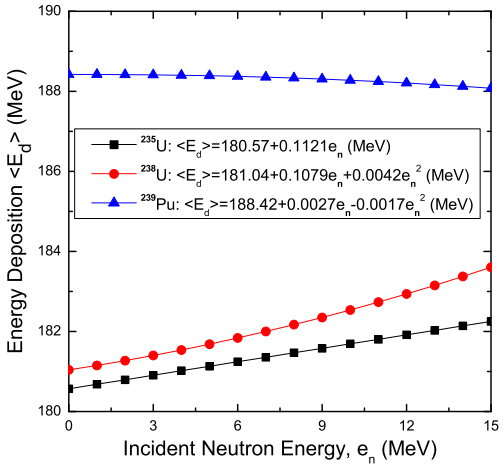

Fig. 29 Average total prompt fission energy deposition as a function of the incident neutron energy. See Eq. (42) for explanation.

2.9.1 Nuclear Heating

Nuclear heating is an important quantity in any nuclear system. It is the topic which should be explored in relation to the energy release presented above and its handling by the processing code NJOY. In general, heating as a function of energy, $H(e_{\text{inc}})$, may be given in terms of KERMA (Kinetic Energy Released in Materials) coefficients[3], $k_{ij}(e_{\text{inc}})$, as

[3] The International Commission on Radiation Units and Measurements in its document ICRU-63 [88] recommends using the name "KERMA coefficient" instead of "KERMA factor".

$$H(e_{\rm inc}) = \sum_i \sum_j \rho_i k_{ij}(e_{\rm inc}) \Phi(e_{\rm inc}), \tag{44}$$

where ρ_i is the number density of the i^{th} material, $k_{ij}(e_{\rm inc})$ is the KERMA coefficient for the i^{th} material and j^{th} reaction at energy $e_{\rm inc}$, and $\Phi(e_{\rm inc})$ is the scalar flux. A rigorous calculation of the KERMA coefficient for each reaction requires knowledge of the total kinetic energy carried away by all secondary particles following that reaction; data that frequently are not available in evaluated files. An alternative technique, known as the energy balance method [89], is used by NJOY. KERMA coefficient calculations by this method require knowledge of the incident particle energy, the reaction Q-value and other terms.

The prompt fission reaction Q-value required for prompt fission KERMA including the energy dependent prompt fission Q-value can be calculated as

$$Q(e_{\rm inc}) = E_R - 8.07 \times 10^6 [\bar{\nu}(e_{\rm inc}) - \bar{\nu}(0)] + 0.307 e_{\rm inc} - E_B - E_{GD}, \tag{45}$$

where E_R is the total energy minus neutron energy, E_B is the total energy released by delayed betas and E_{GD} is the total energy of delayed photons.

Table 4 Prompt fission Q-values in MeV obtained with ENDF/B-VII.0 data[a]. To get total energy deposition, add the incident energy to total Q-values tabulated here.

Nuclide	Incident energy $e_{\rm inc}$	ENDF/B VII.0	Madland	NJOY (old)	NJOY (Eq. 45)
^{235}U	0.0253 eV	180.65	180.57	180.65	180.65
	1.0 MeV	180.19	179.68	179.84	180.19
	14.0 MeV	169.07	168.14	164.24	169.14
^{238}U	0.0253 eV	181.28	181.04	181.30	181.30
	1.0 MeV	181.02	180.15	180.68	181.03
	14.0 MeV	169.59	169.37	164.86	169.76
^{239}Pu	0.0253 eV	188.38	188.42	189.37	188.37
	1.0 MeV	187.58	187.42	187.24	187.59
	14.0 MeV	175.98	174.12	171.10	176.00

[a] Given for the sum of prompt fission products, prompt neutrons, and prompt gammas.

Results based upon new ENDF/B-VII.0 are shown in Table 4. We note that the prompt fission Q-value calculated with the traditional ENDF formulas are now in much better agreement with Madland's calculations.

3 Neutron Data for Other Materials

In addition to actinides, there are three other categories of materials of interest for nuclear technology applications. These are light nuclei that often serve as moderators and coolants, structural materials and fission products.

3.1 Light Nuclei

Several light-element evaluations were contributed to ENDF/B-VII.0, based on R-matrix analysis done at Los Alamos using the EDA code. Among the neutron-induced evaluations were those for ^{1}H, ^{3}H, ^{6}Li, ^{9}Be, and ^{10}B. For the light-element standards, R-matrix results for $^{6}\mathrm{Li}(n,\alpha)$ and $^{10}\mathrm{B}(n,\alpha)$ were contributed to the standards process, which combined the results of two different R-matrix analyses with ratio data using generalized least-squares. Differences persisted between the two R-matrix analyses even with the same data sets that are not completely understood, but probably are related to different treatments of systematic errors in the experimental data.

Below we summarize upgrades that have been made for ENDF/B-VII.0. Where no changes have been made compared to ENDF/B-VI.8 (*e.g.*, for n + ^{2}H), we do not discuss reactions on these isotopes.

^{1}H. The hydrogen evaluation came from an analysis of the $N-N$ system that includes data for $p+p$ and $n+p$ scattering, as well as data for the reaction $^{1}\mathrm{H}(n,\gamma)^{2}\mathrm{H}$ in the forward (capture) and reverse (photodisintegration) directions. The R-matrix parametrization, which is completely relativistic, uses charge independent constraints to relate the data in the $p+p$ system to those in the $n+p$ system. It also uses a new treatment of photon channels in R-matrix theory that is more consistent with identifying the vector potential with a photon "wavefunction".

In the last stages of the analysis, the thermal capture cross section was forced to a value of 332.0 mb (as in ENDF/B-VI.8), rather than the "best" experimental value of 332.6 $\pm$0.7 mb [90], since criticality data testing of aqueous thermal systems showed a slight preference for the lower value. Also, the latest measurement [91] of the coherent $n+p$ scattering length was used, resulting in close agreement with that value, and with an earlier measurement of the thermal scattering cross section [92], but not with a later, more precise value [93].

This analysis also improved a problem with the $n+p$ angular distribution in ENDF/B-VI.8 near 14 MeV, by including new measurements [94, 95] and making corrections to some of the earlier data that had strongly influenced the previous evaluation.

^{3}H. The $n+^{3}$H evaluation resulted from a charge-symmetric reflection of the parameters from a $p+^{3}$He analysis that was done some time ago. This prediction [96] resulted in good agreement with $n+t$ scattering lengths and total cross sections that were newly measured at the time, and which gave a substantially higher total cross

section at low energies than did the ENDF/B-VI evaluation. At higher energies, the differences were not so large, and the angular distributions also remained similar to those of the earlier evaluation.

^{9}Be. The $n+^{9}$Be evaluation was based on a preliminary analysis of the ^{10}Be system that did a single-channel fit only to the total cross section data at energies up to about 14 MeV. A more complete analysis should take into account the multichannel partitioning of the total cross section, especially into the (n,2n) channels. An adequate representation of these multibody final states will probably require changes in the EDA code. For ENDF/B-VII.0 the elastic (and total) cross section was modified to utilize the new EDA analysis which accurately parametrizes the measured total elastic data, while the previous ENDF/B-VI.8 angular distributions were carried over.

Data testing of the file (including only the changes in the total cross sections) appeared to give better results for beryllium reflecting assemblies, and so it was decided to include this preliminary version in the ENDF/B-VII.0 release.

^{16}O. The evaluated cross-section of the ^{16}O(n,α_0) reaction in the laboratory neutron energy region between 2.4 and 8.9 MeV was reduced by 32% at LANL. The ^{16}O(n,α) cross section was changed accordingly and the elastic cross sections were adjusted to conserve unitarity. This reduction was based upon more recent measurements. We note that this led to a small increase in the calculated criticality of LCT assemblies.

3.2 Structural Materials

Structural materials play a prominent role in nuclear applications and hence neutron reaction data are evaluated very carefully.

In the ENDF/B-VII.0 main evaluation effort was concentrated on the major actinides and the fission products (Z = 31 - 68) that together cover more than half of the ENDF/B-VII.0 neutron sublibrary. Outside of these two groups, only few materials were fully or partially evaluated for ENDF/B-VII.0 as described below.

3.2.1 Evaluations of Major Structural Materials

Structural materials fall into a category of priority materials in all major evaluated data libraries. The list is dominated by Cr, Fe and Ni, the most important isotopes being major structural materials ^{52}Cr (natural abundance 83.8%), ^{56}Fe (91.7%) and ^{58}Ni (68.1%), followed by less abundant isotopes ^{50,53}Cr, ^{54,57}Fe, ^{60}Ni, *etc.*

In the United States considerable attention to evaluations of structural materials has been devoted in the past. These evaluations have been performed by the highly experienced team at Oak Ridge National Laboratory up to 20 MeV in the 1980s, in particular in reference to the celebrated ENDF/B-V library. We note that ORNL

supplied complete evaluations in the entire energy range, combining the capabilities in the thermal and resonance region (code SAMMY) with the then advanced nuclear reaction modeling code TNG in the fast neutron region. An example would be 1986 update for iron by Fu *et al.* [97]. Since then, virtually no updates below 20 MeV have been made. In view of the data need for accelerator driven systems in the 1990s, the evaluations of structural materials have been extended to 150 MeV by Los Alamos and incorporated into ENDF/B-VI library. Then, these have been adopted without any change by the latest version of the ENDF/B-VII.0 library which was released in 2006.

3.2.2 New Evaluations for ENDF/B-VII.0

^{nat}**V.** Cross sections for the (n,np) reaction were revised at BNL [98] by adjusting the EMPIRE-2.19 calculations to reproduce two indirect measurements by Grimes *et al.* [99] and Kokoo *et al.* [100] at 14.1 and 14.7 MeV respectively. This resulted in the substantial reduction (about 350 mb at the maximum) of the, (n,np) cross section Similarly, the (n,t) reaction was revised to reproduce experimental results of Woelfle *et al.* [101] The inelastic scattering to the continuum was adjusted accordingly to preserve the original total cross section.

^{191,193}**Ir.** These are two entirely new evaluations performed jointly by T-16 (LANL) and the NNDC (BNL) in view of recent GEANIE data on γ-rays following neutron irradiation. The resolved and unresolved resonance parameters are based on the analysis presented in Ref. [12]. New GNASH model calculations were performed for the γ-rays measured by the GEANIE detector, and related (n,xn) reactions cross sections were deduced [102]. We also include an evaluation of the ^{193}Ir(n,n') reaction to the isomer. The remaining cross sections and energy-angle correlated spectra were calculated with the EMPIRE code. The results were validated against integral reaction rates.

^{208}**Pb.** A new T-16 (LANL) analysis with the GNASH code was performed over the incident neutron energy range from 1.0 to 30.0 MeV. The Koning-Delaroche optical model potential [103] from the RIPL-2 data base was used to calculate neutron and proton transmission coefficients for calculations of the cross sections. Minor adjustments were made to several inelastic cross sections to improve agreement with experimental data. Additionally, continuum cross sections and energy-angle correlated spectra were obtained from the GNASH calculations for (n,n'), (n,p), (n,d), (n,t), and (n,α) reactions. Elastic scattering angular distributions were also calculated with the Koning-Delaroche potential and incorporated in the evaluation at neutron energies below 30 MeV.

This new ^{208}Pb evaluation led to a significant improvement in the lead-reflected critical assembly data. This is especially true for fast assemblies, but some problems remained for thermal assemblies.

3.3 Fission Products

Fission products represent the largest category of nuclei (materials) in the evaluated nuclear data libraries. Defined broadly as materials with Z = 31 - 68, in the latest US library ENDF/B-VII.0 they supply 219 nuclei. We follow this definition with the understanding that it covers also several other important materials such as structural Mo and Zr, and absorbers Cd and Gd.

Many fission product evaluations in ENDF/B had not been revised for considerable amount of time of 30-35 years. Not surprisingly an analysis performed by Wright (ORNL) and MacFarlane (LANL) in 2000 revealed considerable deficiencies in ENDF/B-VI [104].

In this situation, fission product evaluations in ENDF/B-VI.8 were completely abandoned and ENDF/B-VII.0 adopted new or recently developed evaluations. For a set of 74 materials, including 19 materials considered to be of priority, entirely new evaluations were performed using the Atlas-EMPIRE evaluation procedure [6] including those by Kim *et al.* [105, 106]. For the remaining 145 materials, evaluations were adopted from the recently developed International Fission Product Library of Neutron Cross Section Evaluations completed in December 2005 and described in 2009 report [107].

3.3.1 Priority Fission Products

New evaluations were performed for materials considered to be priority fission products. The list includes 19 materials,

- ^{95}Mo, ^{99}Tc, ^{101}Ru, ^{103}Rh, ^{105}Pd, ^{109}Ag, ^{131}Xe, ^{133}Cs, ^{141}Pr,^{153}Eu), ^{143,145}Nd, ^{147,149,150,151,152}Sm, ^{155,157}Gd.

This selection [11] was based on the analysis by DeHart, ORNL, which was performed in 1995 [108]. It was motivated by the need to improve existing evaluations for materials of importance for a number of applications, including criticality safety, burn-up credit for spent fuel transportation, disposal criticality analysis and design of advanced fuels.

3.3.2 Complete Isotopic Chains

As a part of modern approach to evaluation, complete isotopic chains were evaluated for several fission products, including Ge, Nd, Sm, Gd and Dy.

A simultaneous evaluation of the complete isotopic chain for a given element became possible thanks to tremendous progress in the development of evaluation tools in recent years. This includes highly integrated evaluation code systems such as EMPIRE, coupled to experimental database EXFOR and to the library of input parameters RIPL. Complete isotopic chains for Ge, Nd, Sm, Gd and Dy, totaling 37

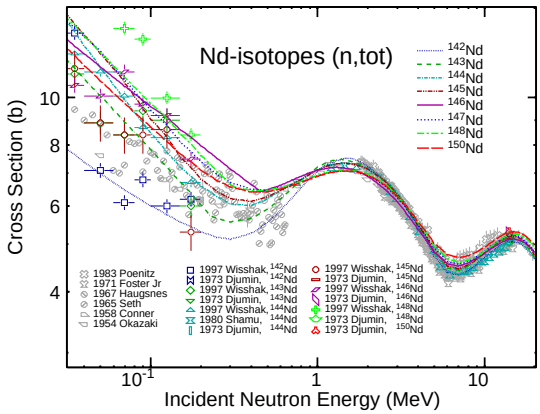

Fig. 30 Total cross sections for Nd isotopes. Note the consistency among different isotopes resulting from the simultaneous evaluation of the full chain of neodymium isotopes.

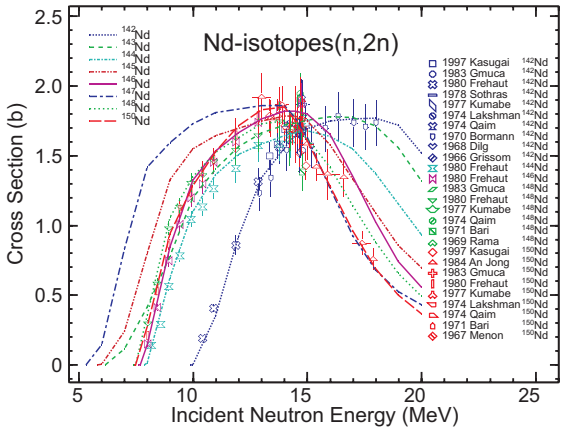

Fig. 31 (n,2n) cross sections for Nd isotopes. Good fit to the available data justifies prediction of cross sections for the radioactive ^{147}Nd.

materials were evaluated for ENDF/B-VII.0. As an example we discuss isotopes of Nd.

A set of neodymium evaluations include two priority fission products, ^{143,145}Nd, another 5 stable isotopes, and the radioactive ^{147}Nd. Neodymium is one of the most reactive rare-earth metals. It is important in nuclear reactor engineering as a fission product which absorbs neutrons in a reactor core. A new evaluation was performed by Kim *et al.* [106]. In Fig. 30 we show total neutron cross sections of all Nd isotopes in comparison with available data measured on isotopic samples as well as on elemental samples.

Of special interest to radiochemical applications is the radioactive ^{147}Nd for which no data exist in the fast neutron region. A good fit to available data on other stable isotopes gives confidence that predictions for ^{147}Nd cross sections are sound. This is illustrated in Figs. 31 and 32 where we show (n,2n) and neutron capture cross sections, respectively, for all Nd isotopes.

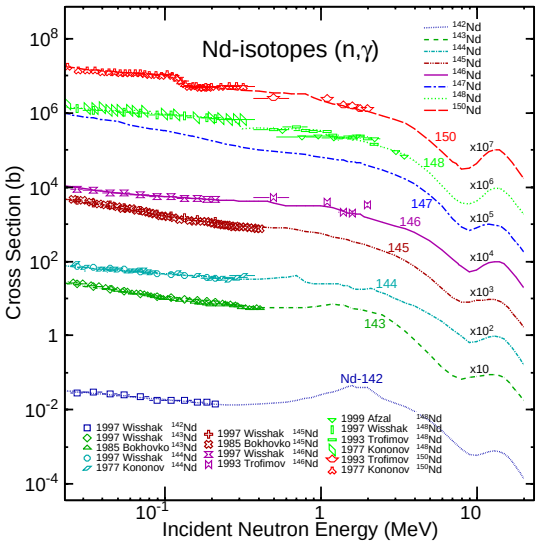

Fig. 32 Neutron capture cross sections for Nd isotopes. Good fit to the available data endorses prediction of cross sections for the radioactive ^{147}Nd.

3.3.3 Specific Case of ^{90}Zr

Zirconium is an important material for nuclear reactors since, owing to its corrosion-resistance and low absorption cross-section for thermal neutrons, it is used in fuel rods cladding. Benchmark testing performed at Bettis and KAPL showed an undesirable drop in the reactivity when the beta version of ENDF/B-VII.0 was used. Taking into account the importance of zirconium in reactor calculations, BNL undertook an entirely new evaluation of the fast neutron region in ^{90}Zr using the EMPIRE code. Good description of the total cross section of ^{90}Zr confirmed the higher elastic scattering cross section, see Fig. 33. The new file met expectations when validated against integral measurements at KAPL.

3.3.4 Remaining Fission Products

Recognizing a need to modernize the fission product evaluations, an international project was conducted during 2001 - 2005 to select the best evaluations from the available evaluated nuclear data libraries. Evaluated nuclear data libraries of five major efforts were considered, namely the United States (ENDF/B-VI.8 and preliminary ENDF/B-VII), Japan (JENDL-3.3, released in 2002), Europe (JEFF-3.0, released in 2000), Russia (BROND-2.2, released in 1992) and China (CENDL-3.0, made available for this project in 2001).

As a result, the International Fission Product Library of Neutron Cross Section Evaluations (IFPL) was created for 219 materials [107]. Afterwards, IFPL was adopted in full by the ENDF/B-VII.0 library, see Table 5 for a summary.

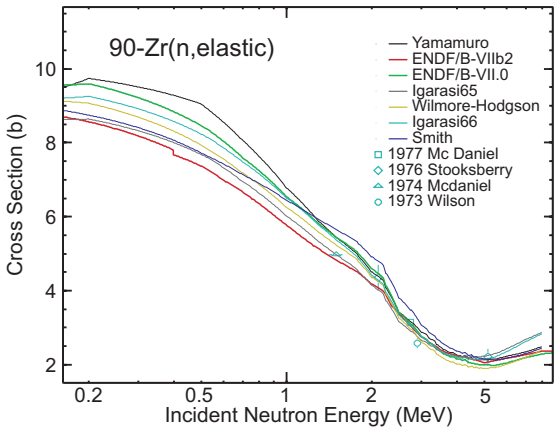

Fig. 33 Comparison of ^{90}Zr elastic cross sections calculated with various optical model potentials. The preliminary ENDF/B-VII evaluation (denoted ENDF/B-VIIb2) yields the lowest cross sections. The ENDF/B-VII.0 evaluation is considerably higher as suggested by the integral experiments.

Table 5 Summary of 219 fission product evaluations included in the ENDF/B-VII.0 library. Full files were taken over from single libraries (data sources) for 135 materials, remaining 84 files were put together from two different data sources.

Library (Data Source)	**Full File**	**Resonance Region**	**Fast Region**
ENDF/B-VI.8, released in 2001	1	3	13
New evals for ENDF/B-VII.0	74	74	-
JEFF-3.1, released in 2005	1	-	-
JENDL-3.3, released in 2002	47	7	56
CENDL-3.0, released in 2001	11	-	15
BROND-2.2, released in 1992	1	-	-
Total number of materials	135	84	84

4 Covariances for Neutron Data

A covariance matrix specifies uncertainties and usually energy-energy correlations of data (cross sections, $\bar{\nu}$, *etc.*) which are required to assess uncertainties of design and operational parameters in nuclear technology applications. Covariances are obtained from the analysis of experimental data and they are stored as variances and correlations in the basic nuclear data libraries.

Early procedures for generating nuclear data covariances were widely discussed in the 1970's and 1980's [109]. Accordingly, many of the presently existing covariance data were developed about 30 years ago for the ENDF/B-V library [110, 111]. This earlier activity languished during the 1990's due to limited interest by users and constrained resources.

More recently, intensive interest in the design of a new generation of nuclear power reactors, as well as in criticality safety and national security applications has stimulated a revival in the demand for covariances as demonstrated at the major Covariance Workshop held in 2008 [112].

4.1 Evaluation Methodology

New covariance data in the ENDF/B-VII.0 neutron sublibrary were produced for 13 materials using the evaluation techniques summarized in Table 6.

Table 6 Summary of methods used for the ENDF/B-VII.0 covariance evaluations. Distinguished are three energy regions, resolved resonances, unresolved resonances and fast neutron region.

Energy region	Evaluation method	Material
Resolved resonances	Direct SAMMY	^{232}Th
	Retroactive SAMMY	$^{152-158,160}$Gd
	Atlas-KALMAN	^{89}Y,^{99}Tc,^{191,193}Ir
Unresolved resonances	Experimental	^{232}Th
	Atlas-KALMAN	^{99}Tc, ^{193}Ir
	EMPIRE-KALMAN	$^{152-158,160}$Gd,^{89}Y,^{191}Ir
Fast neutrons	EMPIRE-KALMAN	$^{152-158,160}$Gd,^{89}Y,^{99}Tc,^{191,193}Ir
	EMPIRE-GANDR	^{232}Th

4.1.1 Resonance Region

Covariances in the resonance region can be produced by three different methods. The most sophisticated approach is based on the code SAMMY [10] , which uses generalized least-squares fits to experimental data. The intermediate Atlas method propagates resonance parameter uncertainties [12] to cross section covariances. The simplest and most transparent method uses uncertainties of thermal cross sections and resonance integrals as estimate of covariances [113].

SAMMY covariance method:

This method is normally applied to actual experimental data as the integral part of simultaneous evaluation of both resonance parameters and their covariances (files MF2 and MF32 in ENDF-6 format terminology [2]). However, out of practical necessity an alternative retroactive procedure is often used. One proceeds in three steps:

First, one either starts with actual experimental data or these are artificially ("retroactively") generated using R-matrix theory and known resonance parameters. In the latter case, usually transmission, capture and fission is calculated assuming realistic experimental conditions. Then, realistic statistical uncertainties are assigned to each data point, and realistic values are assumed for data-reduction parameters such as normalization and background.

Afterwards, initial covariance matrix is established. Let D represent the experimental data and V the covariance matrix for experimental/retroactive data. Values for V (both on- and off-diagonal elements) are derived from the statistical uncertainties of the individual data points, ν_i, and from the uncertainties of the data-reduction parameters, in the usual fashion

$$V_{ij} = \nu_i \delta_{ij} + \sum_k g_{ik} \Delta^2 r_k g_{jk}. \tag{46}$$

In this equation, $\Delta^2 r_k$ represents the uncertainty on the k^{th} data-reduction parameter r_k, and g_{ik} is the partial derivative of the cross section at energy E_i with respect to r_k. Then, the covariance matrix V_{ij} describes all the known experimental uncertainties.

Finally, the generalized least-squares equations are used to determine the set of resonance parameters, P', and associated resonance parameter covariance matrix, M', that fit these data. If P is the original set of resonance parameters (for which we wish to determine the covariance matrix), and T is the theoretical curve generated from those parameters, then, in matrix notation, the least-squares equations are

$$P' = P + M + G^t V^{-1}(D - T) \quad \text{and} \quad M' = (G^t V^{-1} G)^{-1}. \tag{47}$$

Here, G is the set of partial derivatives of the theoretical values T with respect to the resonance parameters P; G is sometimes called the sensitivity matrix.

The solutions of Eq.(47) provide the new parameter values P' and the associated resonance parameter covariance matrix M', fitting all directly measured/retroactive data simultaneously and using the full off-diagonal data covariance matrix for each data set.

Atlas covariance method:

This method combines the wealth of data given in the Atlas of Neutron Resonances [12] with the filtering code KALMAN [114, 115]. Atlas provides values and uncertainties for neutron resonance parameters and also integral quantities such as capture thermal cross sections, resonance integrals and 30-keV Maxwellian averages. The procedure consists of two major steps:

- One starts with the resonance parameters and their uncertainties and uses multilevel Breit-Wigner formalism to compute cross sections along with their sensitivities.
- Uncertainties of resonance parameters are propagated to cross sections with the code KALMAN. Uncertainties of thermal values are obtained by suitable adjustment of resonance parameter uncertainties, if necessary inferring anticorrelation with bound (negative energy) resonances.

An alternative approach would be to take resonance parameter uncertainties, put them into file MF32, and leave the job of propagation of these uncertainties into cross section covariances to well established processing codes.

Low-fidelity covariance method:

This simple, yet extremely transparent and useful method, provides estimate of covariance data using known uncertainties of thermal cross sections and integral quantities. It was proposed by M. Williams [113] in 2004 and later used extensively in the "Low-fidelity Covariance Project" by ANL-BNL-LANL-ORNL collaboration that was completed in 2008 [116].

4.1.2 Fast neutron region

EMPIRE-KALMAN covariance method:

EMPIRE-KALMAN methodology can serve as an example of recently developed covariance methods in the fast neutron region. The KALMAN filter techniques is based on minimum variance estimation and naturally combines covariances of model parameters, of experimental data and of cross sections. This universality is a major advantage of the method.

The key ingredient of the method is the sensitivity matrix, which represents complex nuclear reaction calculations. If we denote the combination of nuclear reaction models as an operator $\hat{\mathbf{M}}$ that transforms the vector of model parameters $\mathbf{p}$ into a vector of cross sections $\boldsymbol{\sigma}(\mathbf{p})$ for a specific reaction channel, then the sensitivity matrix $\mathbf{S}$ can be interpreted as the linear term in the expansion of the operator $\hat{\mathbf{M}}$,

$$\hat{\mathbf{M}}\mathbf{p} = \boldsymbol{\sigma}(\mathbf{p}) \tag{48}$$

and

$$\hat{\mathbf{M}}(\mathbf{p}+\delta\mathbf{p}) = \boldsymbol{\sigma}(\mathbf{p}) + \mathbf{S}\delta\mathbf{p} + \ldots \tag{49}$$

where $\hat{\mathbf{M}}$ is the operator rather than a matrix. In practice, the elements $s_{i,j}$ of the sensitivity matrix are calculated numerically as partial derivatives of the cross sections σ at the energy E_i with respect to the parameter p_j,

$$s_{i,j} = \frac{\partial\sigma(E_i,\mathbf{p})}{\partial p_j}\,. \tag{50}$$

In case of covariance determination, the initial values of the parameters, $\mathbf{p}_0$, are already optimized, *i.e.*, when used in the model calculations they provide the evaluated cross sections. Their covariance matrix $\mathbf{P}_0$ is assumed to be diagonal while the uncertainties of the parameters are estimated using systematics, independent measurements or educated guesses. The model-based covariance matrix (prior) for the cross sections, $\mathbf{C}_0$, can be obtained through a simple error propagation formula,

$$\mathbf{C}_0 = \mathbf{S}\mathbf{P}_0\mathbf{S}^{\mathrm{T}}\,, \tag{51}$$

where superscript T indicates a transposed matrix.

The experimental data, if available, are included through a sequential update of the parameter vector $\mathbf{p}$ and the related covariance matrix $\mathbf{P}$ as

$$\begin{aligned} \mathbf{p}_{n+1} &= \mathbf{p}_n + \mathbf{P}_n \mathbf{S}^{\mathrm{T}} \mathbf{Q}_{n+1} (\boldsymbol{\sigma}_{n+1}^{\mathrm{exp}} - \boldsymbol{\sigma}(\mathbf{p}_n)) \\ \mathbf{P}_{n+1} &= \mathbf{P}_n - \mathbf{P}_n \mathbf{S}^{\mathrm{T}} \mathbf{Q}_{n+1} \mathbf{S} \mathbf{P}_n \,, \end{aligned} \tag{52}$$

Here,

$$\mathbf{Q}_{n+1} = (\mathbf{C}_n + \mathbf{C}_{n+1}^{\mathrm{exp}})^{-1} \,, \tag{53}$$

where $n = 0, 1, 2, \ldots$ and $n+1$ denotes update related to the sequential inclusion of the $(n+1)^{th}$ experimental data set. In particular, the subscript $1 \equiv 0+1$ denotes updating model prior ($n = 0$) with the first experiment. Vector $\mathbf{p}_{n+1}$ contains the improved values of the parameters starting from the vector $\mathbf{p}_n$, and $\mathbf{P}_{n+1}$ is the updated covariance matrix of the parameters $\mathbf{p}_{n+1}$. The $\mathbf{C}_{n+1}^{\mathrm{exp}}$ is the cross section covariance matrix for the $(n+1)^{\mathrm{th}}$ experiment. The updated (posterior) covariance matrix for the cross sections is obtained by replacing $\mathbf{P}_0$ with $\mathbf{P}_{n+1}$ in Eq. (51),

$$\mathbf{C}_{n+1} = \mathbf{S} \mathbf{P}_{n+1} \mathbf{S}^{\mathrm{T}} \,. \tag{54}$$

The updating procedure described above is often called Bayesian, although Eqs. (51 - 54) can be derived without any reference to the Bayes theorem as shown in Ref. [117].

The experimental covariance matrix, $\mathbf{C}_n^{\mathrm{exp}}$, is usually non-diagonal, due to the correlations among various energy points E_i. Assuming that systematic experimental uncertainties are fully correlated, the matrix elements are expressed through the statistical, $\Delta^{\mathrm{sta}}\sigma_n^{\mathrm{exp}}$, and systematic, $\Delta^{\mathrm{sys}}\sigma_n^{\mathrm{exp}}$, experimental uncertainties. This yields

$$c_n^{\mathrm{exp}}(i,i) = (\Delta^{\mathrm{sta}}\sigma_n^{\mathrm{exp}}(E_i))^2 + (\Delta^{\mathrm{sta}}\sigma_n^{\mathrm{exp}}(E_i))^2 \tag{55}$$

and, for $i \neq k$,

$$c_n^{\mathrm{exp}}(i,k) = \Delta^{\mathrm{sys}}\sigma_n^{\mathrm{exp}}(E_i) \times \Delta^{\mathrm{sys}}\sigma_n^{\mathrm{exp}}(E_k) \,. \tag{56}$$

The quality and consistency of the evaluated cross sections can be assessed by scalar quantity

$$\chi^2 = \sum_{n=1}^{N} (\boldsymbol{\sigma}_n^{\mathrm{exp}} - \boldsymbol{\sigma}(\mathbf{p}_{\mathrm{N}}))^{\mathrm{T}} (\mathbf{C}_n^{\mathrm{exp}})^{-1} (\boldsymbol{\sigma}_n^{\mathrm{exp}} - \boldsymbol{\sigma}(\mathbf{p}_{\mathrm{N}})) \,, \tag{57}$$

where $\mathbf{p}_{\mathrm{N}}$ is the final set of model parameters corresponding to the inclusion of N experiments. A value of χ^2 per degree of freedom exceeding unity indicates underestimation of the evaluated uncertainties. It is a fairly common practice to multiply such uncertainties by a square root of χ^2 per degree of freedom to address this issue.

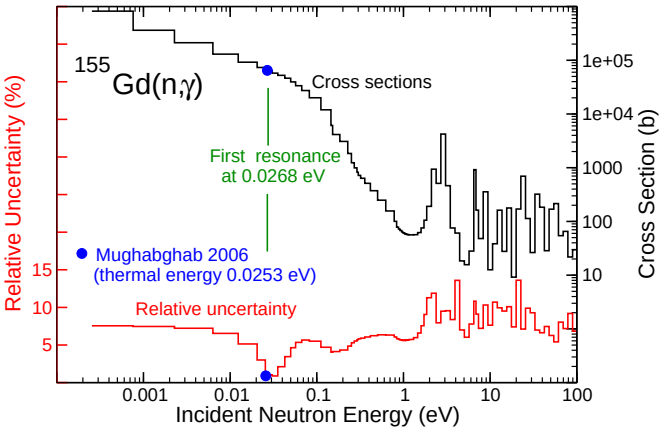

Fig. 34 Relative uncertainties for ^{155}Gd(n,γ) obtained with the retroactive SAMMY method plotted along with the cross sections to show anti-correlation between the two quantities. The experimental cross section (60900 b) and its uncertainty (0.82%) at the thermal energy [12] are well reproduced.

4.2 Sample Case: Gd

Covariance evaluation of Gd isotopes was produced as a sample case for ENDF/B-VII.0. There are 7 stable Gd isotopes, ^{152,154,155,156,157,158,160}Gd and the radioactive ^{153}Gd. All covariances were produced by SAMMY retroactive method in the resolved resonance region and EMPIRE-KALMAN at higher energies.

Fig. 34 shows uncertainties for ^{155}Gd capture cross sections at low energies. The thermal cross section and its uncertainty in the Atlas of Neutron Resonances [12] are very well reproduced. The particular feature that ^{155}Gd shares with ^{157}Gd is a very close vicinity of the first positive resonance to the thermal energy. Therefore, the thermal cross section is determined by the first resonance rather than 1/v dependence typical for other nuclei. Fig. 34 demonstrates also anti-correlation between uncertainties and cross sections in the resonance region. The highest uncertainties are being found between the resonances, *i.e.*, at dips of cross sections. This feature is clearly visible although it is, to some extent, obscured by the group-wise representation that lumps together close resonances.

The covariances for the unresolved resonance and fast neutron regions were produced with the EMPIRE-KALMAN method. In Fig. 35 we show relative uncertainties for ^{157}Gd(n,tot), ^{157}Gd(n,elastic) and ^{157}Gd(n,γ) cross sections for incident neutron energies above 1 keV. Fig. 36 shows the correlation matrix for the ^{157}Gd(n,γ) cross section. This matrix reveals complicated structures with strong correlations aligned within a relatively narrow band along the diagonal.

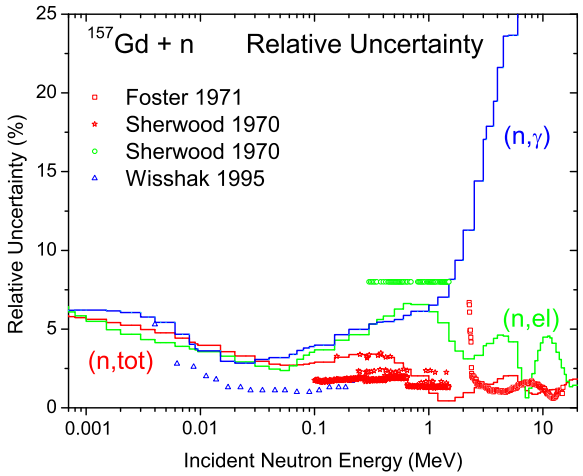

Fig. 35 Relative uncertainties in the unresolved resonance and fast neutron range for the total, elastic and capture cross sections on ^{157}Gd obtained with the EMPIRE-KALMAN method.

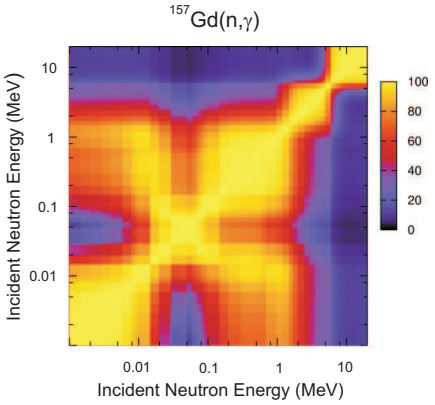

Fig. 36 Correlation matrix for the ^{157}Gd neutron capture cross sections in the fast neutron region obtained with the EMPIRE-KALMAN method.

4.3 Major Actinides

Covariances for major actinides play crucial role in many applications. There was insufficient time to complete new covariance evaluations for these important actinides prior to the release of the ENDF/B-VII.0 library in 2006. This work was completed in 2008, but it has not yet been officially approved by CSEWG (status at the end of 2009).

One of the issues that has been resolved was conversion of huge multi-million line long resonance parameter covariance matrices (MF32 files) into cross section covariances (MF33 files). Such a conversion reduced the size of the files considerably, though the ^{235}U and ^{239}Pu covariance files still remain very large (about 50 MB and 30 MB, respectively).

4.3.1 ^{233,235,238}U Covariances

Evaluation of ^{233,235,238}U covariances was performed by ORNL-LANL collaboration. ORNL covered the resonance region and LANL supplied covariances in the fast neutron region.

Due to huge size of the resonance parameter covariances (MF32) the files were converted into cross section covariances (MF33). Still, the size of the largest ^{235}U file is considerable, in excess of 52 MB.

Preliminary version of these evaluations are available in the recently reestablished ENDF/A library, which contains candidate evaluations for the next release of ENDF/B-VII library. It is expected that all these files will be included into ENDF/B-VII.1 release. As an example of these evaluations, ^{235}U(n,f) covariances are shown in Fig. 37, see also discussion later in this Chapter under the AFCI covariance library.

4.3.2 ^{239}Pu Covariances

Evaluation of ^{239}Pu covariances was also performed by ORNL-LANL collaboration. ORNL covered the resonance region and LANL supplied covariances in the fast neutron region.

The file was also converted into cross section covariances (MF33), its reduced size is 32 MB. Preliminary version of this evaluation is available in the ENDF/A library and it is expected that the file will be included into ENDF/B-VII.1 release.

4.3.3 ^{232}Th Covariances

The covariance evaluation for ^{232}Th includes the resolved resonance, unresolved resonance, and the fast neutron regions as well as $\bar{\nu}$. In the resolved resonance region, a Reich-Moore evaluation was performed [118] in the energy range up to 4 keV using the code SAMMY . The correlation matrix for the radiative capture cross section is shown in Fig. 38. In the unresolved resonance region the experimental method was used [62].

Cross section covariance data in the fast neutron region were generated by the Monte Carlo technique [119] using the EMPIRE code . In the Monte Carlo approach a large collection of nuclear parameter sets (normally more than 1000) is generated by randomly varying these parameters with respect to chosen central val-

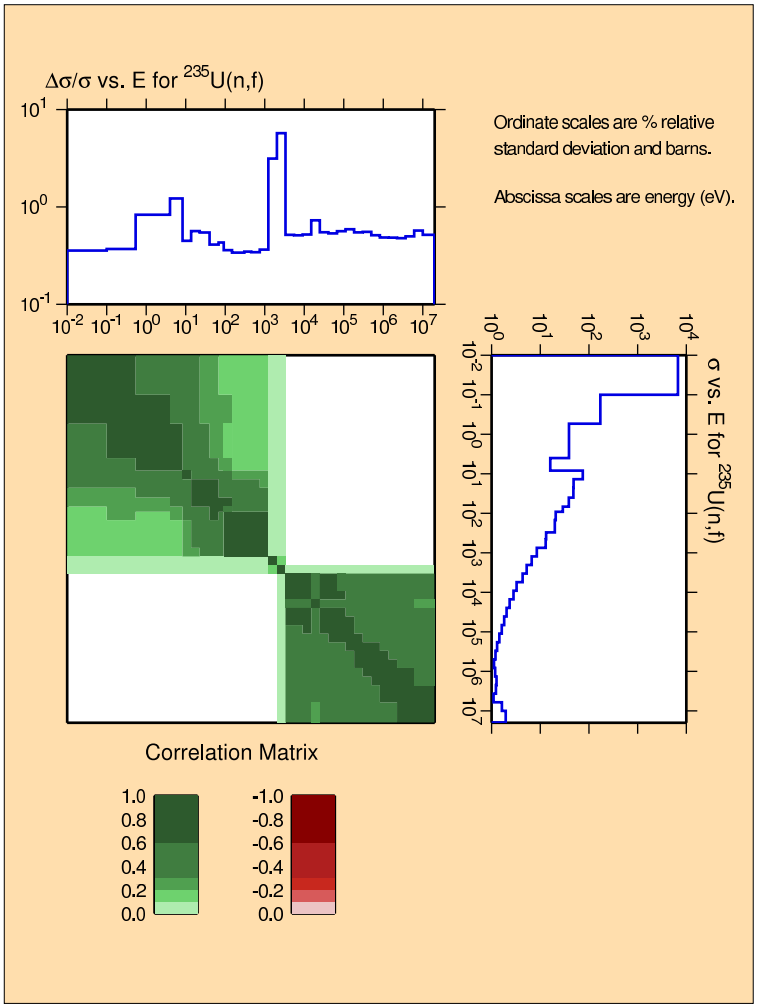

Fig. 37 Covariances for ^{235}U(n,f) taken from ENDF/A (November 2009) which collects candidate evaluations for the next release of ENDF/B-VII. Data are given in 33-energy group representation adopted by the AFCI covariance library: top - cross section uncertainties, right - cross sections, middle - energy-energy correlations.

ues. These parameter sets are then used to calculate a corresponding large collection of nuclear model derived values for selected physical quantities, such as cross sections and angular distributions. These results are subjected to a statistical analysis to generate covariance information. The GANDR code system [120] updates these nuclear model covariance results by merging them with the uncertainty information for available experimental data using the generalized least-squares technique.

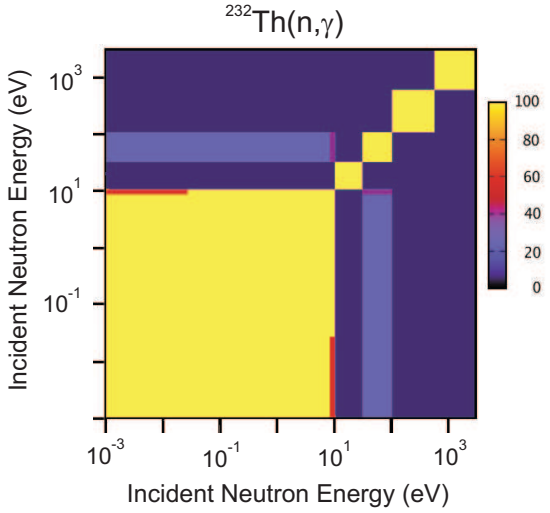

Fig. 38 Correlation matrix for ^{232}Th neutron radiative capture cross sections in the thermal and resolved resonance region.

Covariances for $\bar{\nu}$ were obtained from the unpublished evaluation performed by A. Ignatyuk (Obninsk) for the Russian library BROND-3 (this library has not been released yet) . This evaluation was based on the analysis of experimental data.

4.4 Covariance Libraries

Despite the fact that only limited amount of covariance evaluations have been produced to date (end of 2009), three covariance libraries were created in the US as briefly described below. It should be understood that each of these libraries represents an approximate solution and has, therefore, inherent limitation. This stems from the fact that the development of quality covariances is formidable task which requires considerable resources. This challenge should be addressed by future releases of major evaluated libraries. Accordingly, it is expected that covariances will be part of the next release of the ENDF/B-VII library.

4.4.1 Low-fidelity Covariance Library

Development of this library was funded by the US Nuclear Criticality Safety Program. The library provides the first complete, yet simple, estimate of neutron covariances for 387 materials listed in ENDF/B-VII.0; for details see Little *et al.* [116]. Covariances cover main reaction channels, elastic scattering, inelastic scattering, radiative capture and fission (cross sections and nubars) over the energy range from 10^{-5}eV to 20 MeV. Various approximations were utilized depending on the mass of

the target, the neutron energy range and the neutron reaction. The resulting covariances are not an official part of ENDF/B-VII.0, but they are available for testing in nuclear applications.

In general, at low energies simple estimates were made following the approach proposed by Williams [113]. In the thermal region, defined by the cutoff energy 0.5 eV, experimental uncertainties of thermal cross sections were uniformly adopted. In the epithermal region, from o.5 eV to 5 keV, the uncertainties of resonance integrals were used and uniformly applied. This led to simple and often reasonable estimate of cross section uncertainties. An example is shown in Fig. 39.

In the fast neutron region the model-based estimates of covariances were produced for 307 materials from ^{19}F to ^{209}Bi [121]. To this end EMPIRE code was employed and parametrization from the latest version of the RIPL library [15] was adopted along with global estimates of related model parameters. Parameter uncertainties were propagated into cross section uncertainties.

Light nuclei, $A < 19$, were treated differently. Recent R-matrix evaluations were adopted for three materials; for remaining materials simple estimates were supplied by looking into experimental data in the entire energy region.

Actinides in the fast neutron region were again treated differently. Latest full scale evaluations by ORNL-LANL were used for major actinides, while simple model-based estimates using EMPIRE were used for minor actinides.

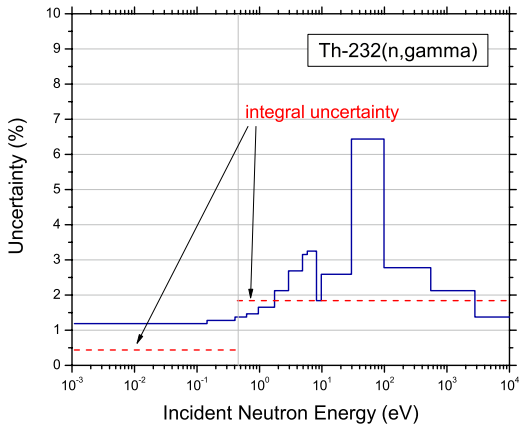

Fig. 39 Low-fidelity uncertainties for ^{232}Th(n,γ) cross sections, labeled as integral quantities, are compared with ENDF/B-VII.0 values.

4.4.2 SCALE-6 Covariance Library

This is the covariance library included in the well-known ORNL reactor licensing code SCALE [122]. The library was produced by selecting covariances from variety of sources as summarized in Table 7 [123].

Table 7 Sources of covariance data in the SCALE-6 covariance library.

Source	Material
ENDF/B-VII.0	^{152,158,160}Gd, ^{232}Th, ^{99}Tc, ^{191,193}Ir
ENDF/A	^{233,235,238}U, ^{239}Pu
ENDF/B-VI.8	^{23}Na, $^{28-30}$Si, ^{45}Sc, ^{51}V, $^{50,52-54}$Cr, ^{55}Mn, $^{54,56-58}$Fe, $^{58,60-62,64}$Ni
	^{63,65}Cu, ^{89}Y, ^{93}Nb, ^{nat}In, ^{185,187}Re, ^{197}Au, $^{206-208}$Pb, ^{209}Bi, ^{241}Am
JENDL-3.3	^{240,241}Pu
LANL new	^{1}H, ^{6}Li, ^{10}B
Low-fidelity	About 200 materials, mostly fission products and minor actinides

It should be noted that inherent limitation of selecting covariances from various sources is inconsistency with basic cross sections, which may or may not be negligible.

4.4.3 AFCI Covariance Library

This library was developed for Advanced Fuel Cycle Initiative funded by the United States DOE Nuclear Energy. It should be suitable for nuclear data adjustment needed for fast reactor applications, such as advanced burner reactor, ABR. The list of materials contains 110 materials, including

- 12 light nuclei,
- 78 structural materials and fission products, and
- 20 actinides.

Covariances are produced by BNL-LANL collaboration [124]. Major reaction channels are covered and covariance data are supplied in 33-energy group representation. It is important to note that these covariances are tested by highly experienced reactor users in Argonne and Idaho National Laboratory.

It is expected that fairly robust version of the AFCI covariance library will be available by the end of 2010. Then, it should serve as the basis for producing ENDF-6 formatted files suitable for inclusion into the next release of ENDF/B-VII. We note that whenever possible, AFCI library adopts new covariance evaluations produced for ENDF/B-VII. As an example, we refer the reader to Fig. 37 where we have shown covariances for ^{235}U(n,f) in AFCI 33-energy group representation.

5 Validation of Neutron Data

Integral data testing of evaluated cross sections plays an essential role for validation purposes. The importance is twofold: Firstly, since many of the integral experiments are very well understood (especially the critical assembly experiments), they provide a strong test of the accuracy of the underlying nuclear data used to

model the assemblies, and can point to deficiencies that need to be resolved. Secondly, such integral data testing can be viewed as a form of "acceptance testing" prior to these data being used in various applications. Many applications, ranging from reactor technologies to defense applications, have a high standard required of a nuclear database before it is adopted for use. Critical assemblies, whilst involving many different nuclear reaction processes, can still be thought of as "single-effect" phenomena that probe the neutronics and nuclear data (but not other phenomena), and therefore an important acceptance test is that a sophisticated radiation transport simulation of the assembly should reproduce the measured k_{eff} to a high degree.

Of necessity the testing of an evaluated data library must be performed after the evaluation process. Ideally though, this testing is not performed as an afterthought, but more as an integral part of the evaluation process. It has been demonstrated many times that a close link between the data evaluators and the data users can provide valuable feedback to the evaluation process - quantifying the sensitivity of performance parameters to specific changes in nuclear data.

We note that ENDF/B-VII.0 benchmarking was largely facilitated by the fact that for the first time benchmark model descriptions were available from the ICSBEP handbook. This criticality safety handbook contains benchmark descriptions of almost 4000 critical assembly configurations (compared to the tens of benchmark descriptions contained in the ENDF-202 Benchmark Specifications used previously). Furthermore this rich collection of benchmark descriptions spans the range of fuel types, compositions, spectra, geometries, *etc*. However, an additional feature of these benchmarks is the evaluation of the benchmark uncertainties, *i.e.*, estimates of the total experimental uncertainties combined with any additional modeling uncertainties [125]. As a result the most diverse and robust aspect of the ENDF/B-VII.0 validation effort was the analysis of hundreds of criticality configurations compared with their benchmark eigenvalues and uncertainties.

5.1 Criticality Testing

In reference to ENDF/B-VII.0, C/E values for k_{eff} (see footnote[4]) have been calculated for hundreds of critical benchmarks using continuous energy Monte Carlo programs including MCNP (versions 4c3 or 5), RCP01, RACER and VIM. These calculations generally use benchmark models derived from the Handbook of the International Criticality Safety Benchmark Evaluation Project (ICSBEP). Benchmark evaluations in this Handbook are revised and extended on an annual basis. Unless otherwise noted, benchmark models derived from the 2004 or 2005 editions of the Handbook were used in the calculations described below.

[4] For the sake of clarity we use the term "C/E value for k_{eff}" rather than the term "normalized eigenvalue". Here, C/E stands for the ratio of calculated to experimental values, and k_{eff} means the effective multiplication factor defined as the ratio of the average number of neutrons produced to the average number of neutrons absorbed per unit time.

Since the C/E values for k_{eff} have all been obtained using continuous energy Monte Carlo calculations there is a stochastic uncertainty associated with each C/E value for k_{eff}. The magnitude of this uncertainty is very small, typically less than 25 pcm (0.025%, see footnote[5]).

A paper by S. C. van der Marck [126] presents independent European data testing of ENDF/B-VII.0, using MCNP4c3 with data processed by NJOY, and also shows extensive neutron transmission benchmark comparisons. Table 8 provides a summary of 730 benchmark criticality experiments that were simulated and compared with measurements.

Table 9 summarizes the average value of C/E-1 (the average deviation of Calculation/Experiment from unity) for these benchmarks. We show for comparison in *italics* the values for the previous ENDF/B-VI.8. While it is important to study the individual benchmark results for a more thorough understanding, it is still very useful to observe the overall averaged behavior shown in Table 9:

- The low-enriched U (LEU) compound benchmarks are modeled much more accurately (owing to improved ^{238}U, as well as ^{16}O and ^{1}H).
- The intermediate-enriched U (IEU) benchmarks are modeled more accurately.
- The Pu and high-enriched U (HEU) fast benchmarks are modeled more accurately.
- The ^{233}U thermal benchmarks are modeled more accurately. Although the ^{233}U fast benchmarks simulations appear to have become worse, this is perhaps more due to deficiencies in modeling of beryllium for two of the assemblies studied - for bare ^{233}U (Jezebel-23 and Flattop-23) the new ENDF/B-VII.0 are clearly much better.
- Lower energy Pu (PU) benchmarks were modeled poorly in ENDF/B-VI.8 and continue to be modeled poorly in the new library.

Table 8 The number of benchmarks per main ICSBEP category for compound, metal and solution systems with thermal, intermediate, fast and mixed neutron spectrum used in ENDF/B-VII.0 validation [126] .

	COMP				MET				SOL	Total
	ther	inter	fast	mix	ther	inter	fast	mix	ther	
Low-enriched U	257				1				49	307
Intermediate-enriched U	6	4					16			26
High-enriched U		6		1	41	5	66	5	87	211
Mixed	34		1				4		10	49
Low energy Pu		1				1	7	6	105	120
^{233}U	8						4		5	17
Total	305	11	1	1	42	6	97	11	256	730

[5] pcm is derived from Italian "per cento mille", meaning per hundred thousands. It is a unit of reactivity, where 1 pcm = 0.00001 Δk/k, *i.e.*, 100 pcm is a 0.1% discrepancy.

Table 9 The average value of $C/E-1$ in pcm (100 pcm = 0.1%) for ENDF/B-VII.0 per main ICSBEP benchmark category. Shown in *italics* are the values for the ENDF/B-VI.8 library.

	COMP				MET				SOL
	ther	inter	fast	mix	ther	inter	fast	mix	ther
LEU	17				-41				123
	-452				*-270*				*107*
IEU	103	219					182		
	-299	*-238*					*712*		
HEU		1744		104	-51	88	147	812	108
		1442		*-273*	*-411*	*-42*	*186*	*462*	*142*
MIX	428		110				193		-254
	377		*978*				*69*		*-257*
PU		1110				4565	229	936	620
		967				*4654*	*375*	*745*	*531*
^{233}U	146						-364*		66
	-380						*-338*		*-292*

*) This becomes -64 pcm versus *-254 pcm* if we restrict ourselves to the well understood UMF-001 and UMF-006 assemblies.

5.2 Fast U and Pu Benchmarks

Fast U and Pu benchmarks were given considerable attention in the validation of the ENDF/B-VII.0 library. Shown below are selected examples for several benchmark categories.

Bare, and ^{238}U reflected, assemblies. A large number of well-known Los Alamos fast benchmark experiments have been incorporated into the ICSBEP Handbook and are routinely calculated to test new cross section data. Unmoderated enriched ^{235}U benchmarks include Godiva (HEU-MET-FAST-001 or HMF1)[6], Flattop-25 and Big-10 assemblies.

Results of MCNP5 k_{eff} calculations with ENDF/B-VI.8 and ENDF/B-VII.0 cross sections for this suite of benchmarks are displayed in Fig. 40. The improved accuracy in calculated k_{eff} for these systems with the new ENDF/B-VII.0 cross sections is readily apparent.

Assemblies with various reflectors. A number of additional highly-enriched uranium benchmarks, either bare or with one of a variety of reflector materials including water, polyethylene, aluminum, steel, lead and uranium have also been calculated with MCNP5 and both ENDF/B-VI.8 and ENDF/B-VII.0 cross sections. The calculated values for k_{eff} are illustrated in Fig. 41. Once again, significant improvement in the calculated k_{eff} is observed with the ENDF/B-VII.0 cross sections.

[6] "HEU-MET-FAST-001" is the identifier assigned in the ICSBEP Handbook for this assembly. It is comprised of 4 parts which, respectively, classify the assembly by fissile materials (PU, HEU, LEU), fuel form (METal, SOLution, COMPound), and energy spectrum (FAST, INTERmediate, THERMal or MIXED), and benchmark number (-NNN). It is also common to use a shorthand form for this identifier, such as HMF1 for HEU-MET-FAST-001.

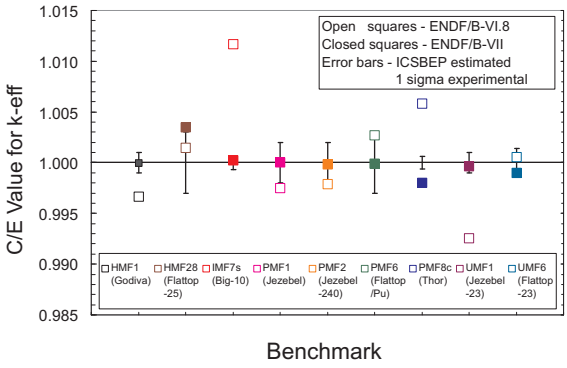

Fig. 40 LANL HEU, Pu and ^{233}U unmoderated benchmark C/E values for k_{eff} calculated with ENDF/B-VI.8 and ENDF/B-VII.0 cross section data.

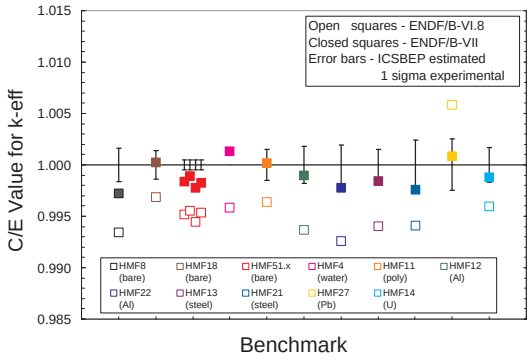

Fig. 41 HEU-MET-FAST benchmark C/E values for k_{eff} calculated with ENDF/B-VI.8 and ENDF/B-VII.0 cross section data.

Pb reflected assemblies. Two reflector elements of particular historical interest are lead and beryllium. Often there are multiple evaluations that contain similar materials, in particular the same core with differing reflectors, thereby facilitating testing of cross section data for individual reflector materials. Such is the situation for lead, displayed in Fig. 42, with calculated k_{eff} for a variety of benchmarks.

The significant improvements in these lead-reflected calculated k_{eff} reflects improvements made in the new ENDF/B-VII.0 ^{208}Pb evaluation, which was based on modern calculational methods together with careful attention to accurately predicting cross section measurements, and by adopting the JEFF-3.1 evaluations for ^{204,206,207}Pb which (together with the JEFF-3.1 file for ^{208}Pb) have reduced this bias by a similar amount in JEFF-3.1 benchmarking.

The situation is not so clear for thermally moderated systems (LCT) as shown in Fig. 42. This Fig. also shows the k_{eff} calculations for the HMF57 benchmark, which consists of either a spherical or cylindrical HEU core with a lead reflector. In any event, the C/E values for k_{eff} are significantly different from unity in most cases regardless of cross section data set.

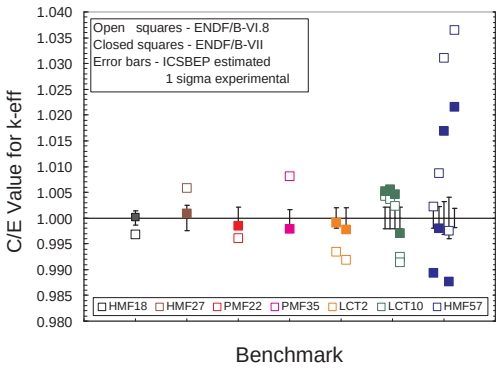

Fig. 42 Bare and lead reflected C/E values for k_{eff} calculated with ENDF/B-VI.8 and ENDF/B-VII.0 cross section data for several HMF, PMF and LCT benchmarks.

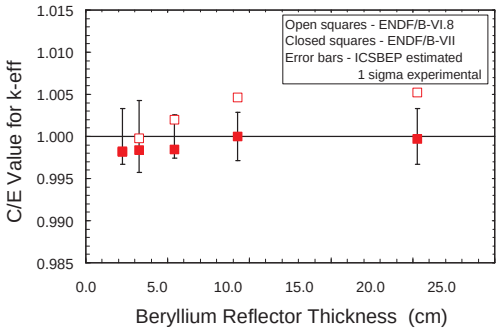

Fig. 43 HEU-MET-FAST-058 benchmark C/E values for k_{eff} with ENDF/B-VI.8 and ENDF/B-VII.0 cross section data as a function of the beryllium reflector thickness.

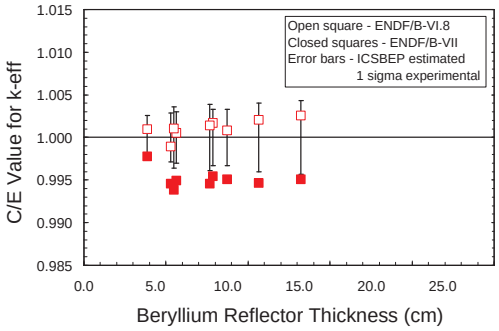

Fig. 44 HEU-MET-FAST-066 benchmark C/E values for k_{eff} for ENDF/B-VI.8 and ENDF/B-VII.0 cross section data as a function of the beryllium reflector thickness. The poorer agreement using ENDF/B-VII.0 appears to be in contradiction to the results shown in Fig. 43.

Be reflected assemblies. C/E values for k_{eff} of beryllium reflected benchmarks are shown in Figs. 43 and 44. These comparisons are useful to assess the changes made in the ^{9}Be cross sections for ENDF/B-VII.0.

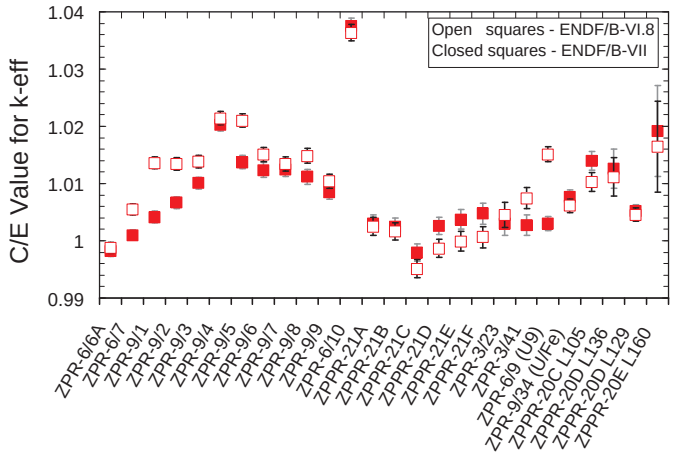

Fig. 45 C/E values for k_{eff} for 26 ZPR (zero power reactor) and ZPPR (zero power physics reactor) benchmarks from Argonne. The ENDF/B-VII results are for the beta2 version, but one does not expect significant changes for ENDF/B-VII.0.

Zero Power Reactor assemblies. The k_{eff} calculations by the code VIM for a suite of 26 Argonne ZPR or ZPPR benchmarks are presented in Fig. 45. These benchmarks come from various areas of the ICSBEP Handbook. These benchmarks exhibit large variation in calculated k_{eff}, with the smallest k_{eff} being biased several tenth of a percent below unity while the maximum positive C/E k_{eff} bias is in excess of 3%. Calculated k_{eff} with ENDF/B-VII.0 cross sections are generally an improvement over those obtained with ENDF/B-VI.8, but significant deviations from unity remain.

5.3 Thermal U and Pu Benchmarks

Thermal benchmarks are of considerable interest to reactor applications. Shown below are selected examples for ^{235}U solution benchmarks, fuel rod U benchamrks, and Pu solution as well as MOX benchmarks.

5.3.1 ^{235}U Solution Benchmarks

Thermal, highly enriched ^{235}U homogeneous solution benchmarks were used to test the accuracy of low energy ENDF/B cross section data sets for many years. The new ENDF/B-VII.0 library, like the old ENDF/B-VI.8 library, performs well for these assemblies. C/E values for k_{eff} have been calculated for a suite of critical assemblies from 14 HEU-SOL-THERM (HST) or LEU-SOL-THERM (LST) benchmark evaluations. These benchmarks have most commonly been correlated versus Above-Thermal Leakage Fraction (ATLF), *e.g.*, $k_{\text{calc}}(\text{ATLF}) = b_0 + b_1 * \text{ATLF}$, where ATLF is the net leakage out of the solution of neutrons whose energies exceed 0.625 eV. Smaller systems with large ATLF test the higher energy cross sections, the ^{235}U fission spectrum, elastic scattering angular distributions and, for reflected systems, the slowing down and reflection of above-thermal neutrons back into the fissile solution.

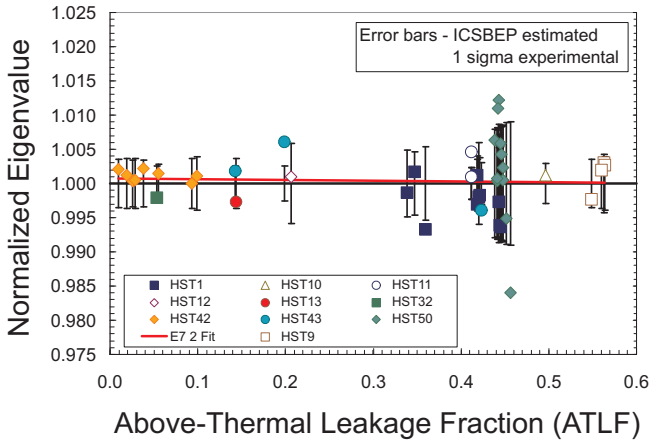

Fig. 46 HEU-SOL-THERM benchmark C/E values for k_{eff} with ENDF/B-VII.0 cross sections.

An important goal in developing the new ENDF/B-VII.0 library was to improve the data files while at the same time retain the good performance seen with ENDF/B-VI.8 (in the homogeneous solution benchmark category). As shown in Fig. 46 this goal has been attained. This result is nontrivial, since we have made changes in the ENDF/B-VII.0 library for ^{16}O (the n,α cross section was significantly reduced) and for hydrogen (a new standard cross section, as well as an updated scattering kernel).

5.3.2 U Fuel Rod Benchmarks

The ^{238}U cross section data in ENDF/B-VII.0 have led to major improvements in the ability to accurately calculate thermal low-enriched uranium benchmark C/E values for k_{eff}. Calculated C/E for k_{eff} for arrays of low-enriched UO_2 fuel rods have histor-

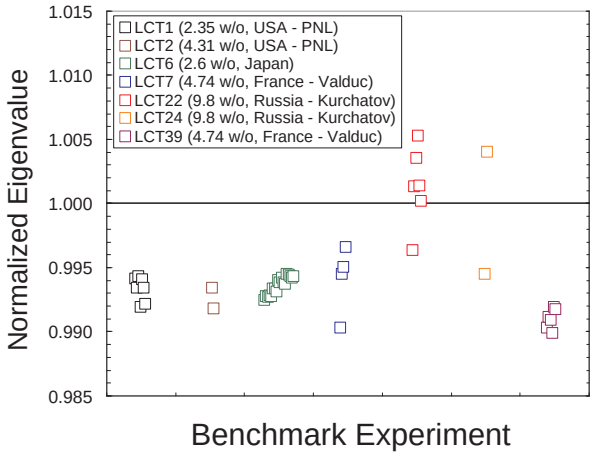

Fig. 47 LEU-COMP-THERM benchmark C/E values for k_{eff} with the old ENDF/B-VI.8 cross sections.

ically been biased with previous data libraries including ENDF/B-VI.8, frequently falling 500 to 1000 pcm below unity. These C/E values have also varied systematically when correlated against parameters such as rod pitch, average fission energy, unit cell H/U ratio or ^{238}U absorption fraction. Some of these characteristics are illustrated in Fig. 47, and 48, which illustrate calculated k_{eff} obtained with MCNP5 and either ENDF/B-VI.8 and/or ENDF/B-VII.0 cross sections.

Results using the new ENDF/B-VII.0 cross sections are significantly more accurate as shown in Fig. 48, which illustrates calculated k_{eff} for the LCT7 benchmark with both ENDF/B-VI.8 and ENDF/B-VII.0 cross sections. The ENDF/B-VI.8 C/E for k_{eff} trend and bias have both been eliminated with the ENDF/B-VII.0 cross section data set.

A summary of all water moderator and reflected LCT k_{eff} reveals that previously identified deficiencies have been largely eliminated. A total of 58 LEU-COMP-THERM benchmarks have been calculated with the ENDF/B-VII.0 cross section data set. The average calculated k_{eff} is 1.0000 with a population standard deviation of 0.0025. This standard deviation represents a significant decrease over that obtained with ENDF/B-VI.8 cross sections and is further evidence for the reduction or elimination in C/E k_{eff} trends, such as versus H/U ratio (Fig. 48), with the ENDF/B-VII.0 cross sections.

The ENDF/B-VII.0 cross section changes that are responsible for the improved C/E k_{eff} are due primarily to (i) ORNL and CEA ^{238}U revisions in the resonance range for ^{238}U, and (ii) the new Los Alamos analysis of ^{238}U inelastic scattering in the fast region. The contribution to the increased calculated criticality of these two revisions are of about the same magnitude. Two additional cross section changes

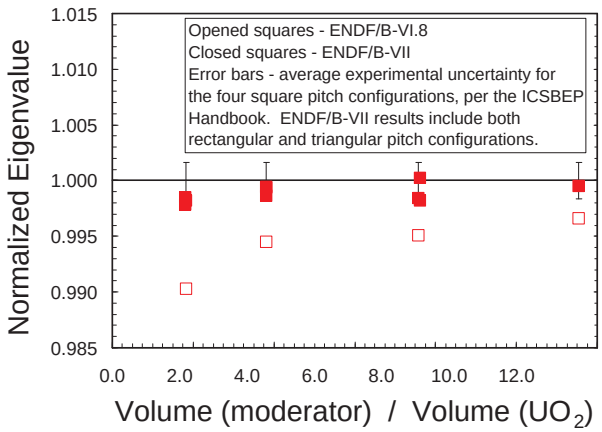

Fig. 48 LEU-COMP-THERM-007 benchmark C/E values for k_{eff} for the ENDF/B-VI.8 and ENDF/B-VII.0 cross sections.

also contributed to increase the calculated k_{eff} of these assemblies: the reduced ^{16}O(n,α) cross section, and a revised scattering kernel for hydrogen bound in water.

5.3.3 Pu Solution and MOX Benchmarks

While excellent calculated k_{eff} results continue to be obtained for thermal uranium solution critical assemblies, the same cannot be said for plutonium solution (PU-SOL-THERM, or PST) assemblies. MCNP5 C/E values for k_{eff}, calculated with ENDF/B-VII.0 cross sections are plotted versus ATLF and versus H/Pu ratio in Figs. 49, 50, respectively. There are obvious variations in these C/E values for k_{eff} when plotted versus ATLF or H/Pu ratio, but it is not obvious what changes in the plutonium cross section evaluation that could also be supported by the underlying microscopic experimental cross section data would mitigate these trends.

The results for a MOX benchmark, six critical configurations from MIX-COMP-THERM-002, show less variation than the solutions, possibly because there are fewer of them. The fuel pins contain 2 wt.% MOX, and the plutonium contains 8% ^{240}Pu. The benchmarks include a highly (several hundred ppm) borated case and a slightly (a few ppm) borated case for each of three lattice pitches. The highly borated cases contain many more fuel pins than the slightly borated cases and exhibit a small positive bias, but all three fall within a band of about a quarter of a percent in reactivity.

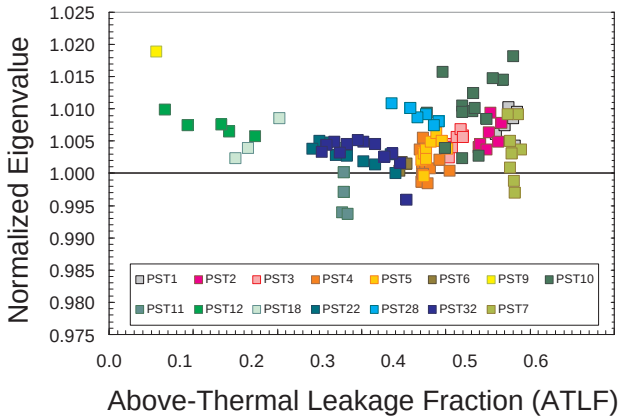

Fig. 49 PU-SOL-THERM benchmark C/E values for k_{eff} with ENDF/B-VII.0 cross sections as a function of the above-thermal leakage fraction.

5.4 Conclusions from Criticality Testing

Hundreds of criticality benchmarks from the ICSBEP Handbook have been calculated to test the accuracy of the ENDF/B-VII.0 cross section library. Significant improvement in C/E values for k_{eff} has been observed in many cases, including bare and reflected fast uranium and plutonium systems and in particular for arrays of low-enriched fuel rod lattices. The C/E values for k_{eff} for bare HEU and Pu assemblies are larger compared to those obtained with ENDF/B-VI.8 data, and now agree very well with the measurements. The reflector bias for the ^{238}U reflected Flattop assemblies has been largely eliminated.

Furthermore, major improvements have been obtained in the calculations for intermediate energy assemblies such as Big-10 and, to a lesser extent, the Argonne ZPR assemblies. Homogeneous uranium solution systems have been calculated accurately with the last several versions of ENDF/B-VI cross sections, and these accurate results are retained with the ENDF/B-VII.0 cross section library. Many fast reflected systems are more accurately calculated with the ENDF/B-VII.0 cross section library, but disturbing discrepancies remain, particularly in lead and beryllium reflected systems (although certain reflector-bias improvements were obtained using the new data for these isotopes).

A significant accomplishment has been excellent C/E for k_{eff} for the LCT assemblies, where the historical underprediction of criticality has been removed. This advance has come from improved ^{238}U evaluation (both in the resonance region and in the fast region), together with revisions to the ^{16}O(n,α) cross section and the hydrogen bound in water scattering kernel. Plutonium solution systems are not cal-

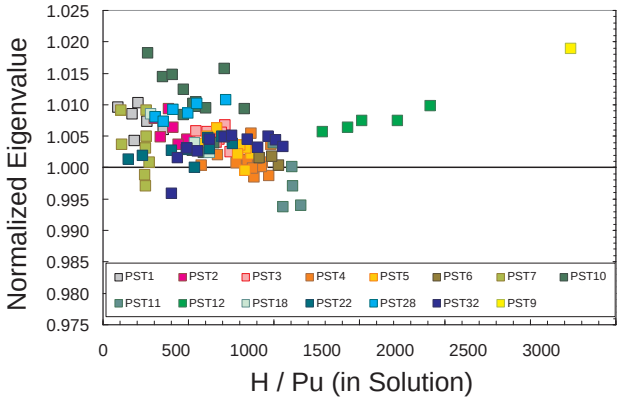

Fig. 50 PU-SOL-THERM benchmark C/E values for k_{eff} with ENDF/B-VII.0 cross sections as a function of the H/Pu ratio.

culated as well as uranium solutions, with C/E values for k_{eff} typically being several tenths of a percent greater than unity. There is a 1.5% spread in these C/E values for k_{eff}, but there does not appear to be a trend as a function of ^{239}Pu abundance. Although advances have been made at Los Alamos to the ^{239}Pu cross sections in the fast region, there has been no recent work on ^{239}Pu at lower energies. Clearly such efforts are needed in the future. Performance of the new ENDF/B-VII.0 evaluations for ^{233}U and ^{232}Th is much improved in both fast and thermal critical assemblies; an analysis of the Np-U composite fast benchmark suggests important improvements have been made in ^{237}Np fission cross section evaluation.

5.5 Delayed Neutron Testing, β_{eff}

Delayed neutron data can be tested against measurements of the effective delayed neutron fraction β_{eff} in critical configurations. Unlike the situation for k_{eff}, only a handful of measurements of β_{eff} have been reported in open literature with sufficiently detailed information. In Ref. [126] more than twenty measurements are listed, including two thermal spectrum cores and five fast spectrum cores:

TCA: A light water moderated low-enriched UO_2 core in the Tank-type Critical Assembly [84].

IPEN/MB-01: A core consisting of 28 $\times$ 26 UO_2 (4.3% enriched) fuel rods inside a light water filled tank [127].

Masurca: Measurements of β_{eff} by several international groups in two unmoderated cores in Masurca (R2 had $\sim$30% enriched uranium, ZONA2 had both pluto-

Table 10 C/E values for β_{eff} of several critical systems, using ENDF/B-VII.0 and other libraries. The uncertainties in the C/E values are statistical uncertainties from the calculations only.

System	C/E β_{eff}			
	ENDF/B-VII.0	ENDF/B-VI.8	JEFF-3.1	JENDL-3.3
TCA	0.998 ± 0.002	1.053 ± 0.011	1.029 ± 0.002	0.987 ± 0.012
IPEN/MB-01	1.008 ± 0.005	1.054 ± 0.005	1.040 ± 0.005	1.019 ± 0.005
Masurca R2	1.012 ± 0.009	1.035 ± 0.009	1.011 ± 0.009	1.018 ± 0.010
Masurca ZONA2	0.973 ± 0.013	0.983 ± 0.015	1.021 ± 0.013	0.994 ± 0.014
FCA XIX-1	0.987 ± 0.010	1.005 ± 0.011	1.010 ± 0.010	0.985 ± 0.011
FCA XIX-2	1.010 ± 0.013	1.003 ± 0.014	1.054 ± 0.013	1.022 ± 0.013
FCA XIX-3	0.981 ± 0.017	1.016 ± 0.016	0.997 ± 0.016	0.996 ± 0.016

nium and depleted uranium), surrounded by a 50-50% UO_2-Na mixture blanket and by steel shielding [128].

FCA: Measurements of β_{eff} in three unmoderated cores in the Fast Critical Assembly (highly enriched uranium; plutonium and natural uranium; plutonium), surrounded by two blanket regions, one with depleted uranium oxide and sodium, the other with only depleted uranium metal [128].

The calculation of β_{eff} for these systems was done using a version of MCNP-4C3 with an extra option added to it as described in Ref. [129]. This method was used earlier to test delayed neutron data from JEFF-3.1 and JENDL-3.3 [130]. The results based on ENDF/B-VII.0 are given in Table 10, as well as the results based on those other libraries. One can see that the calculated β_{eff} now agrees better with experiment as compared to the old ENDF/B-VI.8 (specially for the more thermal systems).

5.6 Reaction Rates in Critical Assemblies

Many different critical assemblies have been developed over the years: Godiva is a bare sphere of highly-enriched uranium (HEU); Jezebel is a bare sphere of plutonium; Jezebel 23 is a bare sphere of ^{233}U. The Flattop experiments involved spherical cores of HEU or plutonium surrounded by ^{238}U reflector material to make the composite systems critical. These different systems all produce neutron spectra within them that are "fast", *i.e.*, the neutrons are predominantly of energies in the 100 keV - few MeV region, but the exact spectra vary from system to system. The neutron spectrum gets softer as one moves out from the center of the assembly, thereby giving additional information about the quality of the cross section data in different energy regimes.

Neutron capture of ^{241}Am is shown in Fig. 51 for different critical assembly spectra. We see good agreement between the calculations and the measurements, except that for the hardest-spectrum system (Jezebel) the measurement appears to be underpredicted by up to 6%. This tells us that the ^{241}Am capture cross section

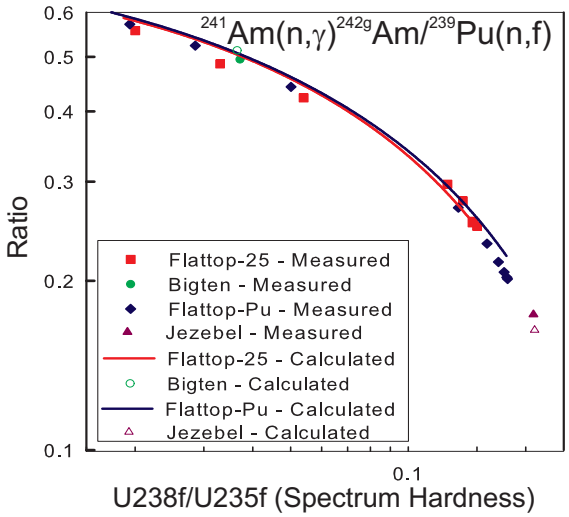

Fig. 51 The integral ^{241}Am neutron capture rate (divided by the ^{239}Pu fission rate) as a function of spectral index for different critical assembly locations. In this case the measurements, which detect the ^{242}Cm, are divided by 0.84 to account for the fraction of ^{242g}Am that beta decays to ^{242}Cm.

to the ground state may be too low in the current evaluation in the $\approx$ 0.5 - 1 MeV region.

5.7 Shielding and Pulsed-sphere Testing

In a paper [126] Steven van der Marck presents extensive data testing results for neutron transmission (shielding) benchmarks. We show some illustrative examples from that paper, focusing on validation benchmarks that test 14 MeV evaluations that have changed between ENDF/B-VI.8 and ENDF/B-VII.0 (*e.g.*, ^{235,238}U, ^{239}Pu, Pb, Li, and Be). These comparisons test the accuracy of the secondary emission spectra of neutrons following nuclear reactions.

Fig. 52 shows an example from the above paper for the FNS (Fusion Neutronics Source) benchmark corresponding to 14 MeV neutrons transmitted through 20 cm lead at an angle of 42.8 degrees. The agreement between simulation and the FNS data is seen to be good, it shows an improvement on the earlier ENDF/B-VI.8 data and provides support for the accuracy of the new ^{208}Pb evaluation.

Numerous high-energy pulsed-sphere experiments [131, 132] have been performed in which small, medium, and large spheres of 32 different materials were pulsed with a burst of high-energy (14 MeV) neutrons at Lawrence Livermore National Laboratory's ICT (Insulated Core Transformer) accelerator facility. Measured time-dependent neutron fluxes at collimated detectors located at a distance of 7 - 10 meters provide a benchmark by which various neutron transport codes and cross-section libraries may be evaluated.

The results can be seen in Fig. 53. The peak on the left hand side corresponds to the transmission of the 14 MeV transmission of source neutrons; the broad peak

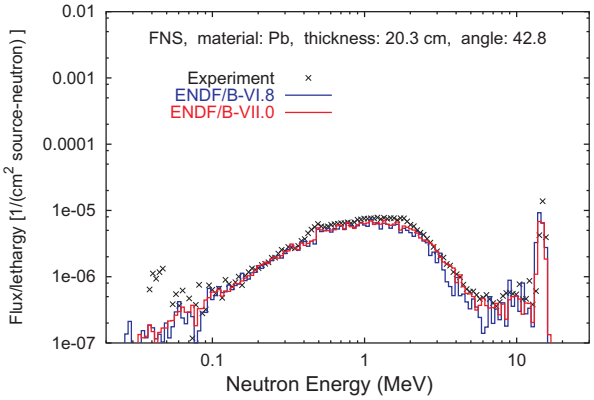

Fig. 52 Simulation of 14 MeV neutron transmission through 20 cm Pb at 42.8 degrees [126].

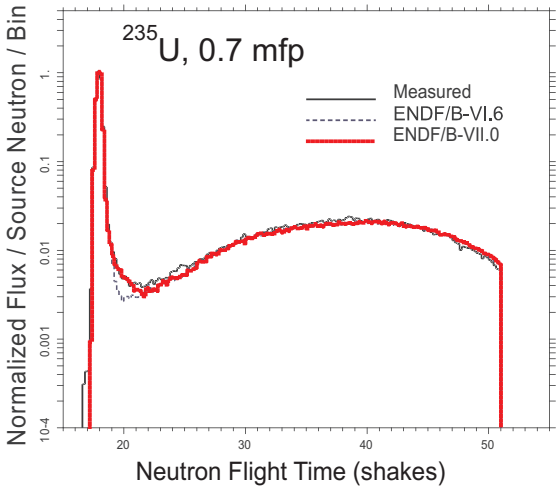

Fig. 53 Comparison of the simulated results using ENDF/B-VI.6 and ENDF/B-VII.0 data for the 0.7 mfp ^{235}U sphere. The experiment used a NE-213 detector biased at 1.6 MeV and located 9.455 m along the 26 degree flightpath. See the footnote for the definition of shake. Note the improved simulation predictions in the minimum region ($E_n \approx 8$ - 12 MeV), where preequilibrium and direct inelastic scattering are present.

further right (lower energies) corresponds to the neutrons created through compound nucleus and fission mechanisms.

Numerous improvements [133, 134, 135, 136] to the simulations have been made since the early implementations of these benchmarks. Simulations were performed by comparing the measured data with calculated results using ENDF/B-VI.6 or ENDF/B-VII.0 data with MCNP for the smallest spheres of ^{235}U, ^{238}U, and ^{239}Pu. With the improvements in the modeling of the pulsed sphere experiments, problems with down-scattering from 14-MeV to the 8-12 MeV energy region had been noted especially for ^{235}U and ^{239}Pu. Recent efforts by Los Alamos National Laboratory to improve the evaluated data for inelastic scattering at these higher incident neutron energies have been incorporated into the ENDF/B-VII.0 evaluations.

As shown in Fig. 53, the ENDF/B-VII.0 library improves the treatment of inelastic scattering for ^{235}U and ^{239}Pu showing much better agreement with the measured data. The improvements in modeling these integral transmission data experiments in the minimum region around 20 shakes[7] can be directly related to the cross section improvements in the fundamental data for an incident energy of 14 MeV and 8-12 MeV emission energies, see Fig. 23.

5.8 Testing of Thermal Values and Resonance Integrals

Important quantities at low neutron energies are thermal capture cross sections and capture resonance integrals. These quantities can be extracted from the ENDF/B-VII.0 files and compared with the data in the recently published Atlas of Neutron Resonances [12].

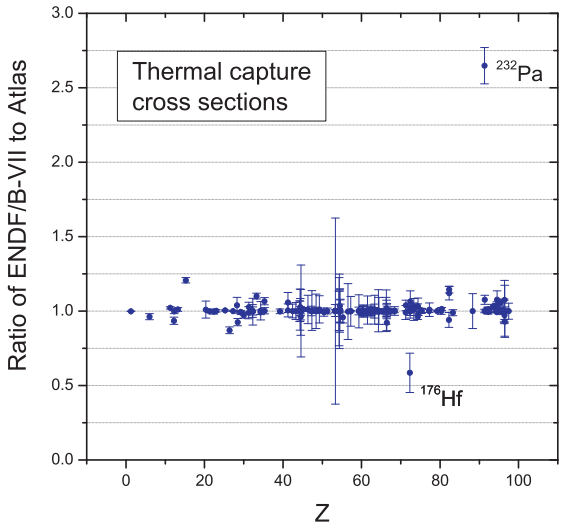

Fig. 54 Thermal neutron capture cross sections in ENDF/B-VII.0 compared to the Atlas of Neutron Resonances [12].

Ratios of capture cross sections at thermal energies are shown in Fig. 54. Overall, there is a fairly good agreement between the values in ENDF/B-VII.0 and the Atlas, although in several instances there are notable discrepancies. The thermal region in ^{232}Pa was revised for ENDF/B-VII.0 by Wright (ORNL) leading to the thermal capture nearly 3 times bigger than the one reported in the Atlas. The origin of this discrepancy is not clear and should be addressed in the future.

Ratios for capture resonances integrals can be seen in Fig. 55. Several comments should be made. Resonance integrals for ^{136}Xe, ^{142}Nd, ^{152}Gd, and ^{232}U: these ratios

[7] A shake is an informal unit of time used in nuclear science, 10^{-8} seconds. The word comes from the expression "two shakes of a lamb's tail" to mean a very short time interval.

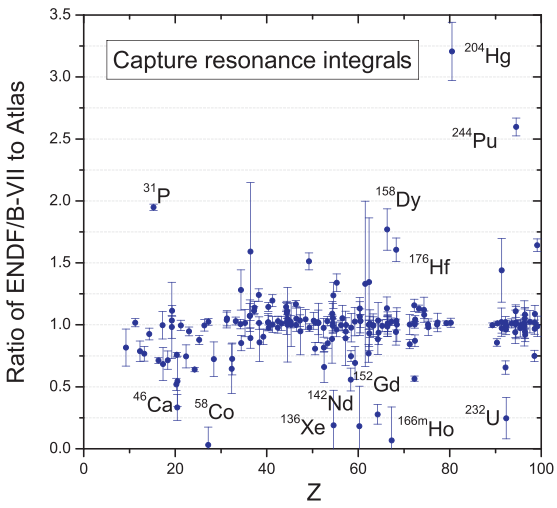

Fig. 55 Neutron capture resonance integrals in ENDF/B-VII.0 compared to the Atlas of Neutron Resonances [12].

deviate from unity since there are inconsistencies between resonance parameters and resonance integral measurements reported in Ref.[12] and the evaluators adopted resonance parameters rather than the experimental integrals. In the extreme case of ^{166m}Ho the experiment is deemed doubtful due to the cadmium cut-off because of the low energy resonance at 0.274 eV. In ^{158}Dy the resolved resonance range is very limited (up to 86 eV) and extrapolation of the unresolved resonance region to such low energies might not be reliable (in particular, the exact position of the lower boundary might play a significant role). The remaining outliers (^{31}P, ^{46}Ca, ^{58}Co, ^{176}Hf, ^{204}Hg, ^{244}Pu) are real discrepancies. These are old evaluations that will have to be updated in future releases of the ENDF/B library.

6 Other Nuclear Data of Interest

Other evaluated nuclear data of interest to nuclear technology applications, primarily to fission reactor applications, are fission yields (also termed fission product yields, FPY), thermal neutron scattering and radioactive decay data.

6.1 Fission Yields

The fission yields from the 1989 LANL evaluation by England and Rides [137] were adopted by ENDF/B-VII.0. In this evaluation fission yield measurements reported in the literature and calculated charge distributions were used to produce a recommended set of yields for the fission products. Independent yields were taken from a

calculated charge distribution model. A Gaussian charge distribution was calculated by using the most probable charge and Gaussian width. The weighted average experimental independent yields, the weighted average experimental cumulative yields, the weighted average experimental cumulative yields and the calculated cumulative yields were combined statistically form a recommended value.

There are two fission product yield sublibraries in ENDF/B-VII.0. Both of them have been taken over from ENDF/B-VII.8 without any change:

- The neutron-induced fission yields sublibrary contains data for 31 actinides. Incident neutron interacts with the target material that undergoes fission which gives rise to extensive number of fission products. There are 31 such target materials, from ^{227}Th to ^{255}Fm; neutron incident energies include the thermal energy of 0.0253 eV, 500 keV and 14 MeV. While for some materials, such as ^{235}U, fission yields are given for all three energies, for many other materials, yields are given only for one or two energies.
- Spontaneous fission yields sublibrary contains 9 materials, ^{238}U, ^{244,246,248}Cm, ^{250,252}CF, ^{253}Es and ^{243,256}Fm. Each of these material undergoes spontaneous fission which again gives rise to extensive set of fission products.

Fission yields can be conveniently retrieved and plotted by Sigma web interface [19] which was developed and continues to be maintained by the NNDC, BNL.

6.2 Thermal Neutron Scattering

In ENDF/B-VII.0 this sublibrary contains 20 evaluations. As described below, seven were reevaluated or updated due to the combined efforts of MacFarlane, Los Alamos, and by Mattes and Keinert, IKE Stuttgart [138]. The remaining evaluations were taken over from the ENDF/B-VI.8 library.

New thermal neutron scattering evaluations were generated by the LEAPR module of the NJOY code [139]. The physical model has been improved over the one used at General Atomics in 1969 to produce the original ENDF/B-III evaluations [140]. The alpha and beta grids have been extended to allow for larger incident energies and to properly represent the features of $S(\alpha,\beta)$ for the various integrations required. The physical constants have been updated for ENDF/B-VII.0 to match the current hydrogen and oxygen evaluations. The changes include additional alpha and beta points, interpolating the rotational energy distributions and translational energies onto the new temperature grid, and slightly reducing the rotational energies to improve the energy region between 0.01 and 0.1 eV.

6.2.1 H_2O and D_2O

H_2O. This evaluation was generated by Mattes and Keinert in 2004 [138]. Water is represented by freely moving H_2O molecule clusters with some temperature de-

pendence to the clustering effect. Each molecule can undergo torsional harmonic oscillations (hindered rotations) with a broad spectrum of distributed modes. The excitation spectra were improved over the older ENDF model, and they are given with a temperature variation. In addition, there are two internal modes of vibration at 205 and 436 meV. The stretching mode was reduced from the older ENDF value of 480 meV to account for the liquid state. Scattering by the oxygen atoms is not included in the tabulated scattering law data. It should be taken into account by adding the scattering for free oxygen of mass 16.

We note that the new H_2O thermal scattering kernel in ENDF/B-VII.0 led to a slight increase in calculated criticality of LEU-COMP-THERM critical assemblies.

D_2O. This was based on the IKE-IAEA-JEFF-3.1 evaluation done by Mattes and Keinert in 2004 [138]. Changes made for ENDF/B-VII include using a more ENDF-like temperature grid and an extension of the α and β grids to improve results for higher incident energies.

6.2.2 O in UO_2 and U in UO_2

Uranium dioxide has a structure similar to fluoride, CaF_2. A lattice dynamical model was developed by Dolling, Cowley, and Woods to fit dispersion curve measurements. In additional to short-range core-core forces, the model includes shell-core, shell-shell, and long-range Coulomb interactions. Weighted frequency distributions were calculated from a dynamical matrix based on this model. The O in UO_2 part is kept separate from the U in O_2 part, and one-fourth of the coherent elastic cross section from the original General Atomics evaluation was included. The various constants were updated to agree with the ENDF/B-VII.0 evaluation of oxygen.

6.2.3 H in ZrH

The lattice dynamics of ZrH were computed from a central force model. The slightly tetragonal lattice of ZrH_2 was approximated by a face-centered-cubic lattice. Four force constants (μ, γ, ν, and δ) were introduced describing respectively the interaction of a zirconium atom with its nearest neighbors (8 H atoms) and its next nearest neighbors (12 Zr atoms), and the interaction of a hydrogen atom with its next nearest neighbors (6 H atoms) and its third nearest atoms (12 H atoms). Eigenvalues and eigenvectors of the dynamical matrix were calculated, and a phonon frequency spectrum was obtained by means of a root sampling technique. Weighted frequency spectra for hydrogen in ZrH were then obtained by appropriate use of the dynamical matrix eigenvectors. The final values of the four force constants were obtained by fitting both specific heat and neutron data. The position of an optical peak observed by neutron scattering techniques to be centered roughly around 0.14 eV determines the constant μ, while the overall width and shape of this peak determine ν and δ, respectively. Existing neutron data are not sufficiently precise to confirm the structure predicted in the optical peak by the central force model. Specific heat data were

used to determine the force constant γ, which primarily determines the upper limit on the phonon energies associated with acoustic modes.

6.2.4 Other modified materials

Liquid methane at 100^oK used the model of Agrawal and Yip as implemented by Picton, modified to include a diffusive component. Solid methane at 22^oK used the model of Picton based on the spectrum of Harker and Brugger. Liquid para and ortho hydrogen at 20^oK were computed with LEAPR. The scattering law is based on the model of Keinert and Sax [141], which includes spin correlations from the Young and Koppel [142] model, diffusion and local hindered motions from an effective translational scattering law based on a frequency distribution, and intermolecular coherence after Vineyard [143].

Data for aluminum are provided for temperatures of 20, 80, 293.6, 400, 600 and 800^oK using frequency distribution of Stedman, Almqvist, and Nilsson [144]. ^{56}Fe was modeled using iron frequency distribution of Brockhouse *et al.* [145].

6.3 Decay Data

The decay data part of the ENDF/B-VII.0 library was produced by Sonzogni (NNDC, BNL) in 2006. This new sublibrary contains 3838 materials and is mostly derived from the Evaluated Nuclear Structure Data File (ENSDF) [146] and the 2005 edition of the Nuclear Wallet Cards [147]. Each material corresponds to the ground state or an isomeric level of a given nucleus. The library provides information for stable and unstable nuclei, from the neutron to ^{283}Rg (Z=111).

For sections of the library corresponding to unstable levels, the half-life, decay modes and energy released during the decay is presented. For stable levels, the only information given is the spin and parity of the level. The energy released can be given with varying degrees of detail. The most basic information includes mean electromagnetic energy (EEM), mean light particle energy (ELP), and mean heavy particle energy (EHP).

For materials whose decay scheme is well known, *i.e.* satisfying that the sum of the average energies for each radiation type is very close to the effective Q-value, the ENSDF database was used and discrete radiation information was provided. In contrast, for materials with unknown or poorly known decay schemes, the Nuclear Wallet Cards database was used. In this case, a simple rule was used to obtain the mean energies. If for instance the level in question undergoes beta decay, it was assumed that EEM and ELP corresponds each to a third of decay Q-value, while the neutrinos take the remaining third. For β-delayed particle emission, it was assumed that the neutrinos carried away a quarter of the available energy and that leptons, baryons and photons took a quarter each.

The measurement of decay characteristics of fission products becomes increasingly difficult as the fission products are further from the valley of stability. Typically, as the β- decay Q-value increases, more weak gamma rays are produced which are difficult to place or simply escape detection. To address this issue, a series of measurements using a ^{252}Cf source and a Total Absorption Gamma Spectrometer (TAGS) were performed at INL, Idaho [148]. Using these data, EEM and ELP values were obtained for 48 materials, which can improve the decay heat predicting power of the library [149]. To obtain the EEM and ELP values from TAGS experiments the evaluator followed the prescription developed by Hagura *et al.* [149], where it is assumed that the decay from excited levels proceeds only by gamma emission, *i.e.*, conversion electrons are neglected. As a result the EEM values is really an upper limit and the ELP a lower one. The effect of electron conversion is expected to be small, less than 10% of EEM. The use of TAGS data in decay data libraries is one of the issues under study by WPEC Subgroup 25 [150].

Additionally, the following features were included:

- Internal conversion coefficients were calculated for all gamma rays of known multipolarity using the code BRICC [151].
- For ^{36}Cl, ^{59}Fe, ^{99}Tc, ^{129}I and ^{137}Cs average β- energies for second forbidden non-unique transitions were calculated using the code SPEBETA [152].
- Theoretical β- decay half-lives and β-delayed neutron emission probabilities (P_n) using the Kratz-Hermann systematics *et al.* [77] were used for some neutron rich nuclides which were produced in the fission of ^{235}U and ^{239}Pu with limited experimental $T_{1/2}$ or P_n information.

6.3.1 Decay heat calculations

A plot of the decay heat following a fission event of ^{235}U can be seen in Fig. 56. The total decay heat is separated into two components, electromagnetic and light particles. The former includes gamma and X-rays, while the latter includes electrons from β- decay as well conversion and Auger electrons. A heavy particle component, including neutrons and alphas is negligible. The data come from the 1989 compilation of Tobias [153]. The effect of the TAGS data is clearly visible. Without including it, many unmeasured weak gamma rays would be missing due to incomplete decay schemes, resulting in artificially high values of electron and neutrino mean energies as well as artificially low values of mean gamma energies.

The JEFF-3.1 decay data library was released in 2005 (correction to TAGS not yet introduced) and shares a similar spirit and scope with the ENDF/B-VII.0 decay data library. One possible way of comparing both libraries would be to plot decay heats without TAGS data for ^{235}U. This is shown in Fig. 57 and, as expected, both libraries give very similar results under this condition.

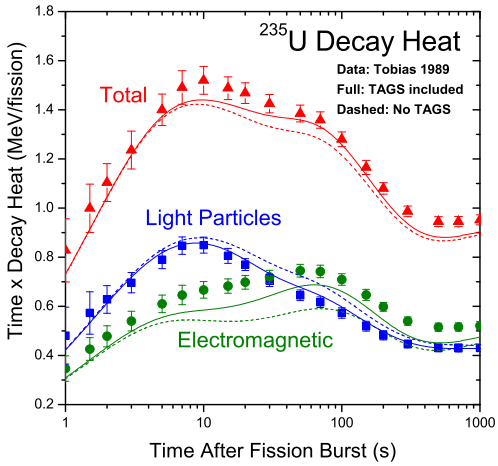

Fig. 56 Decay heat per fission for a ^{235}U sample as a function of time. Shown is the total decay heat and its two components (light particles, electromagnetic).

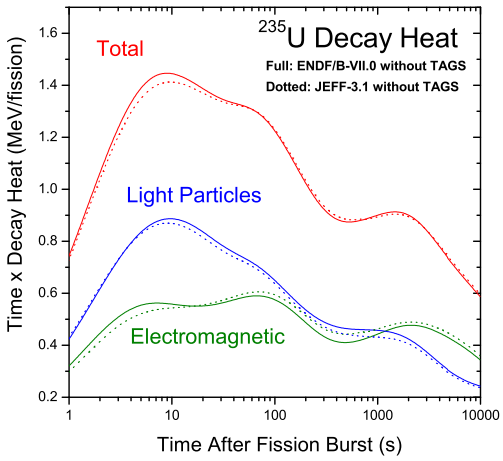

Fig. 57 Decay heat per fission for a ^{235}U sample as a function of time using the ENDF/B-VII.0 and the JEFF-3.1 decay data without TAGS data.

7 Evaluated Nuclear Data Libraries

There are numerous evaluated nuclear data libraries available from various nuclear data centers. National interests and different applications are the two principal factors causing this variety. Countries with strong nuclear program, such as US, European Union, Japan, Russia and China, develop their own general purpose libraries to maintain evaluation expertise and ensure technological independence.

On the other hand, various applications of nuclear technology require special purpose libraries that satisfy particular needs of a given application. These derived libraries add another class to that mentioned above. One should also take into account various versions (releases) of the major libraries. Frequent sharing of evaluations among different libraries, often with some modifications, makes this picture even more complicated.

7.1 Overview of Libraries

A brief overview of evaluated nuclear data libraries should assist users to make the right choice for their application. It should be understood that there is internal dynamics in data development. Therefore, users should always consult webpages of the most prominent data centers to make sure that the library they are interested in is the latest version available.

7.1.1 General Purpose Libraries

General purpose libraries are not limited to any specific application and they are meant to satisfy broad class of users. In practice, though, they often started as libraries for reactor applications.

Evaluations in a general purpose library are usually most complete in terms of physical quantities and nuclear reactions. They have to be suitable for transport calculations and as such have to fulfill quite strict requirements regarding completeness and consistency. Thus, neutron evaluations have to cover thermal, resolved and unresolved resonance as well as fast neutron ranges extending at least up to 20 MeV, contain all major reaction channels, provide cross sections and possibly angular distributions, energy-angle correlated cross sections, and photon production data. Internal consistency implies that individual cross sections must sum up to the total cross section and the integrals of emission spectra correspond to the respective reaction cross sections.

Typically, the general purpose libraries are extensively validated against integral measurements. Sometimes, results of these integral measurements are incorporated into a library. This procedure introduces implicit correlations between various reactions and materials causing such a libray to become an entity, rather than a simple collection of individual evaluations.

Major general purpose libraries are maintained by the following countries:

1. USA – ENDF/B-VII.0, released in 2006; new version is expected in 2011,
2. Europe – JEFF-3.1, released in 2005; new version is expected in 2010,
3. Japan – JENDL-3.3, released in 2002; JENDL-4 is expected in 2010,
4. Russia – BROND-2.2, released in 1992; BROND-3 hast not been completed yet, it is partly available in the selected evaluations of ROSFOND which was released in 2008,

5. China – CENDL-2, released in 1991; CENDL-3 was developed but not internationally released; development of CENDL-4 is underway.

Over the first decade of the 21^{st} century three evaluated data libraries (ENDF/B, JEFF, and JENDL) have been continuously updated and improved. These libraries will be briefly summarized later in this Section.

7.1.2 Special Purpose Libraries

The special purpose libraries address particular exigencies of certain applications. Typical examples of such libraries are:

- International Reactor Dosimetry File, IRDF [154]
- European Activation File, EAF [155],
- Standards neutron cross section library [156], and
- Fusion Evaluated Nuclear Data Library, FENDL [157].

Evaluations in these libraries are not as comprehensive as those in the general purpose libraries but excel in certain features that would be impractical or too costly to be implemented in the general purpose files.

For example, activation library does not have to cover the full energy range, does not require spectra and angular distributions but does need to provide cross sections for the reactions leading to the radioactive products. Often, these are meta-stable states that are rarely considered in the general purpose libraries. There is no internal consistency requirement, but the amount of materials in the activation library is usually far larger than in the general purpose libraries.

The dosimetry libraries are similar to the activation ones but cover very limited number of well known reactions that are used for determination of neutron spectra. Cross section covariances are critical for spectra deconvolution and are mandatory in the dosimetry libraries.

On top of this pyramid are libraries of standards that include cross sections and covariances for an even smaller number of reactions that are known to a very high accuracy. The evaluation of standards is particularly thorough and is predominantly based on detailed analysis of precise experimental data. Since standards are used as reference in many measurements they are a potential source of correlations among seemingly independent experiments. Therefore, cross-correlations among standards cross sections are required in the standards library. These libraries provide by far most accurate and reliable data but their coverage is very fragmentary.

Another type of special purpose libraries are those which are created as a selection of evaluations from various major libraries to better serve particular application. The prominent example is FENDL [157], the international library compiled under auspices of the IAEA in support of the fusion programme.

Some examples of special purpose libraries:

IRDF-2002: The International Reactor Dosimetry File [154] is a standardized, updated, and benchmarked evaluated cross section library of neutron dosimetry

reactions with uncertainty information for use in lifetime management assessments of nuclear power reactors and other neutron metrology applications such as boron neutron capture therapy, therapeutic use of medical isotopes, nuclear physics measurements, and reactor safety applications. It contains damage cross sections, decay data, standard spectra, and dosimetry cross sections in ENDF-6 pointwise and groupwise representation. Development of IRDF-2002 was coordinated by IAEA during 2001-2004.

INDL/TSL: An improved set of thermal neutron scattering law data prepared for 10 elements/compounds in 2004-2006 by M. Mattes and J. Keinert under auspices of the IAEA.

IAEA-Standards, 2006: The most respected international library of neutron cross section standards [156]. It contains data for 9 reactions including covariances. The library relies on a very careful evaluation of the selected set of most precise and reliable experiments. ENDF/B-VII.0 adjusted its neutron sublibrary to these cross sections and the whole set is available in its standards sublibrary.

EAF-2003: The Europen Activation File [158] is the most extensive library of neutron activation cross sections. It contains 12 617 excitation functions on 774 different targets from ^{1}H to ^{257}Fm stored in the extended ENDF-6 format (EAF format). The ENDF-6 formatted version is included as JEFF-3.1/A sublibrary in the general purpose library JEFF-3.1.

EAF-2007: Extension of the European Activation File to proton- and deuteron-induced reactions [155] in addition to the traditional neutron-induced data [158]. The deuteron-induced library contains 66,864 reactions, while the proton-induced library contains 67,925 reactions. The library makes extensive use of model calculations with the TALYS code [159].

JENDL/AC-2008: The JENDL Actinoid File 2008 is a consistent set of new evaluations for 79 actinides ($89 \leq Z \leq 100$) released in 2008 with the intention of being included in JENDL-4.

MINSK: The library of original evaluations for 17 actinides developed by Maslov *et al.* (Minsk, Belarus) between 1995 and 2003. it contains data for isotopes of Th, Pa, U, Np, Pu, Am, and Cm.

MENDL-2: The neutron reaction data library for nuclear activation and transmutation at intermediate energies developed by Shubin (IPPE Obninsk) *et al.* around 1995-98. It contains production cross-sections for the formation of radioactive product nuclides for incident neutrons with energies up to 100 MeV. The 505 nuclides included cover the range from ^{26}Al to ^{210}Po with half-lives larger than one day.

ENDF/HE-VI: The high-energy library developed by S. Perlstein (BNL) and T. Fukahori (JAERI) in 1990's containing neutron and proton data for ^{12}C, ^{56}Fe, ^{208}Pb, and ^{209}Bi up to 1000 MeV.

7.1.3 Derived Libraries

Derived libraries are obtained from the libraries discussed above by processing them with a dedicated computer code such as NJOY [160]. In most cases this processing is carried out to reconstruct cross sections in the resonance region, perform their Doppler broadening at a given temperature (pointwise representation) and to provide averages over certain energy intervals (groupwise representation). Derived libraries are generally needed for transport calculations (*e.g.*, ACE libraries used in the Monte Carlo MCNP code [161]).

The derived libraries may also be adjusted to reproduce particular set of integral experiments. In most cases such adjustment is performed on the groupwise library and is targeting very well defined application such as sodium cooled fast reactors. The performance of the adjusted library is superior when it is used for the intended application but it might be poor for other applications. This is a consequence of the selection of integral experiments and adoption of energy-group structure that are tailored for the intended application.

7.2 ENDF-6 Format

Use of the ENDF-6 format is common for most of the evaluated nuclear data libraries. Only some of the activation and derived libraries deviate from this standard. Otherwise, all major libraries are using ENDF-6 format that has been accepted internationally. This unification had a great impact on the world-wide cooperation, greatly facilitated by exchanging files between the national libraries and easy comparison of the data.

The ENDF format has been developed by the Cross Section Evaluation Working Group (CSEWG) and it is maintained by the National Nuclear Data Center. The work started in 1966, the first version was released in 1968, and then in 1970, 1972, 1975, 1979 and 1990 along with the subsequent releases of the US ENDF library. The current version, ENDF-6 [2], has been used for both the ENDF/B-VI and ENDF/B-VII library implying that new version of the format has not been developed for the ENDF/B-VII. We note that to differentiate it from the library which is denoted with Roman numerals (say, ENDF/B-VI), the ENDF format is always denoted with the Arabic numeral (ENDF-6).

For historic reasons, the ENDF-6 format uses 80-character records conforming to the old-fashioned versions of FORTRAN. It is organized in a strict hierarchical structure. Any library is a collection of material evaluations from a recognized evaluation group. It is divided into sub-libraries that distinguish between different incident particles and types of data, namely neutron induced reactions, proton induced reactions, thermal scattering data, fission yields, decay data, *etc*. The sublibraries contain the data for different materials identified by MAT numbers. Each material evaluation contains data blocks referred to as “Files” and denoted with MF numbers.

File 1: MF=1 is the descriptive part of the numerical file with details of evaluation, it also contains $\bar{\nu}$ values.

File 2: MF=2 contains neutron resonance parameters. Neither thermal constants, nor cross sections in the resonance region are provided, these are reconstructed from resonance parameters by processing codes.

File 3: MF=3 contains cross sections. The minimum required energy range for neutron reactions is from the threshold or from 10^5 eV up to 20 MeV, but higher energies are allowed. There is a section for each important reaction or sum of reactions. The reaction MT-numbers for these sections are chosen based on the emitted particles.

Files 4-6: Energy and angle distributions for emitted neutrons and other particles or nuclei. File 4 is used for simple two-body reactions (elastic, discrete inelastic). Files 4 and 5 are used for simple continuum reactions, which are nearly isotropic and emit only one important particle. File 6 is used for more complex reactions that require energy-angle correlation, that are important for heating or damage, or that have several important products, which must be tallied.

Files 8-10: If any of the reaction products are radioactive, they should be described further in File 8. This file indicates how the production cross section is to be determined (from File 3, 6, 9 or 10) and gives minimal information on the further decay of the product. Additional decay information can be retrieved from the decay data sub-library when required. Branching ratios (or relative yields) for the production of different isomeric states of a radionuclide may be given in File 9. Alternatively, radionuclide isomer-production cross sections can be given in File 10.

Files 12-15: For compatibility with earlier versions, photon production and photon distributions can be described using File 12 (photon production yields), File 13 (photon production cross sections), File 14 (photon angular distributions), and File 15 (photon energy distributions). File 12 is preferred over File 13 when strong resonances are present (capture, fission).

Files 30-40: Covariance data are given in Files 30-40, with $\bar{\nu}$ covariances in File 31, resonance parameter covariances in File 32, and cross section covariances in File 33.

A concise list of basic definitions and constants used in the ENDF-6 format is given in Tab. 11. For detailed description we refer to the extensive manual [2].

7.3 ENDF/B-VII.0 (United States, 2006)

The ENDF/B-VII.0 library , released by the U.S. Cross Section Evaluation Working Group (CSEWG) in December 2006, contains data primarily for reactions with incident neutrons, protons, and photons on almost 400 isotopes, based on experimental data and theory predictions. The new library plays an important role in nuclear technology applications, including transport simulations supporting national security, nonproliferation, advanced reactor and fuel cycle concepts, criticality safety,

Table 11 ENDF-6 Format: Selected Definitions and Constants. See [2] for more details .

File	Section	Quantity
MF=1		General information
MF=1	MT=451	Description of the evaluation
	MT=452	Average number of neutrons per fission, $\bar{\nu}$ ($\bar{\nu} = \bar{\nu}_d + \bar{\nu}_p$)
	MT=455	Average number of delayed neutrons per fission, $\bar{\nu}_d$
	MT=456	Average number of prompt neutrons per fission, $\bar{\nu}_p$
	MT=458	Energy release in fission for incident neutrons
	MT=460	β-delayed photon spectra
MF=2		Resonance parameters
MF=2	MT=151	Resolved resonance parameters, flag LRU=1
	MT=151	Unresolved resonance parameters, flag LRU=2
MF=3		Reaction cross sections
MF=3	MT=1	Total cross sections
	MT=2	Elastic cross sections
	MT=4	Sum of all inelastic cross sections
	MT=5	Sum of cross sections for all reaction channels not given explicitly under other MT numbers
	MT=16	(n,2n) cross sections
	MT=17	(n,3n) cross sections
	MT=18	(n,xf) total fission cross sections
	MT=19	(n,f) first chance fission cross sections
	MT=20	(n,nf) second chance fission cross sections
	MT=21	(n,2nf) third chance fission cross sections
	MT=22	(n,n'α) cross sections
	MT=28	(n,n'p) cross sections
	MT=51	(n,n'$_1$) cross sections (inelastic scattering to the 1^{st} excited level)
	MT=52	(n,n'$_2$) cross sections (inelastic scattering to the 2^{nd} excited level)
	MT=91	(n,n'$_{cont}$) cross sections (inelastic scattering to continuum)
	MT=102	(n,γ) cross sections
	MT=103	(n,p) cross sections
	MT=105	(n,t) cross sections
	MT=107	(n,α) cross sections
	MT=601	(n,p$_1$) cross sections for the (n,p) reaction leaving residual nucleus in the 1^{st} excited level
	MT=600	(n,p$_0$) cross sections for the (n,p) reaction leaving residual nucleus in the ground state
	MT=801	(n,α_1) cross sections for the (n,α) reaction leaving residual nucleus in the 1^{st} excited level
MF=4		Angular distributions of emitted particles expressed as normalized probability distributions
MF=4	MT=2	Angular distributions for elastic scattering
	MT=51	Angular distributions for inelastic scattering to the 1^{st} excited level
MF=5		Energy distributions (spectra) of emitted particles expressed as normalized probability distributions
MF=5	MT=16	Spectra of emitted neutrons, photons and recoils for the (n,2n) reaction (neutron spectra contain both cascading neutrons)
MF=6		Energy-angle distributions of emitted particles (for a given reaction should contain subsections for all reaction products including γ's and recoils)
MF=6	MT=5	Energy-angle distributions of products for all reactions lumped into MT=5 (reactions are identified by the residual nuclei)
	MT=91	Energy-angle distributions of continuum neutrons (only those neutrons that were not followed by any other particle emission are counted)
	MT=28	Energy-angle distributions of neutrons, protons, residual nuclei and photons emitted in the (n,n'p) reaction
MF=7		Thermal neutron scattering on moderating materials
MF=7	MT=2	Elastic thermal neutron scattering
	MT=4	Inelastic thermal neutron scattering
MF=8		Decay data and fission-product yields
MF=8	MT=454	Independent fission product yields
	MT=459	Cumulative fission product yields
	MT=457	Radioactive decay data
MF=9		Multiplicities for production of radioactive nuclei (activation/isomeric cross sections expressed as a fraction of the respective cross sections in MF=3)
MF=10		Absolute cross sections for production of radioactive nuclei (similar to MF=9 but without reference to MF=3)
MF=12		Multiplicities for photon production and branching ratios for γ transitions between discrete levels (respective cross sections in MF=3 must be used for absolute values)

File	Section	Quantity
MF=13		Absolute photon spectra and photon production cross sections (similar to MF=12 but without reference to MF=3)
MF=14		Angular distributions for discrete and continuum photons
MF=15		Energy spectra for continuum photons (normalized distributions to be multiplied by the respective cross sections in MF=3)
MF=23		Electromagnetic interaction cross sections (such as total, coherent and incoherent (Compton) elastic scattering for photons and elastic scattering, brehm--sstrahlung and ionization for electrons)
MF=23	MT=501	Total cross section for incident photons
	MT=502	Photon coherent scattering cross section
	MT=516	Pair production cross section
	MT=522	Photoelectric absorption cross section
	MT=527	Electro-atomic brehmsstrahlung cross section
MF=26		Spectra and angular distributions of photons and electrons emitted in inter--action of photons or electrons with atoms
MF=27		Atomic form factors or scattering functions for angular distribution of photons
MF=28		Atomic relaxation data (emission of X-rays and electrons from ionized atoms)
MF=31		Covariances for nubar ($\bar{\nu}$)
MF=32		Covariances for resonance parameters
MF=33		Covariances for cross sections
MF=33	MT=1	Covariances for total cross sections
	MT=2	Covariances for elastic cross sections
	MT=851-870	Covariances for cross sections of lumped channels
MF=34		Covariances for angular distributions of emitted particles
MF=35		Covariances for energy spectra of emitted particles
MF=40		Covariances for activation cross sections

NLIB	Library	Full name
0	ENDF/B	US Evaluated Nuclear Data File
1	ENDF/A	US Evaluated Nuclear Data File for preliminary or incomplete evaluations
2	JEFF	Joint European evaluated File
3	EFF	European Fusion File (now in JEFF)
4	ENDF/HE	US High Energy file
5	CENDL	Chinese Evaluated Nuclear Data Library
6	JENDL	Japanese Evaluated Nuclear Data Library
21	IFPL	NEA International Fission Product Library
33	FENDL	IAEA Fusion Evaluated Nuclear Data Library
34	IRDF	IAEA International Reactor Dosimetry File
37	FENDL/A	FENDL Activation file
41	BROND	Russian Biblioteka (library) of Recommended Neutron Data

Symbol	Definition	Recommended value
m_n	neutron mass	1.008 664 916 amu
m_e	electron mass	$5.485\,799\,110 \times 10^{-4}$ amu
m_p	proton mass	1.007 276 467 amu
m_d	deuteron mass	2.013 553 213 amu
m_t	triton mass	3.015 500 713 amu
m_h	^{3}He mass	3.014 932 244 amu
m_α	α-particle mass	4.001 506 179 amu
amu	atomic mass unit	$931.494\,013 \times 10^6$ eV
e	elementary charge	$1.602\,176\,462 \times 10^{-19}$ C
h	Planck's constant	$4.135\,667\,27 \times 10^{-15}$ eV s
$\hbar/2\pi$	Planck's const./2π	$6.582\,118\,89 \times 10^{-16}$ eV s
k	Boltzmann's constant	$8.617\,342 \times 10^{-5}$ eV/K
c	Speed of light	299 792 458 m/s
N_A	Avogadro's number	$6.022\,141\,99 \times 10^{23}$ 1/mol

fusion, medicine, space applications, nuclear astrophysics, and nuclear physics facility design.

Major releases of the US ENDF/B library are summarized in Table 12. After an initial two-year release cycle, CSEWG moved to ever longer release cycles. Recent releases occurred at widely-spaced intervals: ENDF/B-V was released in 1978, ENDF/B-VI in 1990, followed by this ENDF/B-VII.0 release in 2006. However, interim releases have occurred more frequently and ENDF/B-VI had upgrades embodied in eight releases, the last one occurring in October 2001 and referred to as ENDF/B-VI.8 [162].

Table 12 Major releases of the ENDF/B library of the United States. The library is maintained by the Cross Section Evaluation Working Group, CSEWG, established in 1966.

ENDF/B	I	II	III	IV	V	VI	VII
Year	1968	1970	1972	1974	1978	1990	2006

7.3.1 Overview of the ENDF/B-VII.0 Library

The ENDF/B-VII.0 library contains 14 sublibraries, summarized in Table 13 according to the identification number NSUB. The number of materials (isotopes or elements) are given for both the new (VII.0) and previous (VI.8) versions of the ENDF/B library. Although the ENDF/B library is widely known for evaluated neutron cross sections, it also contains a considerable amount of non-neutron data.

Out of the total of 14 sublibraries, there are two new sublibraries; 7 sublibraries were considerably updated and extended, and the remaining 5 sublibraries were taken over from ENDF/B-VI.8 without any change:

1. The photonuclear sublibrary is new; it contains evaluated cross sections for 163 materials (all isotopes) mostly up to 140 MeV. The sublibrary has been supplied by Los Alamos National Laboratory (LANL) and it is largely based on the IAEA-coordinated collaboration completed in 2000 [163].
2. The photo-atomic sublibrary has been taken over from ENDF/B-VI.8. It contains data for photons from 10 eV up to 100 GeV interacting with atoms for 100 materials (all elements). The sublibrary has been supplied by Lawrence Livermore National Laboratory (LLNL).
3. The decay data sublibrary has been completely re-evaluated and considerably extended by the National Nuclear Data Center, BNL.
4. The spontaneous fission yields were taken over from ENDF/B-VI.8. The data were supplied by LANL.
5. The atomic relaxation sublibrary was taken over from ENDF/B-VI.8. It contains data for 100 materials (all elements) supplied by LLNL.

Table 13 Contents of the ENDF/B-VII.0 library, with ENDF/B-VI.8 shown for comparison. NSUB stands for the sublibrary number, given in the last two columns are the number of materials (isotopes or elements).

No.	NSUB	Sublibrary name	Short name	ENDF/B- VII.0 materials	ENDF/B-VI.8 materials
1	0	Photonuclear	g	163	-
2	3	Photo-atomic	photo	100	100
3	4	Radioactive decay	decay	3838	979
4	5	Spontaneous fission yields	s/fpy	9	9
5	6	Atomic relaxation	ard	100	100
6	10	Neutron	n	393	328
7	11	Neutron fission yields	n/fpy	31	31
8	12	Thermal scattering	tsl	20	15
9	19	Standards	std	8	8
10	113	Electro-atomic	e	100	100
11	10010	Proton	p	48	35
12	10020	Deuteron	d	5	2
13	10030	Triton	t	3	1
14	20030	^{3}He	he3	2	1

6. The neutron reaction sublibrary represents the heart of the ENDF/B-VII.0 library. The sublibrary has been considerably updated and extended, it contains 393 materials, including 390 isotopic evaluations and 3 elemental ones (C, V and Zn). These evaluations can be considered to be complete[8] since they contain data needed in neutronics calculations. Important improvements were made to the actinides by LANL, often in collaboration with ORNL. Evaluations in the fission product range (Z = 31 - 68) have been entirely changed. Of the 393 materials, about 2/3 of the evaluations are based upon recent important contributions from the U.S. evaluators. The remaining evaluations were adopted from other sources (mostly the JENDL-3.3 library). LLNL provided β-delayed γ-ray data for ^{235}U and ^{239}Pu, for the first time in ENDF/B.
7. Neutron fission yields were taken over from ENDF/B-VI.8. The data were supplied by LANL.
8. The thermal neutron scattering sublibrary contains thermal scattering-law data, largely supplied by LANL, with several important updates and extensions [138]).
9. The neutron cross section standards sublibrary is new. Although standards traditionally constituted part of the ENDF/B library, in the past these data were stored on a tape. As the concept of tapes has been abandoned in ENDF/B-VII.0 the new sublibrary (short name *std*, sublibrary number NSUB = 19), has been introduced. Out of 8 standards materials, 6 were newly evaluated, while the ^{3}He(n,p) and ^{nat}C(n,n) standards were taken over from ENDF/B-VI.8. The standard cross sections were adopted by the neutron reaction sublibrary except for the thermal cross section for ^{235}U(n,f) where a slight difference occurs to satisfy thermal data

[8] The only exception is ^{253}Es that contains (n,γ) dosimetry cross sections.

testing. These new evaluations come from the international collaboration coordinated by the IAEA [156].
10. The electro-atomic sublibrary was taken over from ENDF/B-VI.8. It contains data for 100 materials (all elements) supplied by LLNL.
11. The proton-induced reactions were supplied by LANL, the data being mostly to 150 MeV. There are several updates and several new evaluations.
12. The deuteron-induced reactions were supplied by LANL. This sublibrary contains 5 evaluations.
13. The triton-induced reactions were supplied by LANL. This sublibrary contains 3 evaluations.
14. Reactions induced with ^{3}He were supplied by LANL. This sublibrary contains 2 evaluations.

7.3.2 Processing and Data Verification

The ENDF/B-VII.0 library was issued in its basic format defined by the ENDF-6 Formats Manual [2]. For practical applications the library must be processed so that basic data are converted into formats suitable as input for applied codes such as the Monte Carlo transport code MCNP and the reactor licensing code SCALE [122]. Recommended processing codes:

- Los Alamos code NJOY-99 [160, 164] , to be obtained from RSICC [165] or NEA Data Bank [166], with patches available at the LANL T-2 webpage [167].
- Two codes are available for processing of covariance data, ERRORJ [168] – since recently a part of the NJOY package, and PUFF [169] – a module of the Oak Ridge processing code AMPX [170].

Data verification was performed by the National Nuclear Data Center, BNL:

- Checking the library by ENDF-6 utility codes (CHECKR, FIZCON, PSYCHE) [171] for possible formatting problems and inconsistencies in physics.
- Processing of photonuclear, neutron, thermal scattering and proton sublibraries by NJOY-99 to ensure that a processed library suitable for neutronics calculations can be produced.
- Use of the processed files by the Monte Carlo codes MCNP [161] and MCNPX [172] in simple neutronics test to ensure that neutronics calculations can be performed.
- Processing of covariance data to ensure that multigroup data for applied calculations can be produced.

Data validation is a complex process described earlier in this chapter. CSEWG used continuous energy Monte Carlo transport codes and validation focused on the neutron reaction and thermal neutron scattering sublibraries. These are the best validated sublibraries. The neutron standards sublibrary contains a special category of data where the highest quality was achieved. The photonuclear sublibrary was subject to partial validation, and the decay data sublibrary went through some limited

testing. The remaining 9 sublibraries were not included in the ENDF/B-VII.0 validation process.

7.4 JEFF-3.1 (Europe, 2005)

The Joint Evaluated Fission and Fusion (JEFF) Project is a collaborative effort among the European member countries of the NEA Data Bank. The initial objective was to improve performance for existing reactors and fuel cycles. More recently, the goal is to provide users with a more extensive set of data for a wider range of applications, including innovative reactor concept (Gen-IV), transmutation of radioactive waste, fusion, and medical applications. These data include neutron- and proton-induced reactions, radioactive decay, fission yields, thermal scattering law and photo-atomic interactions.

The JEFF-3.1 version of the library was released in May 2005, for summary description see JEFF Report 19 [18]. The library combines the efforts of the JEFF and EFF/EAF (European Fusion File/European Activation File) working groups. The neutron general purpose sublibrary contains 381 materials from ^{1}H to ^{255}Fm. The activation sublibrary is based on the EAF-2003 and contains cross sections for neutron reactions on 774 targets; radioactive decay sublibrary contains 3 852 isotopes of which only 226 are stable; proton sublibrary covers 26 materials from ^{40}Ca to ^{209}Bi; thermal scattering law sublibrary includes 9 materials; neutron-induced-fission-yield sublibrary covers 19 isotopes from ^{232}Th to ^{245}Cm, and spontaneous-fission-yield sublibrary contains ^{242,244}Cm and ^{252}Cf.

The JEFF-3.0 library was upgraded mainly because of underprediction of the reactivity for low-enriched uranium systems relevant to light water reactors. The reactivity issue was linked to the ^{238}U cross sections and the improved evaluation was assembled as a result of the broad international effort. Transport calculations proved that the predictions of this reactivity was appreciably improved.

New evaluations or major revisions were performed for Ti sotopes (IRK Vienna), Ca, Sc, Fe, Ge, Pb, and Bi isotopes (NRG Petten), ^{103}Rh, ^{127,129}I, Hf isotopes, ^{236,237,238}U and ^{214}Am (CEA). For other isotopes, more recent evaluations from other libraries were adopted. Revised thermal scattering data have been produced for all important moderator and structural materials.

The JEFF project put considerable effort to validation of the library, which was done particularly carefully from the point of view of nuclear reactor applications. The overall performance of the library is excellent.

7.5 JENDL-3.3 (Japan, 2002)

JENDL-3.3 is the Japanese evaluated library which was released in 2002, see the summary paper by Shibata *et al.* [173]. The library is largely based on evaluations

that originated in Japan, thus representing probably the most extensive source of independent evaluations, just after the US effort.

The objective of the JENDL effort is to supply Japanese evaluated data for fast breeder reactors, thermal reactors, fussion neutronics and shielding calculations, as well as other applications. The JENDL-3.3 library contains data for 337 materials, from 10^{-5} to 20 MeV. Major issues in the previous version of the library, JENDL-3.2, were addressed: overestimation of criticality values for thermal fission reactors was improved by the modification of fission cross sections and fission neutron spectra for ^{235}U; incorrect energy distributions of secondary neutrons from important heavy materials were replaced by the statistical model results; inconsistency between elemental and isotopic evaluations were removed for medium-heavy nuclides.

JENDL-3.3 also contains covariances for 20 most important materials. Of them, 16 materials have been originally developed for JENDL-3.2 covariance file, made available in March 2002 [174] and adopted shortly afterwards with minor modifications by JENDL-3.3. Additional three materials were produced for JENDL-3.3, while the dosimetry material ^{55}Mn was taken over. The list of resulting 20 materials includes actinides, structural materials and light nuclides, which are of interest primarily for fast reactor applications:

- ^{1}H, ^{10,11}B, ^{16}O, ^{23}Na, ^{48}Ti, V, ^{52}Cr, ^{55}Mn, ^{56}Fe, ^{59}Co, ^{58,60}Ni, ^{90}Zr, ^{233,235,238}U, ^{239,240,241}Pu.

A new version of the library, JENDL-4, is under development, with a release expected in 2010.

7.6 Web Access to Nuclear Data

Several major webpages offer evaluated nuclear data. These are regularly maintained by the four well established data centers:

1. National Nuclear Data Center (NNDC), USA, www.nndc.bnl.gov
2. International Atomic Energy Agency, Nuclear Data Section (IAEA-NDS), Vienna, www-nds.iaea.org
3. Nuclear Energy Agency, Data Bank (NEA-DB), Paris, www.nea/fr/html/dbdata
4. Nuclear Data Center, Japan Atomic Energy Agency (NDC-JAEA), Japan, wwwndc.tokai-sc.jaea.go.jp

The NNDC has probably the largest portfolio of data with web retrieval capabilities, including both nuclear structure (ENSDF, NuDat, Chart of Nuclides) and nuclear reactions (EXFOR, ENDF, Sigma).

For the readers of the present Handbook of most interest would be **Sigma** nuclear reaction retrieval and plotting system, which was developed by the NNDC to satisfy needs of both professional users and those without knowledge of complex ENDF-6 formatting system. Sigma uses the latest web technologies to provide

browsing and search tools as well as interactive graphics. It can be easily accessed at www.nndc.bn.gov/sigma and includes the following capabilities:

- Retrieval, Browsing, Search
- Plotting
  - Cross Sections
  - Angular Distributions, Energy Spectra
  - Covariances (MF33)
  - Fission Yields
- Computations (ratios, integrals, weighting)
- Thermal Values and Resonance Integrals

Sigma offers data from the following nuclear reaction libraries:

- ENDF/B-VII.0 (USA, 2006)
- JEFF-3.1 (Europe, 2005)
- JENDL-3.3 (Japan, 2002)
- ROSFOND (Russia, 2008)
- ENDF/B-VI.8 (USA, 2001)
- ENDF/A (USA, selected files only)
- EXFOR (NRDC network, experimental data, latest version)

The IAEA Nuclear Data Service (Vienna) offers major nuclear reaction data libraries as well as number of smaller libraries and specialized results of the IAEA-coordinated data projects. Its signature nuclear reaction retrieval system is **ENDF**, which is also offered by the NNDC as an alternative to Sigma.

The NEA Data Bank (Paris) data services are more restricted, focusing on nuclear reaction data and nuclear reaction computer codes. Its signature nuclear reaction data retrieval and plotting system is Java based **JANIS**.

The Nuclear Data Center of the Japan Atomic Energy Agency (Tokai-mura) offers data services with the focus on data included in the Japanese Evaluated Nuclear Data Library, JENDL.

Acknowledgements To write this Chapter would not be possible without results produced by the dedicated work of numerous scientists and colleagues over years, both in the United States and abroad. We are particularly grateful to members of CSEWG and many other colleagues who contributed to ENDF/B-VII.0 and other nuclear data libraries. We owe special thanks to the authors of the "Big Paper" on ENDF/B-VII.0 [1] which supplied most of the figures and served as the basis for preparing this Chapter.

References

1. M. Chadwick, P. Obložinský, M. Herman, N. Greene, R. McKnight, D. Smith, P. Young, R. MacFarlane, G. Hale, S. Frankle, A. Kahler, T. Kawano, R. Little, D. Madland, P. Moller, R. Mosteller, P. Page, P. Talou, H. Trellue, M. White, W. Wilson, R. Arcilla, C. Dunford, S. Mughabghab, B. Pritychenko, D. Rochman, A. Sonzogni, C. Lubitz, T. Trumbull, J. Weinman, D. Brown, D. Cullen, D. Heinrichs, D. McNabb, H. Derrien, M. Dunn, N. Larson, L. Leal, A. Carlson, R. Block, J. Briggs, E. Cheng, H. Huria, M. Zerkle, K. Kozier, A. Courcelle, V. Pronyaev, and S. van der Marck, "ENDF/B-VII.0: Next generation evaluated nuclear data library for nuclear science and technology," *Nuclear Data Sheets*, vol. 107, no. 12, pp. 2931–3118, 2006.
2. M. Herman and A. Trkov, "ENDF-6 Formats Manual: Data Formats and Procedures for the Evaluated Nuclear Data File ENDF/B-VI and ENDF/B-VII," Tech. Rep. BNL-90365-2009, Brookhaven National Laboratory, 2009.
3. P. G. Young and E. D. Arthur, "GNASH: A preequilibrium statistical nuclear model code for calculations of cross sections and esmission spectra," Tech. Rep. LA-6947, Los Alamos National Lab, Los Alamos, 1977.
4. P. G. Young, E. D. Arthur, and M. B. Chadwick, "Comprehensive nuclear model calculations: Introduction to the theory and use of the GNASH code," Tech. Rep. LA-12343-MS, Los Alamos National Lab, Los Alamos, 1992.
5. P. G. Young, E. D. Arthur, and M. B. Chadwick, "Comprehensive nuclear model calculations: Theory and use of the GNASH code," in *Proc. of the IAEA Workshop on Nuclear Reaction Data and Nuclear Reactors* (A. Gandini and G. Reffo, eds.), (Singapore), pp. 227–404, Trieste, Italy, April 15 - May 17, 1996, World Scientific Publishing, Ltd., 1998.
6. M. Herman, R. Capote, B. Carlson, P. Obložinský, M. Sin, A. Trkov, H. Wienke, and V. Zerkin, "EMPIRE: Nuclear Reaction Model Code System for Data Evaluation," *Nuclear Data Sheets*, vol. 108, no. 12, pp. 2655–2715, 2007.
7. M. Herman, R. Capote, B. Carlson, P. Obložinský, M. Sin, A. Trkov, and V. Zerkin, "EMPIRE nuclear reaction model code, version 2.19 (Lodi)." www.nndc.bnl.gov/empire219/, March 2005.
8. J. Raynal, *Notes on ECIS.* CEA-N-2772, Commissariat à l'Energie Atomique, 1994.
9. G. M. Hale, "Use of R-matrix methods in light element evaluations," in *Proc. Int. Symp. on Nuclear Data Evaluation Methodology* (C. Dunford, ed.), pp. 306–314, Brookhaven National Lab, Upton, NY, World Scientific, Singapore, 1992.
10. N. M. Larson, "Updated users' guide for SAMMY: Multilevel R-matrix fits to neutron data using Bayes' equations," Tech. Rep. ORNL/TM-9179/R7, Document ENDF-364, Oak Ridge National Lab, TN, 2006.
11. S. Oh, J. Chang, and S. F. Mughabghab, "Neutron cross section evaluations of fission products below the fast neutron region," Tech. Rep. BNL-NCS-67469, Brookhaven National Lab., 2000.
12. S. F. Mughabghab, *Atlas of Neutron Resonances: Thermal Cross Sections and Resonance Parameters*. Amsterdam: Elsevier, 2006.
13. A. Ignatyuk, P. Obložinský, M. Chadwick, *et al.*, "Handbook for calculations of nuclear reaction data: Reference Input Parameter Library (RIPL-1)," Technical report TECDOC-1034, IAEA Vienna, 1998.
14. P. Young, M. Herman, P. Obložinský, *et al.*, "Handbook for Calculations of Nuclear Reaction Data: Reference Input Parameter Library-2," TECDOC-1506, IAEA, Vienna, 2005.
15. R. Capote, M. Herman, P. Obložinský, *et al.*, "RIPL - Reference Input Parameter Library for Calculation of Nuclear Reactions and Nuclear Data Evaluations," *Nuclear Data Sheets*, vol. 110, p. 3107, 2009.
16. S. F. Mughabghab, M. Divadeenam, and N. E. Holden, *Neutron Cross Sections: Z=1-60*, vol. 1A. New York: Academic Press, 1981.
17. S. F. Mughabghab, *Neutron Cross Sections: Z=61-100*, vol. 1B. New York: Academic Press, 1984.

18. "The JEFF-3.0 Nuclear Data Library," Tech. Rep. JEFF Report 19, OECD Nuclear Energy Agency, 2005.
19. B. Pritychenko and A. Sonzogni, "Sigma: Web Retrieval Interface for Nuclear Reaction Data," *Nuclear Data Sheets*, vol. 109, p. 2822, 2008.
20. L. M. Bollinger and G. E. Thomas, "p-Wave Resonances of ^{238}U," *Phys. Rev.*, vol. 171, p. 1293, 1968.
21. S. T. Perkins and G. E. Gyulassy, "An Integrated System for Production of Neutronics and Photonics Calculational Constants," Tech. Rep. UCRL-50400, Vol. 12, Univ. of California, 1972.
22. C. E. Porter and R. G. Thomas, "Fluctuations of Nuclear Reaction Widths," *Phys. Rev.*, vol. 104, pp. 483–491, Oct 1956.
23. A. Lane and J. Lynn *Proc. Phys. Soc. (London)*, vol. A70, p. 557, 1957.
24. F. Fröhner, B. Goel, and U. Fischer, "FITACS computer code," Tech. Rep. Report ANL-83-4, p.116, Kernforschungszentrum Karslruhe, 1982. Note: Presented at Specialists' Meeting on Fast Neutron Capture Cross Sections, ANL.
25. P. Axel, "Electric dipole ground state transition width strength function and 7 MeV photon interaction," *Phys. Rev.*, vol. 126, p. 671, 1962.
26. D. M. Brink, *Unpublished*. D. Phil. thesis, Oxford University, 1955.
27. J. Kopecky and M. Uhl, "Test of gamma-ray strength functions in nuclear-reaction model-calculations," *Phys. Rev. C*, vol. 41, pp. 1941–1955, 1990.
28. S. F. Mughabghab and C. L. Dunford, "A dipole-quadrupole interaction term in E1 photon transitions," *Phys. Lett.*, vol. B 487, p. 155, 2000.
29. V. Plujko and M. Herman, *Handbook for calculations of nuclear reaction data, RIPL-2*, ch. 7: Gamma-ray strength functions, p. 120. No. TECDOC-1506, IAEA, Vienna, 2006.
30. C. Dunford, "Compound nuclear analysis programs COMNUC and CASCADE," Tech. Rep. T1-707-130-013, Atomics International, 1971.
31. H. M. Hofmann, J. Richert, J. W. Tepel, and H. A. Weidenmüller, "Direct reactions and Hauser-Feshbach theory," *Ann. Phys.*, vol. 90, p. 403, 1975.
32. C. Kalbach, "Systematics of continuum angular distributions: Extensions to higher energies," *Phys. Rev. C*, vol. 37, pp. 2350–2370, 1988.
33. E. Běták and P. Obložinský, "Code PEGAS: Preequilibrium exciton model with spin conservation and gamma emission," Tech. Rep. INDC(SLK)-001, IAEA/Slovak Academy of Sciences, 1993. Note: DEGAS is an extended version of the code PEGAS using two-parameteric p-h level densities.
34. M. Blann, "New precompound decay model," *Phys. Rev. C*, vol. 54, p. 1341, 1996.
35. M. Blann and M. B. Chadwick, "New precompound model: Angular distributions," *Phys. Rev. C*, vol. 57, p. 233, 1998.
36. M. Blann and M. B. Chadwick, "Precompound Monte-Carlo model for cluster induced reactions," *Phys. Rev. C*, vol. 6203, p. 4604, 2000.
37. T. Tamura, T. Udagawa, and H. Lenske, "Multistep direct reaction analysis of continuum spectra in reactions induced by light ions," *Phys. Rev.*, vol. C26, p. 379, 1982.
38. H. Nishioka, J. J. M. Verbaarschot, H. A. Weidenmüller, and S. Yoshida, "Statistical theory of precompound reactions: multistep compound process," *Ann. Phys.*, vol. 172, p. 67, 1986.
39. M. Herman, G. Reffo, and H. A. Weidenmüller, "Multistep-compound contribution to precompound reaction cross section," *Nucl.Phys.*, vol. A536, p. 124, 1992.
40. G. Hale, "Covariances from Light-Element R-Matrix Analyses," *Nuclear Data Sheets*, vol. 109, p. 2812, 2008.
41. N. Bohr and J. Wheeler, "The mechanism of nuclear fission," *Phys. Rev.*, vol. 56, pp. 426–450, 1939.
42. Y. Frenkel, "On the splitting of heavy nuclei by slow neutrons," *Phys. Rev.*, vol. 55, pp. 987–987, 1939.
43. S. Bjornholm and J. Lynn, "The double-humped fission barrier," *Rev. Mod. Phys.*, vol. 52, pp. 725–931, 1980.
44. D. G. Madland and J. R. Nix, "New calculation of prompt fission neutron-spectra and average prompt neutron multiplicities," *Nucl. Sci. and Eng.*, vol. 81, pp. 213–271, 1982.

45. P. Young, M. Chadwick, R. MacFarlane, P. Talou, T. Kawano, D. Madland, W. Wilson, and C. Wilkerson, "Evaluation of Neutron Reactions for ENDF/B-VII: $^{232-241}$U and ^{239}Pu," *Nuclear Data Sheets*, vol. 108, no. 12, pp. 2589 – 2654, 2007.
46. L. C. Leal, H. Derrien, N. M. Larson, and A. Courcelle, "An Unresolved Resonance Evaluation for ^{235}U," in *PHYSOR Conference*, Chicago, Illinois, April 25-29, 2004.
47. H. Weigmann, J. Hambsch, W. Mannhart, Mamoru Baba, Liu Tingjin, N. Kornilov, D. Madland, and P. Staples, "Fission neutron spectra of ^{235}U," Report NEA/WPEC-9, OECD, 2003.
48. G. Boykov *et al. Sov. J. Nucl. Phys.*, vol. 53, p. 392, 1991.
49. A. Courcelle, "First conclusions of the WPEC Subgroup-22," in *Proc. of the Inter. Conf. on Nuclear Data for Science and Technology* (R. Haight, M. Chadwick, T. Kawano, and P. Talou, eds.), (New York, USA), pp. 462–467, Santa Fe, Sept 26 - Oct 1, 2004, Amer. Inst. of Physics, 2005.
50. H. Derrien, A. Courcelle, L. Leal, N. M. Larson, and A. Santamarina, "Evaluation of ^{238}U Resonance Parameters from 0 to 20 keV," in *Proc. of the Inter. Conf. on Nuclear Data for Science and Technology* (R. Haight, M. Chadwick, T. Kawano, and P. Talou, eds.), (New York, USA), pp. 276–281, Santa Fe, Sept 26 - Oct 1, 2004, Amer. Inst. of Physics, 2005.
51. A. Trkov *et al.*, "Revisiting the ^{238}U thermal capture cross-section and gamma emission probabilities from ^{239}Np decay," *Nucl. Sci. Eng.*, vol. 150, pp. 336–348, 2005.
52. M. López Jiménez, B. Morillon, and P. Romain, "Overview of Recent Bruyères-le-Châtel Actinide Evaluations," in *Proc. of the Inter. Conf. on Nuclear Data for Science and Technology* (R. Haight, M. Chadwick, T. Kawano, and P. Talou, eds.), (New York, USA), pp. 314–316, Santa Fe, Sept 26 - Oct 1, 2004, Amer. Inst. of Physics, 2005.
53. T. Ethvignot *et al. Phys. Lett. B*, vol. 575, p. 221, 2003.
54. Y. Kanda and M. Baba, "WPEC-SG4 Report: ^{238}U Capture and Inelastic Cross Sections," Tech. Rep. NEA/WPEC-4, NEA Paris, 1999.
55. P. Staples *et al. Nucl. Phys. A*, vol. 591, pp. 41–60, 1995.
56. R.W. Lougheed *et al.* , "^{239}Pu and ^{241}Am (n,2n) cross section measurements near 14 MeV," Tech. Rep. UCRL-ID-145592, Lawrence Livermore National Lab, CA, 2001.
57. S. Bjornholm and J. E. Lynn, "The double-humped fission barrier," *Rev.Mod.Phys.*, vol. 52, p. 725, 1980.
58. A. Trkov, "2nd IAEA Research Co-ordination Meeting on Evaluated Nuclear Data for Thorium-Uranium Fuel Cycle," Technical report INDC(NDS)-447, IAEA, Vienna, 2003.
59. A. Trkov, "Evaluated Nuclear Data for Th-U Fuel Cycle Summary Report of the Third Research Coordination Meeting," Technical report INDC(NDS)-494, IAEA, Vienna, 2006.
60. L. Leal and H. Derrien, "Evaluation of the resonance parameters for ^{232}Th in the energy range 0 to 4 keV," technical report, Oak Ridge National Lab, 2006.
61. D. Olsen and R. Ingle, "Measurement of Neutron Transmission Spectra through ^{232}Th from 8 MeV to 4 keV," Report ORNL/TM-7661(ENDF-307), Oak Ridge National Lab, 1981.
62. I. Sirakov, P. Schillebeeckx, R. Capote, and A. Trkov, "^{232}Th: Evaluation of the average resonance parameters and their covariances in the unresolved resonance region from 4 to 100 keV." Private Communication, September 2006.
63. R. Capote, M. Sin, and A. Trkov, "Evaluation of fast neutron induced reactions on ^{232}Th and ^{231,233}Pa up to 60 MeV." private communication, 2006.
64. M. Herman, P. Obložinský, R. Capote, M. Sin, A. Trkov, A. Ventura, and V. Zerkin, "Recent developments of the nuclear reaction model code EMPIRE," in *Proc. of the Inter. Conf. on Nuclear Data for Science and Technology* (R. Haight, M. Chadwick, T. Kawano, and P. Talou, eds.), (New York, USA), p. 1184, Santa Fe, Sept 26 - Oct 1, 2004, Amer. Inst. of Physics, 2005.
65. M. Sin, R. Capote, M. Herman, P. Obložinský, A. Ventura, and A. Trkov, "Improvement of the fission channel in the EMPIRE code," in *Proc. of the Inter. Conf. on Nuclear Data for Science and Technology* (R. Haight, M. Chadwick, T. Kawano, and P. Talou, eds.), (New York, USA), p. 1249, Santa Fe, Sept 26 - Oct 1, 2004, Amer. Inst. of Physics, 2005.
66. E. S. Soukhovitskii, R. Capote, J. M. Quesada, and S. Chiba, "Dispersive coupled-channel analysis of nucleon scattering from ^{232}Th up to 200 MeV," *Phys.Rev. C*, vol. 72, p. 024604, 2005.

67. W. Hauser and H. Feshbach, "The inelastic scattering of neutrons," *Phys. Rev.*, vol. 87, pp. 366–373, 1952.
68. M. Sin, R. Capote, A. Ventura, M. Herman, and P. Obložinský, "Fission of light actinides: ^{232}Th(n,f) and ^{231}Pa(n,f) reactions," *Phys. Rev. C*, vol. 74, no. 1, p. 014608, 2006.
69. A. Ignatyuk, V. Lunev, Y. Shubin, E. Gai, and N. Titarenko, "Evaluation of n + ^{232}Th cross sections for the energy range up to 150 MeV." Provided to the IAEA CRP on Th-U cycle, 2006.
70. A. Trkov and R. Capote, "Validation of ^{232}Th evaluated nuclear data through benchmark experiments," in *Proc. of the Inter. Conf. on Nuclear Energy for New Europe 2006*, Portorož, Slovenia, September 18-21, 2006, 2006.
71. W. Younes and H. C. Britt, "Neutron-induced fission cross sections simulated from (t,pf) results," *Phys. Rev. C*, vol. 67, no. 2, p. 024610, 2003.
72. C. Plettner, H. Ai, C. W. Beausang, *et al.*, "Estimation of (n,f) cross sections by measuring reaction probability ratios," *Phys. Rev. C*, vol. 71, no. 5, p. 051602, 2005.
73. J. Frehaut, "Coherent evaluation of nu-bar (prompt) for ^{235,238}U and ^{239}Pu," Tech. Rep. JEFDOC-17, NEA, JEFF project, 2000.
74. M. Brady and T. England, "Delayed neutron data and group parameters for 43 fissioning systems," *Nucl. Sci. Eng.*, vol. 103, pp. 129–149, 1989.
75. G.R. Keepin, *Physics of Neutron Kinetics*. New York: Addison-Wesley, 1965.
76. W. Wilson and T. England, "Delayed neutron study using ENDF/B-VI basic nuclear data," *Prog. Nucl. Energy*, vol. 41, pp. 71–107, 2002.
77. B. Pfeiffer, K.-L. Kratz, and P.Moller, "Status of delayed-neutron data: half-lives and neutron emission probabilities," *Prog. Nucl. Energy*, vol. 41, pp. 39–69, 2002.
78. G. Audi, O. Bersillon, J. Blachot, and A. Wapstra, "The NUBASE evaluation of nuclear and decay properties," *Nucl. Phys.*, vol. A729, p. 3, 2003.
79. T. England and B. Rider, "Nuclear modeling of the ^{239}Pu(n,xn) excitation function," Tech. Rep. LA-UR-94-3106 ENDF-349, Los Alamos National laboratory, Los Alamos, 1993.
80. J. Conant and P. Palmedo, "Delayed neutron data," *Nuc. Sci. Eng.*, vol. 44, p. 173, 1971.
81. R. Tuttle, "Delayed neutron data," *Nuc. Sci. Eng.*, vol. 56, p. 37, 1975.
82. T. Ohsawa and T. Oyama, "Possible fluctuations in delayed neutron yields in the resonance region of U-235," in *Proc. of the Specialists' Meeting on Delayed Neutron Nuclear Data* (J. Katakura, ed.), (Tokai-mura, Japan), p. 43, JAERI, Amer. Inst. of Physics, 1999.
83. T. Ohsawa and F.-J. Hambsch, "An interpretation of energy-dependence of delayed neutron yields in the resonance region for ^{235}U and ^{239}Pu," *Nuc. Sci. Eng.*, vol. 148, p. 50, 2004.
84. K. Nakajima, "Re-evaluation of the effective delayed neutron fraction measured by the substitution technique for a light water moderated low-enriched uranium core," *J. Nucl. Sci. Techn.*, vol. 38, pp. 1120–1125, 2001.
85. T. Sakurai and S. Okajima, "Adjustment of Delayed Neutron Yields in JENDL-3.2," *J. Nuc. Sci. Tech.*, vol. 39, pp. 19–30, 2002.
86. S. van der Marck, "Benchmarking ENDF/B-VII beta1." CSEWG 2005 meeting report, www.nndc.bnl.gov/csewg/, 2005.
87. D. Madland, "Total prompt energy release in the neutron-induced fission of ^{235}U, ^{238}U, and ^{239}Pu," *Nucl. Phys.*, vol. A772, p. 113, 2006.
88. ICRU-Report-63, in *Nuclear Data for Neutron and Proton Radiotherapy and for Radiation Protection*, Bethesda, MD: Inter. Com. on Radiation Units and Measurements, 2000.
89. D. Muir, "Gamma rays, Q-values and kerma factors," Tech. Rep. LA-6258-MS, Los Alamos National Lab, Los Alamos, 1976.
90. D. Cokinos and E. Melkonian, "Measurement of the 2200 m/sec neutron-proton capture cross section," *Phys. Rev.*, vol. C15, p. 1636, 1977.
91. K. Schoen *et al.*, "Precision neutron interferometric measurements and updated evaluations of the n-p and n-d coherent neutron scattering lengths," *Phys. Rev.*, vol. C67, p. 044005, 2003.
92. T. L. Houk, "Neutron-proton scattering cross section at a few electron Volts and charge independence," *Phys. Rev.*, vol. C3, p. 1886, 1971.

93. W. Dilg, "Measurement of the neutron-proton total cross section at 132 eV," *Phys. Rev.*, vol. C11, p. 103, 1975.
94. N. Boukharaba *et al.*, "Measurement of the n-p elastic scattering angular distribution at E_n = 10 MeV," *Phys. Rev.*, vol. C65, p. 014004, 2002.
95. W. Buerkle and G. Mertens, "Measurement of the neutron-proton differential cross section at 14.1 MeV," *Few Body Systems*, vol. 22, p. 11, 1997.
96. G. M. Hale *et al.*, "Neutron-triton cross sections and scattering lengths obtained from p-^{3}He scattering," *Phys. Rev.*, vol. C42, p. 438, 1990.
97. C. Fu and D. Hetrick, "Update of ENDF/B-V Mod-3 Iron: Neutron-Producing Reaction Cross Sections and Energy-Angle Correlations," ORNL/TM-9964, ENDF-341, Oak Ridge National Laboratory, 1986.
98. D. Rochman, M. Herman, and P. Obložinský, "New evaluation of ^{51}V(n, np+pn) and (n, t) cross sections for the ENDF/B-VII library," *Fusion Engineering and Design*, vol. 81, pp. 2109–2113, August 2006.
99. S. Grimes *et al.*, "Charged particle-producing reactions of 15-MeV neutrons on ^{51}V and ^{93}Nb," *Phys. Rev. C*, vol. 17, p. 508, 1978.
100. O. Kokoo, I. Murata, and A. Takahashi, "Measurements of double-differential cross sections of charged-particle emission reactions for several structural elements of fusion power reactors by 14.1-MeV incident neutrons," *Nucl. Sci. Eng.*, vol. 132, p. 16, 1999.
101. R. Woelfle *et al. Radiochimica Acta*, vol. 50, p. 5, 1990.
102. T. Kawano *et al.*, "Production of isomers by neutron-induced inelastic scattering on ^{193}Ir and influence of spin distribution in the preequilibrium process," *Nucl. Instr. Meth.*, vol. 562, p. 774, 2006.
103. A. J. Koning and J. P. Delaroche, "Local and global nucleon optical models from 1 keV to 200 MeV," *Nucl.Phys.*, vol. A713, p. 231, 2003.
104. R. Q. Wright and R. E. MacFarlane, "Review of ENDF/B-VI fission-product cross sections," Tech. Rep. ORNL/TM-13723, Oak Ridge National Lab, Oak Ridge, TN, 2000.
105. H.-I. Kim, Y.-O. Lee, M. Herman, S. F. Mughabghab, P. Obložinský, and D. Rochman, "Evaluation of Neutron Induced Reactions for 32 Fission Products," Tech. Rep. BNL-77775-2007-IR, Brookhaven National Lab, 2006.
106. H.-I. Kim, M. Herman, S. F. Mughabghab, P. Obložinský, D. Rochman, and Y.-O. Lee, "Evaluation of Neutron Cross Sections for a Complete Set of Nd Isotopes," *Nucl. Sci. Eng.*, vol. 160, p. 168, 2008.
107. P. Obložinský *et al.*, "Evaluated Data Library for the Bulk of Fission Products," Tech. Rep. NEA/WPEC-23, OECD Nuclear Energy Agency, Paris, 2009.
108. M. D. DeHart, "Sensitivity and parametric evaluations of significant aspects of burnup credit for PWR spent fuel packages," Tech. Rep. ORNL/TM-12973, Oak Ridge National Lab, 1995.
109. D. L. Smith, *Probability, Statistics, and Data Uncertainties in Nuclear Science and Technology*. American Nuclear Society, 1991.
110. R. Kinsey, "ENDF-201: ENDF/B Summary Documentation," Tech. Rep. BNL-NCS-17541, National Nuclear Data Center, BNL, July 1979. Note: 3rd Edition, ENDF/B-V Library.
111. B. Magurno, R. Kinsey, and F. Scheffel, "Guidebook for the ENDF/B-V Nuclear Data Files," Tech. Rep. EPRI NP-2510, BNL-NCS-31451, ENDF-328, Brookhaven National Lab and Electric Power Research Institute, July 1982.
112. P. Obložinský, ed., *Workshop on Neutron Cross Section Covariances, Port Jefferson, June 24-28*, vol. 109 of *Nuclear Data Sheets*, 2008.
113. M. Williams, "Generation of Approximate Covariance Data." ORNL memo, August 2004.
114. T. Kawano, T. Ohsawa, K. Shibata, and H. Nakashima, "Evaluation of Covariance for Fission Neutron Spectra," Tech. Rep. 99-009, JAERI, 1999.
115. K. Kosako and N. Yanano, "Preparation of a covariance processing system for the evaluated nuclear data file, JENDL," Tech. Rep. JNC TJ-9440, 99-003, JAERI, 1999.
116. R. Little, T. Kawano, G. Hale, *et al.*, "Low-fidelity Covariance Project," *Nuclear Data Sheets*, vol. 109, p. 2828, 2008.
117. D. W. Muir, "Evaluation of correlated data using partinioned least squares: a minimum-variance derivation," *Nucl. Sci. Eng.*, vol. 101, pp. 88–93, 1989.

118. H. Derrien, L. C. Leal, and N. M. Larson, "Evaluation of ^{232}Th Neutron Resonance Parameters in the Energy Range 0 to 4 keV," Tech. Rep. ORNL/TM-2006/53, Oak Ridge National Lab, 2006.
119. D. Smith, "Covariance matrices for nuclear cross sections derived from nuclear model calculations," report ANL/NDM-159 November, Argonne National Lab, 2004.
120. A. Trkov, "Summary report of a technical meeting on covariances of nuclear reaction data: GANDR project," INDC(NDS)-471, IAEA, Vienna, 2005.
121. M. Pigni, M. Herman, and P. Obložinský, "Extensive set of cross section covariance estimates in the fast neutron region," *Nucl. Sci. Eng.*, vol. 162, pp. 25–40, 2009.
122. "SCALE: A modular code system for performing standardized computer analysis for licensing evaluation." NUREG/CR-0200, Rev. 6 (ORNL/NUREG/CSD-2/R6), Vols. I, II, and III, May 2000. Available from the Radiation Safety Information Computational Center at Oak Ridge National Lab as CCC-545, 2000.
123. M. Williams and B. Rearden, "SCALE-6 Sensitivity/Uncertainty Methods and Covariance Data," *Nuclear Data Sheets*, vol. 109, p. 2797, 2008.
124. P. Obložinský, C. Mattoon, M. Herman, S. Mughabghab, M. Pigni, P. Talou, G. Hale, A. Kahler, T. Kawano, R. Little, and P. Young, "Progress on Nuclear Data Covariances: AFCI-1.2 Covariance Library," Tech. Rep. unpublished, Brookhaven National Laboratory and Los Alamos National Laboratory, 2009.
125. J. B. Briggs *et al.*, "International handbook of evaluated criticality safety benchmark experiments," Tech. Rep. NEA/NSC/DOC(95)04/I, Nuclear Energy Agency, Paris, France, 2004.
126. S. C. van der Marck, "Benchmarking ENDF/B-VII.0," *Nuclear Data Sheets*, vol. 107, pp. 3061–3118, December 2006.
127. A. dos Dantos, R. Diniz, L. Fanaro, R. Jerez, G. de Andrade e Silva, and M. Yamaguchi, "The experimental determination of the effective delayed neutron parameters of the IPEN/MB-01 reactor," (Chicago), PHYSOR, 2004.
128. S. Okajima, T. Sakurai, J. Lebrat, V. Averlant, and M. M., "Summary on international benchmark experiments for effective delayed neutron fraction," *Progress in Nuclear Energy*, vol. 41, p. 285301, 2002.
129. R. Klein Meulekamp and S. van der Marck, "Re-evaluation of the effective delayed neutron fraction measured by the substitution technique for a light water moderated low-enriched uranium core," *Nucl. Sci. Eng.*, vol. 152, pp. 142–148, 2006.
130. S. van der Marck, R. Klein Meulekamp, A. Hogenbirk, and A. Koning, "Benchmark results for delayed neutron data," (New York, USA), pp. 531–534, Santa Fe, Sept 26 - Oct 1, 2004, Amer. Inst. of Physics, 2005.
131. C. Wong *et al.*, "Livermore pulsed sphere program: Program summary through July 1971," Tech. Rep. UCRL-51144, Rev I, and Addendum (1973), Lawrence Livermore National Lab, 1972.
132. W. Webster *et al.*, "Measurements of the neutron emission spectra from spheres of N, O, W, U-235, U-238, and Pu-239, pulsed by 14 MeV neutrons," Tech. Rep. UCID-17332, 1976.
133. A. Marchetti and G. Hedstrom, "New Monte Carlo simulations of the LLNL pulsed-sphere experiments," Tech. Rep. UCRL-ID-131461, Lawrence Livermore National Lab, 1998.
134. S. Frankle, "LLNL pulsed-sphere measurements and detector response functions," Tech. Rep. X-5:SCF-04-004 and LA-UR-05-5878, Los Alamos National Lab, Los Alamos, 2004.
135. S. Frankle, "Possible impact of additional collimators on the LLNL pulsed-sphere experiments," Tech. Rep. X-5:SCF-04-001 and LA-UR-05-5877, Los Alamos National Lab, Los Alamos, 2004.
136. J. Bucholz and S. Frankle, "Improving the LLNL pulsed-sphere experiments database and MCNP models," *Trans. Am. Nucl. Soc.*, pp. 433–435, 2002.
137. T. England and B. Rider, "Evaluation and compilation of fission product yields," Tech. Rep. ENDF-349, Los Alamos National Lab, 1992.
138. M. Mattes and J. Keinert, "Thermal neutron scattering data for the moderator materials H_2O, D_2O, and ZrH_x in ENDF-6 format and as ACE library for MCNP(X) codes," report INDC(NDS)-0470, IAEA, April 2005.

139. R. E. MacFarlane, "New thermal neutron scattering files for ENDF/B-VI release 2," Tech. Rep. LA-12639-MS (1994), Los Alamos National Lab, Los Alamos, 1994.
140. J. Koppel and D. Houston, "Reference manual for ENDF thermal neutron scattering data," report GA-8774 revised and reissued as ENDF-269 by the National Nuclear Data Center, General Atomic, July 1978.
141. J. Keinert and J. Sax, "Investigation of neutron scattering dynamics in liquid hydrogen and deuterium for cold neutron sources," *Kerntechnik*, vol. 51, p. 19, 1987.
142. J. A. Young and J. U. Koppel, "Slow neutron scattering by molecular hydrogen and deuterium," *Phys. Rev.*, vol. 135, pp. A603–A611, Aug 1964.
143. G. H. Vineyard, "Frequency factors and isotope effects in solid state rate processes," *J. of Physics and Chemistry of Solids*, vol. 3, no. 1-2, pp. 121–127, 1957.
144. R. Stedman, L. Almqvist, and G. Nilsson, "Phonon-frequency distributions and heat capacities of Aluminum and Lead," *Phys. Rev.*, vol. 162, pp. 549–557, Oct 1967.
145. B. N. Brockhouse, H. E. Abou-Helal, and E. D. Hallman, "Lattice vibrations in iron at 296^{o}K," *Solid State Commun.*, vol. 5, p. 211, 1967.
146. "ENSDF, Evaluated Nuclear Structure Data File." www.nndc.bnl.gov/ensdf, 2006.
147. J. Tuli, "Nuclear Wallet Cards." Electronic version, www.nndc.bnl.gov/wallet, 2005.
148. R. Greenwood, R. Helmer, M. Putnam, and K. Watts, "Measurement of β- decay intensity distributions of several fission-product isotopes using a total absorption γ-ray spectrometer," *Nucl.Instrum.Methods Phys.Res.*, vol. A390, p. 95, 1997.
149. N. Hagura, T. Yoshida, and T. Tachibana, "Reconsideration of the theoretical supplementation of decay data in fission-product decay heat summation calculations," *J. of Nucl. Science and Tech.*, 2006.
150. T. Yoshida *et al.*, "Validation of Fission Product Decay Data for Decay Heat Calculations." WPEC Subgroup-25, www.nea.fr/html/science/projects/SG25, 2006.
151. I. Band, M. Trzhaskovskaya, C. Nestor Jr., P. Tikkanen, and S. Raman, "Dirac-Fock internal conversion coefficients," *At. Data Nucl. Data Tables*, vol. 81, p. 1, 2002.
152. P. Cassette, "SPEBETA programme de calcul du spectre en energie des electros emis par des radionucleides emetterus beta," Tech. Rep. CEA Technical Note LPRI/92/307/J, CEA Saclay, 1992.
153. A. Tobias and R. Mills. (private communication), 1989.
154. P. J. Griffin and R. Paviotti-Corcuera, "Summary Report of the Final Technical Meeting on International Reactor Dosimetry File: IRDF-2002," Tech. Rep. INDC(NDS)-448, IAEA, Vienna, Austria, October 2003.
155. R. Forrest, J. Kopecky, and J.-C. Sublet, "The European Activation File: EAF-2007 neutron-induced cross section library," Tech. Rep. FUS 435, United Kingdom AEA, 2007.
156. A. Carlson, V. Pronyaev, D. Smith, *et al.*, "International Evaluation of Neutron Cross Section Standards," *Nuclear Data Sheets*, pp. 3215–3325, 2009.
157. D. Lopez Aldama and A. Trkov, "FENDL-2.1 Update of an evaluated nuclear data library for fusion applications," Tech. Rep. INDC(NDS)-467, IAEA, Vienna, Austria, December 2004.
158. R. Forrest, J. Kopecky, and J.-C. Sublet, "The European Activation File: EAF-2003 Cross Section Library," Tech. Rep. FUS 486, United Kingdom AEA, 2002.
159. A. Koning, S. Hilaire, and M. Duijvestijn, "TALYS: Comprehensive nuclear reaction modeling," in *Proc. of the Inter. Conf. on Nuclear Data for Science and Technology* (R. Haight, M. Chadwick, T. Kawano, and P. Talou, eds.), (New York, USA), pp. 1154–1159, Santa Fe, Sept 26 - Oct 1, 2004, Amer. Inst. of Physics, 2005.
160. R. E. MacFarlane and D. W. Muir, "The NJOY nuclear data processing system, version 91," Tech. Rep. LA-12740-M, Los Alamos National Lab, NM, 1994.
161. X5-MCNP-Team, "MCNP - A General Monte Carlo N-Particle Transport Code, Version 5, Volume I: Overview and Theory," Tech. Rep. LA-UR-03-1987, Los Alamos National Lab, April 2003.
162. CSEWG-Collaboration, "Evaluated Nuclear Data File ENDF/B-VI.8." www.nndc.bnl.gov/endf, released in October 2001.

163. M. Chadwick, P. Obložinský, A. Blokhin, *et al.*, "Handbook on Photonuclear Data for Applications: Cross-sections and Spectra," Tech. Rep. IAEA-TECDOC-1178, International Atomic Energy Agency, October 2000.
164. R. MacFarlane and A. Kahler, "NJOY-99 nuclear data processing code, version released in 2006." unpublished.
165. RSICC, "Webpage, Radiation Safety Information Computational Center." www-rsicc.ornl.gov, 2009.
166. NEA, "Webpage, Nuclear Energy Agency Data Bank." www.nea.fr/html/databank/, 2009.
167. LANL, "Webpage, T-2 Information Service, Los Alamos National Lab." t2.lanl.gov, 2009.
168. K. Kosako, "Covariance Data Processing Code: ERRORJ," in *the Specialists' Meeting of Reactor Group Constants* (J. Katakura, ed.), JAERI, Tokai, Japan, February 22-23, 2001. JAERI-Conf 2001-009.
169. D. Wiarda and M. Dunn, "PUFF-IV: Code System to Generate Multigroup Covariance Matrices from ENDF/B-VI Uncertainty Files ." Oak Ridge National Lab, Radiation Safety Information Computational Center (RSICC) Code Package PSR-534, 2006.
170. M. Dunn and N. Greene, "AMPX-2002: A Cross Section Processing System for Generating Nuclear Data for Criticality Safety Applications," Tech. Rep. Trans. Am. Nucl. Soc., ORNL, 2002.
171. C. Dunford, "ENDF Utility Codes, version 7.02." www.nndc.bnl.gov/nndcscr/endf/endf-util-7.02/, 2005.
172. "MCNPX Transport Code for Charged Particles." mcnpx.lanl.gov, 2006.
173. K. Shibata, T. Kawano, T. Nakagawa, *et al.*, "Japanese Evaluated Nuclear Data Library Version 3 Revision-3: JENDL-3.3," *J. Nucl. Sci. Tech.*, vol. 39, pp. 1125–1136, 2002.
174. K. Shibata, A. Hasegawa, O. Iwamoto, *et al.*, "JENDL-3.2 Covariance File," *J. Nucl. Sci. Tech.*, vol. Suppl.2, pp. 40–43, 2002.

Contents

Index